Journal of Medicinal Chemistry

Article

Design, Synthesis, and Pre-Clinical Efficacy of Novel Non-Retinoid Antagonists of Retinol Binding Protein 4 in the Mouse Model of Hepatic Steatosis

Christopher L. Cioffi, Boglarka Racz, András Váradi, Emily Freeman, Michael P Conlon, Ping Chen, Lei Zhu, Douglas B. Kitchen, Keith Barnes, William Martin, Paul Pearson, Graham Johnson, William S. Blaner, and Konstantin Petrukhin

J. Med. Chem., **Just Accepted Manuscript** • DOI: 10.1021/acs.jmedchem.9b00352 • Publication Date (Web): 11 May 2019

Design, Synthesis, and Pre-Clinical Efficacy of Novel Non-Retinoid Antagonists of Retinol Binding Protein 4 in the Mouse Model of Hepatic Steatosis

Christopher L. Cioffi,*[€] Boglarka Racz,[§] Andras Varadi,[§] Emily E. Freeman,[†] Michael P. Conlon,[†] Ping Chen,[†] Lei Zhu,[&] Douglas B. Kitchen,[&] Keith D. Barnes,[†] William H. Martin,[‡] Paul G. Pearson,[¶] Graham Johnson,[£] William S. Blaner[¥] and Konstantin Petrukhin*[§]

[€]Albany College of Pharmacy and Health Sciences, Departments of Basic and Clinical Sciences and Pharmaceutical Sciences, 106 New Scotland Ave, Albany, NY 12208

[§]Department of Ophthalmology, Columbia University Medical Center, New York, NY 10032

[†]AMRI, Department of Medicinal Chemistry, East Campus, 3 University Place, Rensselaer, NY 12144

[&]AMRI, Computer Assisted Drug Discovery, East Campus, 3 University Place, Rensselaer, NY 12144

[‡]WHM Consulting LLC, 111 Sterling City Road, Lyme, CT 06371

[¶] Pearson Pharma Partners, 31194 La Baya Drive, Westlake Village, CA 91361

[£]NuPharmAdvise LLC, 3 Lakeside Drive, Sanbornton, NH 03269

[¥]Department of Medicine, Columbia University Medical Center, New York, NY 10032

Abstract: Retinol-binding protein 4 (RBP4) serves as a transporter for all-*trans* retinol (**1**) in the blood and it has been proposed to act as an adipokine. Elevated plasma levels of the protein have been linked to diabetes, obesity, cardiovascular diseases, and non-alcoholic fatty liver disease (NAFLD). Recently, adipocyte-specific overexpression of RBP4 was reported to cause hepatic steatosis in mice. We previously identified an orally bioavailable RBP4 antagonist that significantly lowered RBP4 serum levels in *Abca4*$^{-/-}$ knockout mice with concomitant normalization of complement system protein expression and reduction of bisretinoid formation within the retinal pigment epithelium (RPE). We describe herein the discovery of novel RBP4 antagonists **48** and **59**, which reduce serum RBP4 levels by >80% in mice upon acute oral dosing. Furthermore, **59** demonstrated efficacy in the transgenic adi-hRBP4 murine model of hepatic steatosis, suggesting that RBP4 antagonists may also have therapeutic utility for the treatment of NAFLD.

▪ INTRODUCTION

Retinol-binding protein 4 (RBP4) is a serum protein belonging to the lipocalin family that transports the essential vitamin all-*trans*-retinol (vitamin A, **1**) (Figure 1) from the hepatic stores to peripheral tissues.[1] RBP4-mediated transport of **1** from the liver to target tissues requires formation of a tertiary complex between holo-RBP4 (RBP4 bound to **1**) and transthyretin (TTR)[2] as circulating apo-RBP4 (RBP4 not bound to **1**) associates poorly with TTR and due to its low molecular weight (21 kDa), is rapidly cleared via glomerular filtration.[3] Inhibition of holo-RBP4 formation by displacing **1** from the ligand-binding

pocket of RBP4 by selective antagonists prevents RBP4-TTR complexation from occurring, which in turn leads to a reduction in circulating levels of RBP4 and **1**. Cellular uptake of **1** is facilitated by STRA6 (stimulated by retinoic acid gene 6 protein), which functions as a high affinity RBP4 membrane receptor and a retinol channel in many vitamin A-dependent tissues and blood-organ barriers.[4] Until recently, transport of **1** was the only function attributed to RBP4. Consistent with its major role as a carrier of hepatic **1**, 60-80% of circulating RBP4 derives from the liver where it is secreted bound to **1**[5] with extra-hepatic secretion, mainly from adipocytes, accounting for approximately 20-40% of circulating levels of the protein.[6-8] Recently, emerging epidemiologic evidence suggested that modestly enhanced circulating levels of RBP4 might have important metabolic effects. Numerous, but not all, epidemiological studies established an association of elevated serum RBP4 levels with obesity,[8, 9] insulin resistance,[8-11] cardiovascular disease,[12, 13] pro-atherogenic conditions,[8] hepatic steatosis,[9] and type 2 diabetes.[8, 11] It has been theorized that RBP4 may act as an adipokine (a cytokine produced by adipocytes) involved in the mediation of insulin sensitivity and the regulation of energy metabolism.[2] Consistent with this hypothesis, it was reported that RBP4 secreted from cultured adipocytes may activate cytokine production from co-cultured macrophages through TLR4 and JNK pathway activation that does not involve the RBP4 receptor STRA6.[13, 14] It was suggested that retinol binding may not be required for RBP4 to act as a pro-inflammatory metabolic effector, given that apo-RBP4 was shown to induce an inflammatory response in endothelial cells by stimulating the expression of pro-inflammatory signaling molecules in a retinol- and STRA6-independent fashion.[15]

Conversely, it has been reported that RBP4 signaling depends on retinol binding and involves the STRA6 receptor.[16, 17] Despite the progress made in the characterization of RBP4 as a putative adipokine, it is not fully understood how modestly elevated serum RBP4 levels in humans may mechanistically contribute to the pathogenesis of a variety of metabolic disorders. Three mouse models mimicking the increase in circulating levels of serum RBP4 were used to probe the role of RBP4 in mediating adverse metabolic consequences. Transgenic mice ectopically expressing human RBP4 in muscle from a muscle-specific promoter have approximately 3-fold higher circulating levels of serum RBP4.[18] These mice were reported to develop high-fat diet (HFD)-induced insulin resistance,[9] although two subsequent studies could not replicate this finding.[19, 20] Adeno-associated virus-driven overexpression of murine RBP4 in the mouse liver yielded a 2- to 3-fold increase in levels of serum RBP4.[21] However, no effect on glucose and energy homeostasis was detected in response to this significant increase in liver-secreted circulating RBP4.[21] In a remarkable contrast to the two previous models, low-level transgenic expression of human RBP4 in the mouse adipose tissue led to a strong metabolic phenotype, which comprised hepatic steatosis, dyslipidemia, and reduced glucose tolerance.[22] Given that hepatic steatosis observed in this model resulted from increased hepatic uptake of adipose-derived circulating non-esterified fatty acids,[22] it may be suggested that adipose-secreted RBP4 facilitates trafficking of the adipose-derived fatty acids to the liver through a yet to be defined mechanism. Interestingly, earlier crystal structures of heterologously expressed RBP4 display fortuitous fatty acid ligands from the expression host in the ligand binding pocket of RBP4.[23, 24] Furthermore, recent x-ray

crystallographic and mass spectrometry findings reported by Monaco and coworkers confirmed that in addition to binding retinoids, RBP4 is also capable of binding fatty acids,[25] which may potentially relate to the RBP4 role as a facilitator of fatty acid trafficking. We previously described the discovery new classes of non-retinoid RBP4 antagonists[26, 27] that we studied in animal models of retinal disease.[28] In light of the aforementioned studies, it seems reasonable to suggest that synthetic RBP4 ligands may also serve as important pharmacological tools in assessing the role of RBP4 in the pathogenesis of metabolic disorders such as non-alcoholic fatty liver disease (NAFLD) and non-alcoholic steatohepatitis (NASH). Here we report the characterization of a new class of non-retinoid RBP4 antagonists and their assessment in the mouse transgenic model of hepatic steatosis.

Protein Data Bank (PDB) high-resolution x-ray crystal structures providing binding poses of various ligands bound to RBP4 were studied during our structure-based drug design efforts to discover novel non-retinoid RBP4 antagonists. These structural data include RBP4 co-crystallized with **1** (PDB ***1rbp***), **1** bound to the RBP4-TTR tertiary complex (PDB ***3bsz***), RBP4 co-crystallized with the retinoid RBP4 antagonist fenretinide (**2**) (PDB ***1fel***), and RBP4 co-crystallized with the non-retinoid RBP4 antagonist A1120 (**3**) (PDB ***3fmz***).[26, 27] Initial rational design efforts derived from the aforementioned structural data provided optimized bicyclic antagonists **4** and BPN-14136 (**5**). Importantly, **5** presented exceptional *in vitro* RBP4 binding and functional antagonist activity, desirable ADME characteristics, and a favorable pharmacokinetic (PK) profile. In addition, **5** dramatically reduced circulating RBP4 levels *in vivo* with good pharmacokinetic/pharmacodynamic

correlation (PK/PD) in rodents. Furthermore, **5** significantly reduced lipofuscin bisretinoid accumulation and normalized complement system protein expression in the retinal pigment epithelium (RPE) of *Abca4*$^{-/-}$ mice, a model that recapitulates the phenotype of Stargardt disease.[28]

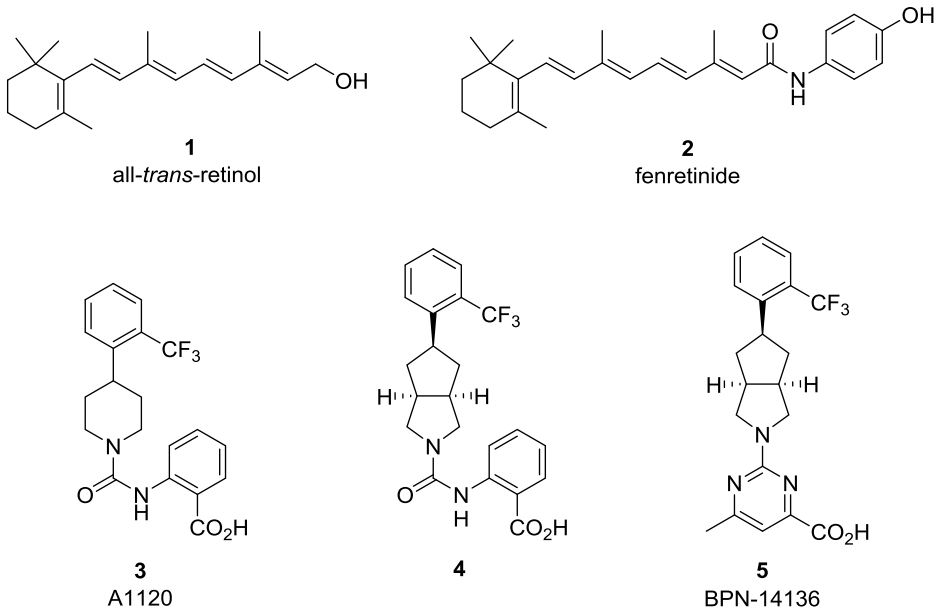

Figure 1. All-*trans*-retinol or vitamin A (**1**), the retinoid RBP4 antagonist fenretinide (**2**), the non-retinoid piperidine-based RBP4 antagonist A1120 (**3**), and the rationally designed bicyclic analogues **4** and BPN-14136 (**5**).

Buoyed by the *in vitro* and *in vivo* profiles of **5**, we sought to further build upon our findings and expand our compound portfolio by developing additional structurally diverse series of RBP4 antagonists. Our objective was to identify novel chemical matter devoid of a carboxylic acid. Carboxylic acids are present on numerous drugs and our earlier RBP4 antagonists utilized this functional group effectively. The carboxylic acid can confer numerous benefits such as reducing CNS exposure, however some carboxylic acid bearing

compounds have also been reported to present idiosyncratic drug toxicity liabilities that have been associated with acyl glucuronidation formation.[29] Thus, we sought to further expand our chemical matter portfolio by developing diverse series that could avoid potential acyl glucuronidation liabilities should they arise. Drawing from the reported *N*-benzyl imidazole RBP4 antagonist **6** (*h*RBP4 SPA IC_{50} = 0.44 ± 0.18 μM)[30] (Figure 2) and guided by our previously reported ***3fmz***-derived computational docking model,[26, 27] we implemented a structure-activity relationship (SAR) strategy involving the design and synthesis of novel compounds presenting 2- and 3-carboxamido fused [5,6]-bicyclic heteroaromatic "bottom group" appendages. Our goal was to reduce the number of rotatable bonds of **6** by fusing the pendent benzyl group phenyl ring directly to the imidazole ring via a [5,6]-bicyclic heteroaromatic framework. We hypothesized that motifs that remove these rotatable bonds but still project an aromatic ring toward the opening of the binding pocket may provide novel chemical matter with improved potency and physicochemical properties relative to **6**.

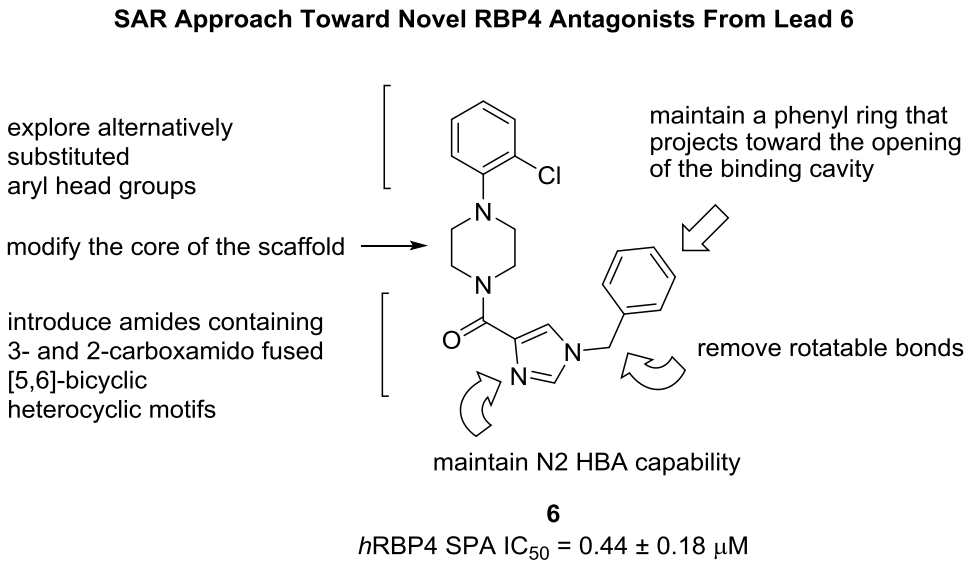

Figure 2. *N*-benzyl imidazole RBP4 antagonist **6** and the SAR strategy used to discover novel RBP4 antagonists containing 2- and 3-carboxamido fused [5,6]-bicyclic heteroaromatic appendages.

Figure 3 highlights how we initially executed our medicinal chemistry work plan. Novel analogues were synthesized with the 4-(2-(trifluoromethyl)phenyl)piperidine core scaffold of **3** and in some cases with the bicyclic core system of **4** and **5**. We began our campaign by exploring 3-carboxamides of various fused bicyclic heteroaromatic systems appended to both cores followed by subsequent syntheses of analogues bearing 2-carboxamido fused bicyclic heteroaromatic systems. Select piperidine core analogues bearing a 3-carboxamido [1,2,4]triazolo[4,3-a]pyridine-6-carbonitrile bottom group motif with alternatively fluorinated 2-trifluoromethylphenyl head groups were also later prepared.

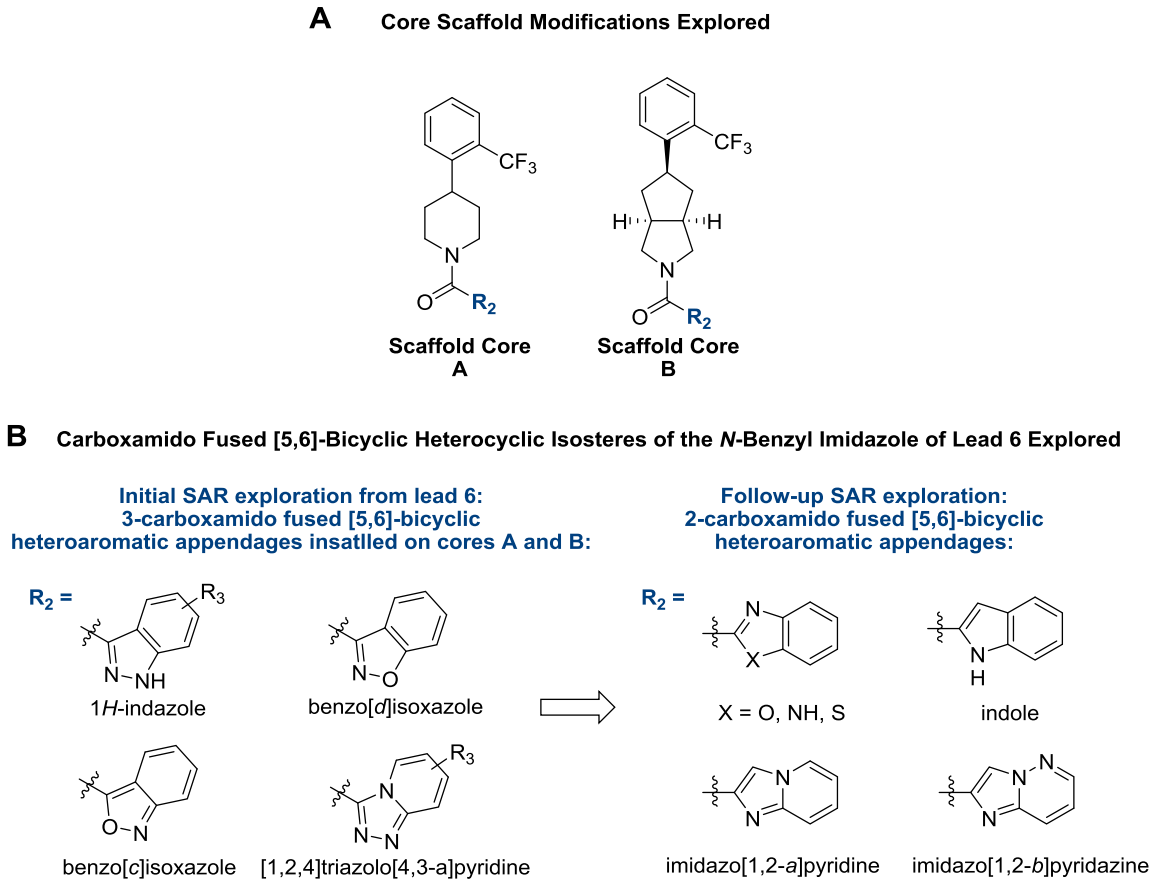

Figure 3. The structure-based drug design strategy used to discover novel RBP4 antagonists containing 3- and 2-carboxamido fused [5,6]-bicyclic heteroaromatic appendages starting from lead **6**. (A) The piperidine (**A**) and bicyclic octahydrocyclopenta[c]pyrrole (**B**) scaffold core systems used in the SAR campaign. (B) The initial 3-carboxyamido and subsequent 2-carboxyamido fused [5,6]-bicyclic heteroaromatic bottom group motifs explored.

▪ CHEMISTRY

The syntheses of compounds possessing 1*H*-indazole-3-carboxamides (**11–18**) are presented in Scheme 1.[31] Tertiary alcohol **8** is manufactured via addition of lithiated **7** to

N-benzyl-4-piperidinone. Elimination of **8** upon treatment with thionyl chloride yields tetrahydropyridine **9**, which was reduced and *N*-benzyl de-protected in one-pot via a Pd/C-catalyzed ammonium formate reduction. Treatment of the resultant piperidine freebase with HCl provided hydrochloride salt **10**, which underwent facile amide formation with various 1*H*-indazole-3-carboxylic acids to generate amide analogues **11**–**18** using HBTU as the peptide coupling agent.

Scheme 1[a]

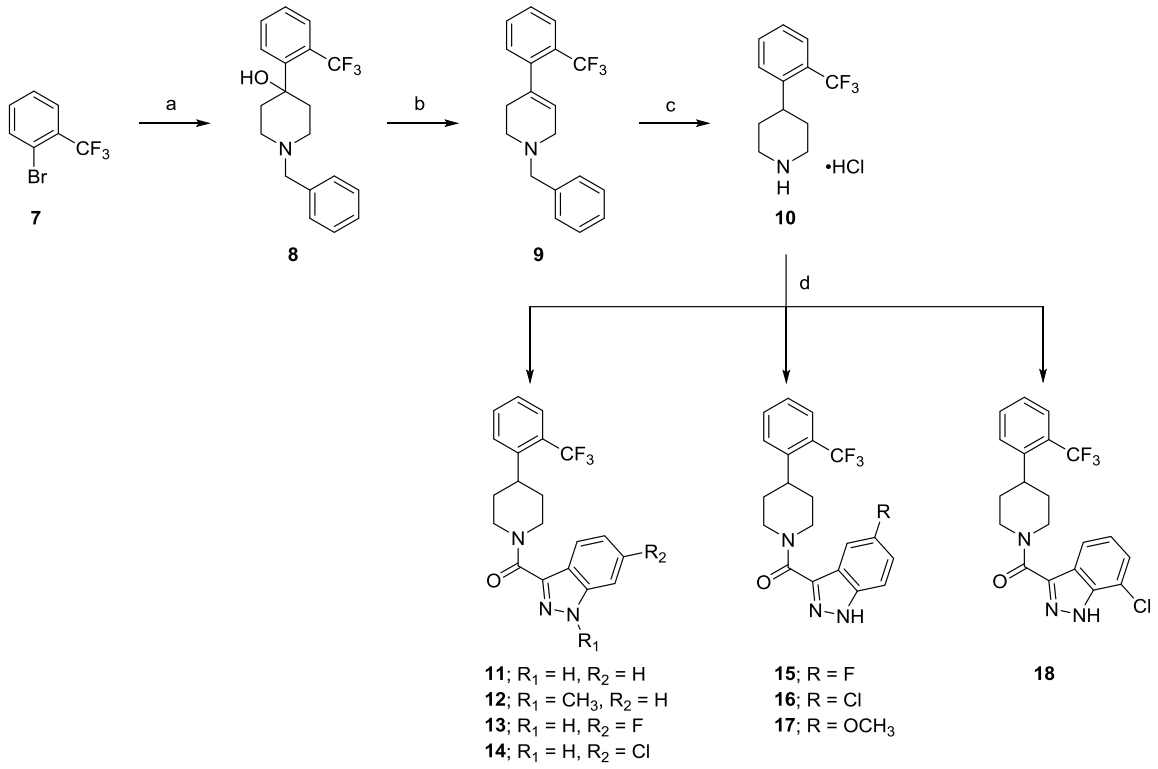

[a]Reagents and conditions: (a) (i) *n*-BuLi, THF, -78 °C, 40 min; (ii) 1-benzylpiperidin-4-one, THF, -78 °C; (b) $SOCl_2$, 0 °C, 2 h; (c) (i) HCO_2NH_4, 10% Pd/C, CH_3OH, reflux, 2 h; (ii) 4.0 M HCl solution in 1,4-dioxane, CH_3CN, rt, 2 h; (d) substituted indazole-3-carboxylic acid, HBTU, Et_3N, DMF, rt, 16 h.

The syntheses of N1-substituted-1*H*-indazole-3-carboxamides **19–21** are highlighted in Scheme 2. Alkylation of 1*H*-indazole **13** with either iodoethane or 2-iodopropane gave **19** and **20**, respectively. Formation of desired oxetane **21** was achieved via alkylation between **13** and iodooxetane.

Scheme 2[a]

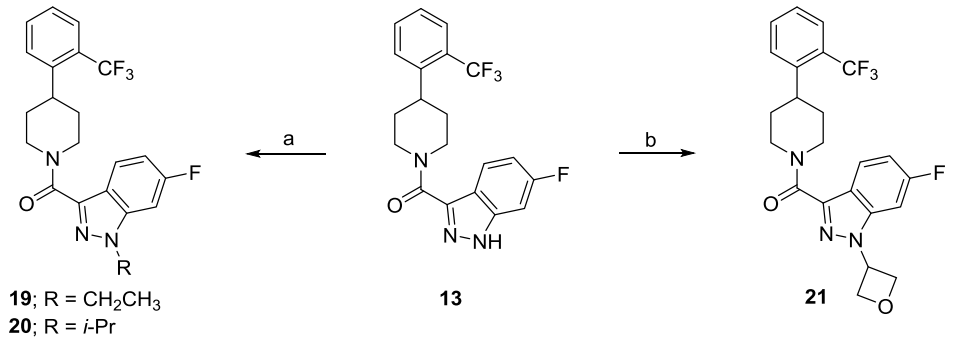

[a]Reagents and conditions: (a) iodoethane or 2-iodopropane, K_2CO_3, DMF, rt, 4h; (b) 3-iodooxetane, K_2CO_3, DMF, 60 °C, 24 h.

The syntheses of benzo[*d*]isoxazole-3-carboxamide **22** and benzo[*c*]isoxazole-3-carboxamide **23** are depicted in Scheme 3. HBTU-facilitated peptide coupling of benzo[*d*]isoxazole-3-carboxylic acid or benzo[*c*]isoxazole-3-carboxylic acid with piperidine hydrochloride **10** afforded **22** and **23**, respectively.

Scheme 3[a]

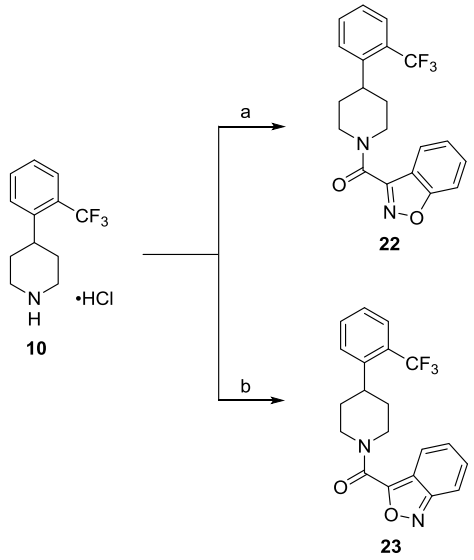

[a]Reagents and conditions: (a) benzo[*d*]isoxazole-3-carboxylic acid, HBTU, Et_3N, DMF, rt, 16 h; (b) benzo[*c*]isoxazole-3-carboxylic acid, HBTU, Et_3N, DMF, rt, 16 h.

We previously disclosed the synthesis of bicyclic intermediate **31**, which is highlighted in Scheme 4.[32] Reduction and subsequent *N*-Boc protection of dione **24** gave unsaturated isoindole **25**, which underwent oxidative cleavage to provide di-acid **26**. Dieckman condensation followed by de-carboxylation gave ketone intermediate **27**, which was converted to racemic vinyl triflate (±)-**28**. Compound (±)-**28** underwent Pd-catalyzed Suzuki cross-coupling reaction to give styrene (±)-**29**, which underwent Pd/C-catalyzed hydrogenation to provide *endo*-isomer **30** exclusively. *N*-Boc de-protection with 2.0 M HCl in Et_2O afforded hydrochloride salt **31**.

Scheme 4[a]

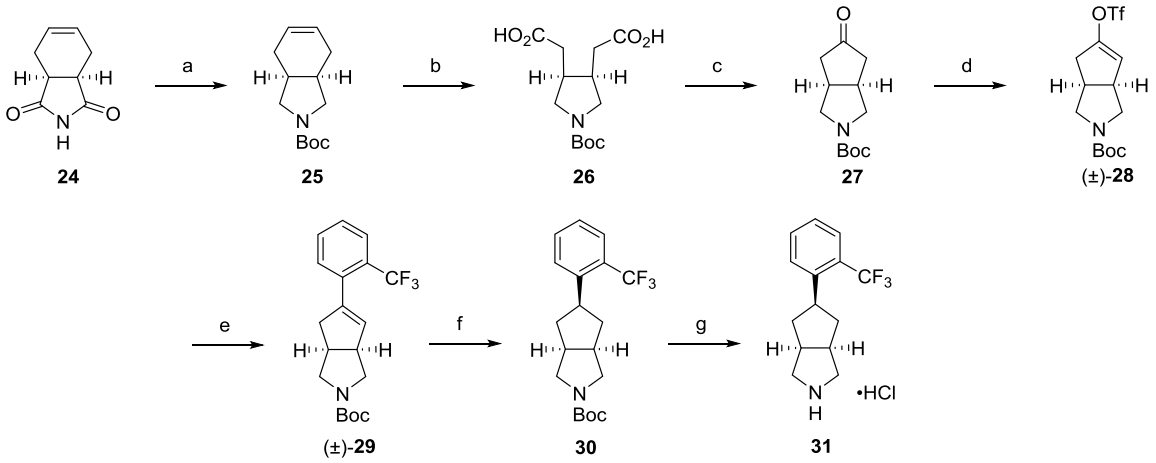

[a]Reagents and conditions: (a) (i) $LiAlH_4$ (1.0 M solution in THF), THF, 70 °C, 16 h; (ii) Boc_2O, CH_2Cl_2, rt, 16 h; (b) (i) $NaIO_4$, RuO_2•H_2O, CH_3CN, CCl_4, H_2O, rt, 24 h; (c) Ac_2O, NaOAc, 120 °C, 3 h; (d) (i) LiHMDS (1.0 M solution in THF), THF, -78 °C, 30 min; (ii), $PhN(SO_2CF_3)_2$, THF, -78 °C to rt, 3 h; (e) (2-(trifluoromethyl)phenyl)boronic acid, $Pd(PPh_3)_4$, 2.0 M Na_2CO_3, DME, 80 °C, 6 h; (f) H_2 (40 psi), 10% Pd/C, CH_3OH, rt, 16 h; (g) 2.0 M HCl in Et_2O, CH_2Cl_2, 0 °C to rt, 24 h.

[1,2,4]Triazolo[4,3-*a*]pyridine analogues **34–43** were accessed via the synthetic routes presented in Scheme 5. [1,2,4]Triazolo[4,3-*a*]pyridine-3-carboxylic acids **33a–33e** were produced in two steps via initial condensation of ethyl 2-oxoacetate with 5-substituted 2-hydrazinylpyridines **32a–32e** followed by a $PhI(OAc)_2$-mediated ring cyclization. The carboxylic acids **33a–33e** subsequently underwent amide formation with intermediates **10** and **31** to afford the desired analogues **34–43**.

Scheme 5[a]

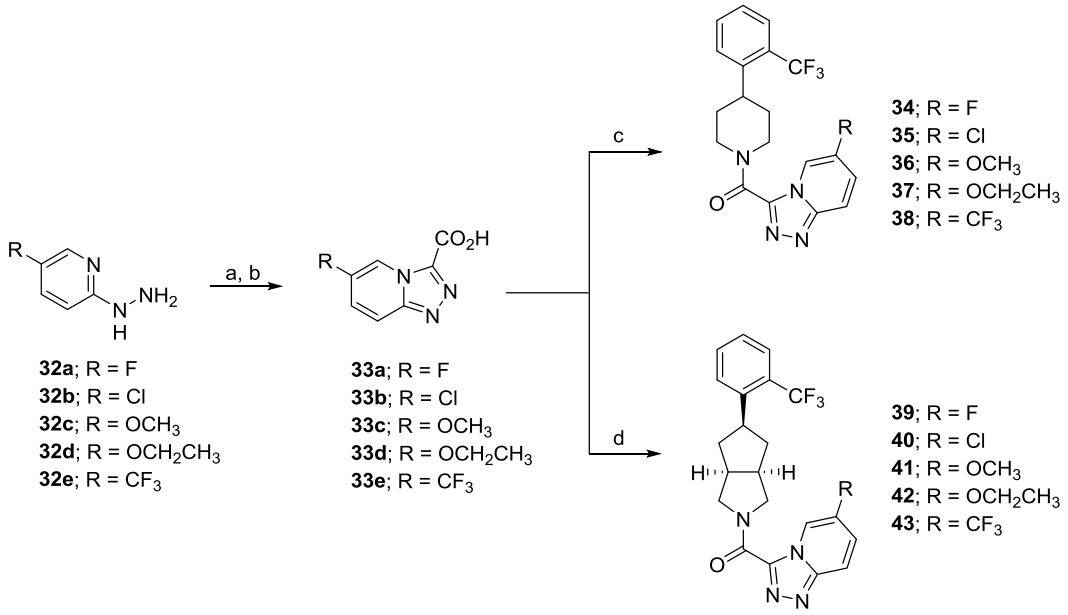

[a]Reagents and conditions: (a) (i) substituted 2-hydrazinylpyridine, ethyl 2-oxoacetate, CH_3OH, 60 °C, 1 h; (ii) $PhI(OAc)_2$, CH_2Cl_2, rt, 1 h; (b) (i) $LiOH{\bullet}H_2O$, THF, H_2O, rt, 20 min; (ii) 2.0 N aqueous HCl; (c) **10**, HBTU, *i*-Pr_2NEt, DMF, rt, 16 h; (d) **31**, HBTU, *i*-Pr_2NEt, DMF, rt, 16 h.

Acid **44** served as an access point for both piperidine and bicyclic-containing core analogues **48–53**. HBTU-mediated peptide coupling between **44** and amines **10** and **31** furnished compounds **45** and **46**, respectively. These intermediary aryl bromides were converted to the nitrile-bearing analogues **48** and **51** via Pd-catalyzed cyanation with $ZnCN_2$. Methylation of **45** to provide **49** was achieved with $Fe(acac)_3$ and CH_3MgBr. Analogue **52** was obtained via carbonylation of **46** with $Mo(CO)_6$ in CH_3OH followed by hydrolysis of the resulting methyl ester with $LiOH{\bullet}H_2O$. Urea **53** was furnished via a Pd-catalyzed amination between **46** and *N*,*N*-dimethylurea. The synthesis of sulfonamide analogue **54** began with a Pd-catalyzed carbon-sulfur cross-coupling between **46** and

benzyl thiol to furnish an intermediary benzyl mercaptan, which was then converted to the sulfonyl chloride and treated with *N*-methylamine.

Scheme 6[a]

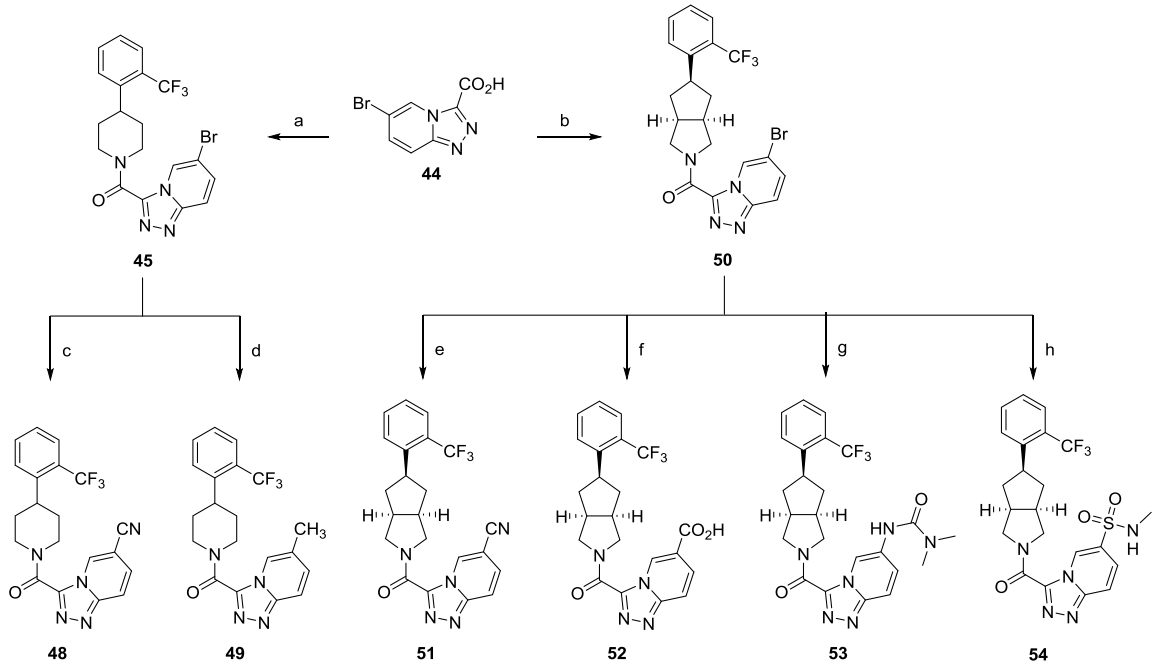

[a]Reagents and conditions: (a) **10**, HBTU, *i*-Pr_2NEt, DMF, rt, 16 h; (b) **31**, HBTU, *i*-Pr_2NEt, DMF, rt, 16 h; (c) $ZnCN_2$, $Pd(PPh_3)_4$, DMF, 130 °C (microwave irradiation), 30 min; (d) $Fe(acac)_3$, CH_3MgBr (1.4 M solution in THF/toluene) NMP, THF, rt, 1 h; (e) $ZnCN_2$, $Pd(PPh_3)_4$, DMF, 130 °C (microwave irradiation), 30 min; (f) (i) $Mo(CO)_6$, $Pd(OAc)_2$, xantphos, Cs_2CO_3, CH_3OH, 1,4-dioxane, 80 °C, 2 h; (iii) LiOH•H_2O, THF, H_2O, rt, 30 min; (iv) 2 N aqueous HCl; (g) *N*,*N*-dimethylurea, $Pd(OAc)_2$, xantphos, Cs_2CO_3, 1,4-dioxane, 100 °C, 6 h; (h) (i) benzyl thiol, *i*-Pr_2NEt, $Pd(OAc)_2$, xantphos, 1,4-dioxane, 110 °C, 16 h; (ii) NCS, HOAC, H_2O, rt, 3 h; (iii) *N*-methylamine, *i*-Pr_2NEt, CH_2Cl_2, rt, 2 h.

A subset of analogues presenting alternatively fluorinated 2-trifluoromethyl phenyl groups were designed to further explore the hydrophobic β-ionone binding pocket of

RBP4 (**59**, **62**, **63**, **65**) (Schemes 7 and 8). The preparation of fluorinated analogue **59** is depicted in Scheme 7. Conversion of **55** to vinyl triflate **56** was followed by Pd-catalyzed Suzuki cross-coupling to furnish tetrahydropyridine **57**. Hydrogenation of **57** followed by *N*-Boc de-protection with 2.0 M HCl in Et_2O provided piperidine hydrochloride salt **58**. HBTU-mediated peptide coupling between **58** and carboxylic acid **44** followed by Pd-catalyzed cyanation with $Zn(CN)_2$ afforded desired analogue **59**.

Scheme 7[a]

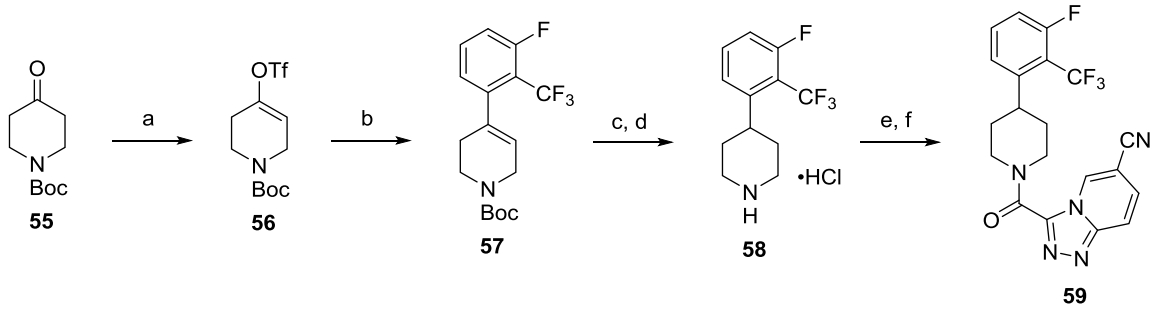

[a]Reagents and conditions: (a) (i) LiHMDS (1.0 M solution in THF), THF, -78 °C, 1 h; (ii), $PhN(SO_2CF_3)_2$, THF, -78 °C to 0 °C, 3 h; (b) (3-fluoro-2-(trifluoromethyl)phenyl)boronic acid, $Pd(PPh_3)_4$, 2.0 M aqueous K_2CO_3, DME, 80 °C, 6 h; (c) 10% Pd/C, H_2 (30 psi), EtOH, rt, 18 h; (d) 2.0 M HCl in Et_2O, CH_2Cl_2, rt, 18 h; (e) **44**, HBTU, *i*-Pr_2NEt, DMF, rt, 16 h; (e) $Zn(CN)_2$, $Pd(PPh_3)_4$, DMF, 130 °C (microwave irradiation), 30 min.

The preparation of fluorinated analogues **61**, **62** and **64** is shown in Scheme 8. Suzuki cross-coupling between vinyl triflate **56** and (5-fluoro-2-(trifluoromethyl)phenyl)boronic acid or (4-fluoro-2-(trifluoromethyl)phenyl)boronic acid followed by *N*-Boc de-protection gave intermediary tetrahydropyridines **60a** and **60b**, respectively. PtO_2-mediated

hydrogenation of these tetrahydropyridines gave corresponding piperidine intermediates that readily underwent amide formation with **44**. Cyanation of these amides using the aformentioned Pd-catalyzed conditions with $Zn(CN)_2$ yielded **61** and **62**, respectively. The synthesis of fluorinated aryl head group analogue **64** followed a route previously described for the preparation of compound **59** with the exception that tetrahydropyridine hydrogenation to give piperidine intermediate **63** was conducted with PtO_2 under 1 atm instead of 10% Pd/C at 30 psi of H_2. *N*-Boc de-protection of **63** followed by peptide coupling with **44** and subsequent Pd-catalyzed cyanation led to desired compound **64**.

Scheme 8[a]

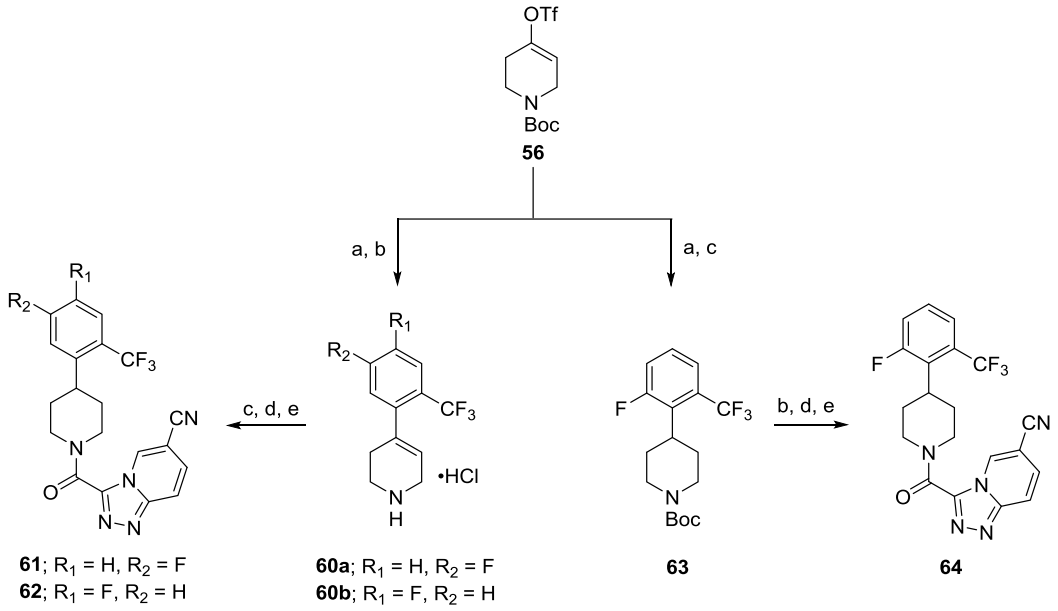

[a]Reagents and conditions: (a) (i) substituted aryl boronic acid, $Pd(PPh_3)_4$, 2.0 M aqueous K_2CO_3, DME, 80 °C, 6 h; (b) 2.0 M HCl in Et_2O, CH_2Cl_2, rt, 18 h; (c) (i) PtO_2, H_2 (1 atm), HOAc, EtOAc, rt, 72 h; (ii) 2.0 M HCl in Et_2O, CH_2Cl_2, rt, 18 h; (d) **44**, HBTU, Et_3N, *i*-Pr_2NEt, rt, 16 h; (e) $ZnCN_2$, $Pd(PPh_3)_4$, DMF, 130 °C (microwave irradiation), 30 min.

The syntheses of various 2-carboxamido fused [5,6]-bicyclic heteroaromatic analogues (**65**–**72**) are highlighted in Scheme 9. These analogues were prepared peptide coupling between the respective heteroaromatic 2-carboxylic acid and **10** in the presence of HBTU.

Scheme 9[a]

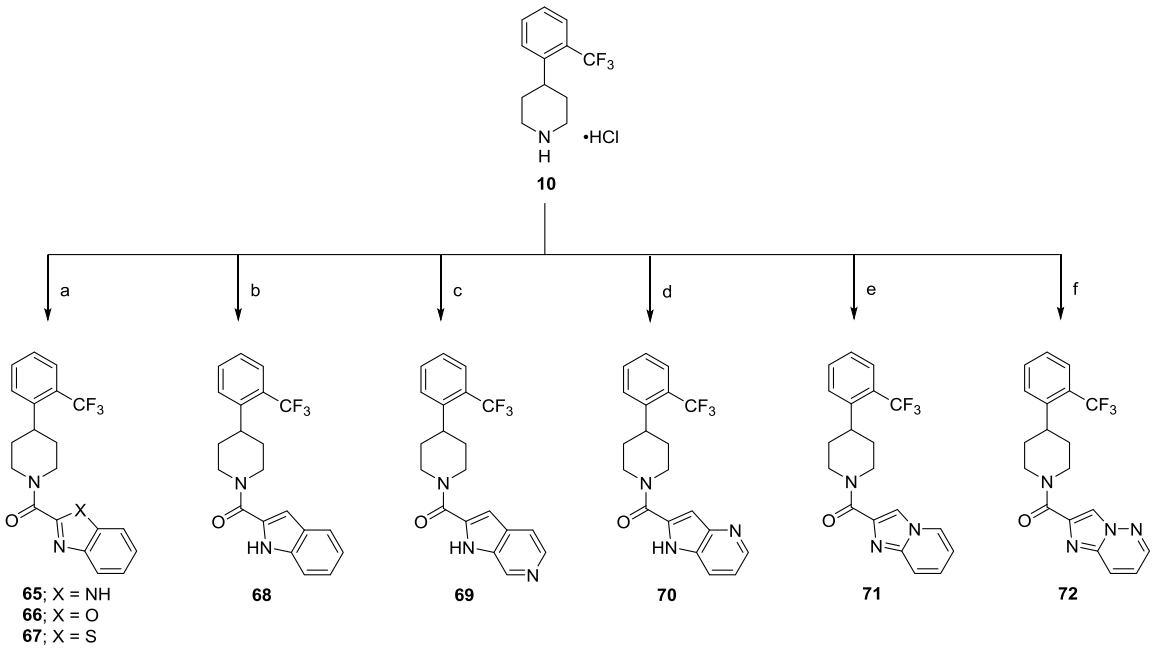

[a]Reagents and conditions: (a) 1*H*-benzo[*d*]imidazole-2-carboxylic acid, benzo[*d*]oxazole-2-carboxylic acid or benzo[*d*]thiazole-2-carboxylic acid, HBTU, *i*-Pr_2NEt, DMF, rt, 16 h; (b) **10**, 1*H*-indole-2-carboxylic acid, HBTU, *i*-Pr_2NEt, DMF, rt, 16 h; (c) 1*H*-pyrrolo[2,3-*c*]pyridine-2-carboxylic acid, HBTU, *i*-Pr_2NEt, DMF, rt, 16 h; (d) 1*H*-pyrrolo[3,2-*b*]pyridine-2-carboxylic acid, HBTU, *i*-Pr_2NEt, DMF, rt, 16 h; (e) imidazo[1,2-*a*]pyridine-2-carboxylic acid, HBTU, *i*-Pr_2NEt, DMF, rt, 16 h; (f) imidazo[1,2-*b*]pyridazine-2-carboxylic acid, HBTU, *i*-Pr_2NEt, DMF, rt, 16 h.

The syntheses of a series of follow-up 6-substituted imidazo[1,2-*b*]pyridazine-2-carboxamide analogues (**74**–**78**) were generated from key intermediate **73** as depicted in Scheme 10. Methylation of **73** to give **74** was achieved via a Pd(dppf) cross-coupling with trimethylboroxine. Nucleophilic aromatic substitution of **73** with $NaOCH_3$ provided methoxy analogue **75**. The installation of the cyclopropyl ring of **76** was achieved via a of $Pd(OAc)_2$ cross-coupling reaction with **73** and potassium cyclopropyltrifluoroborate in the presence di-(1-admantyl)-*n*-butylphosphine, and Cs_2CO_3. Lastly, heating **73** in neat pyrrolidine or morpholine yielded the desired nucleophilic aromatic substitution products **77** and **78**, respectively.

Scheme 10[a]

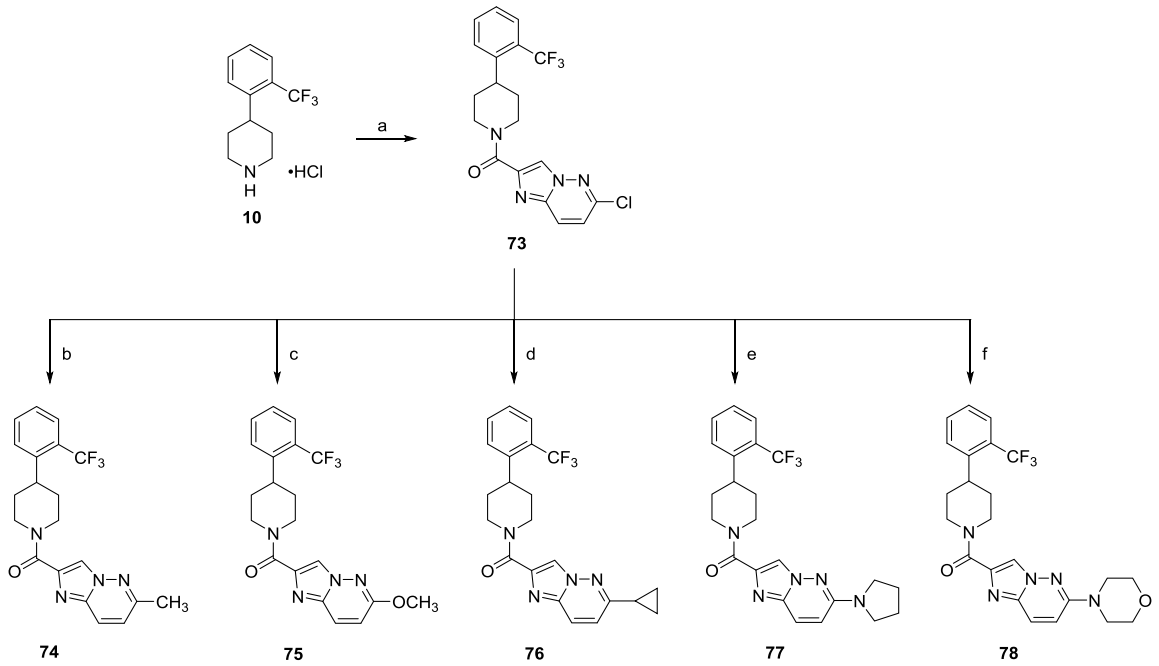

[a]Reagents and conditions: (a) 6-chloroimidazo[1,2-b]pyridazine-2-carboxylic acid, HBTU, *i*-Pr_2NEt, DMF, rt, 16 h; (b) trimethylboroxine, Pd(dppf), K_2CO_3, 1,4-dioxane, H_2O, 110 °C, 5 h; (c) $NaOCH_3$,

CH_3OH, 70 °C, 1 h; (d) potassium cyclopropyltrifluoroborate, $Pd(OAc)_2$, di-(1-admantyl)-*n*-butylphosphine, Cs_2CO_3, toluene, H_2O, 100 °C, 3 h; (e) pyrrolidine (neat), 100 °C, 3 h; (f) morpholine (neat), 120 °C, 2 h.

▪ RESULTS AND DISCUSSION

The reported PDB high-resolution x-ray crystal structures ***3fmz*** (co-crystal structure of **3** bound to RBP4)[30, 33] and ***4psq*** (co-crystal structure of **6** bound to RBP4)[30] provided critical data that was used in support of our structure-based drug design efforts toward novel fused [5,6]-bicyclic heteroaromatic amide-containing analogues (Figure 4). The structural data show **3** and **6** binding within the internal binding cavity of RBP4 with similar geometric alignment. The core piperidine ring of **3** and piperazine ring of **6** both reside in the relatively narrow β-barrel channel of the binding cavity and their respective 2-trifluoromethyl substituted aryl head group projecting into the vacuous and hydrophobic β-ionone pocket where van der Waals contacts are made (Figure 4). The urea of **3** and the carboxamide of **6** both accept an H-bond from backbone amide Leu37. A salt bridge forms between the carboxylic acid of **3** and Arg121 toward the opening of the binding pocket (Figure 4, A). Furthermore, two key H-bonds are also established between the acid of **3**, Tyr90, and Gln98 while the phenyl ring of **3** also engages in an edge-to-face π-π binding interaction with Phe96. In contrast, the N2 imidazole nitrogen of **6** engages in an H-bond with the Arg121 ηNH_2 group while the *N*-benzyl appendage projects toward the opening of the binding cavity (Figure 4, B). The key H-bond binding interactions with Leu37 and Arg121 described for **3** and **6** are hypothesized to play a crucial role in the induction and

stabilization of conformational changes within RBP4 loops β3-β4 and β5-β6 that prohibit complexation between RBP4 and TTR and afford antagonist functional activity.[14, 21, 22, 30]

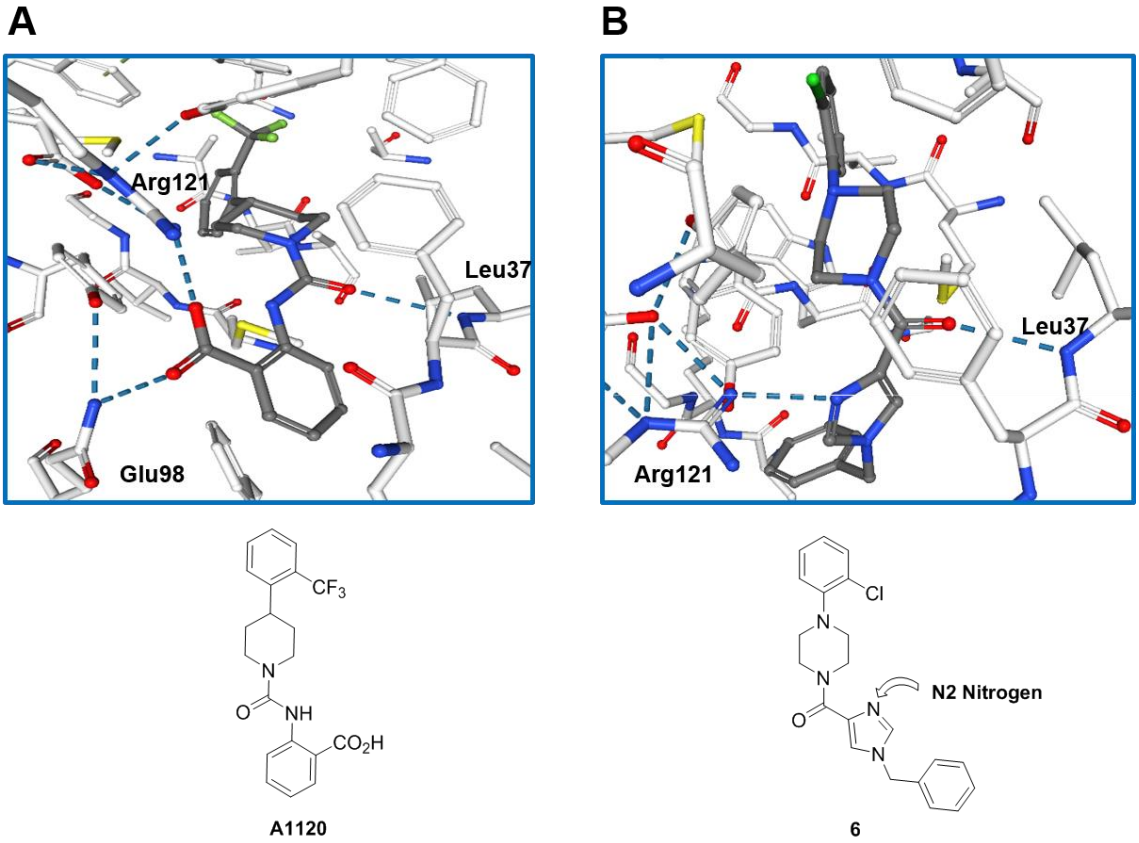

Figure 4. (A) Binding conformation of anthranilic acid antagonist **3** and key H-bond interactions with RBP4 as depicted within ***3fmz***. The image is in stick model format. Carbon atoms are shown as grey for the ligand and white for the protein, oxygen atoms are red, nitrogen atoms are blue, chlorine atoms are green, and sulfur atoms are yellow. H-bonds are indicated as blue dotted lines and the residues undergoing H-bond interactions with **3** are labeled. The urea carbonyl of **3** engages in an H-bond interaction with backbone Leu37 while Arg121 forms a salt bridge and Glu98 H-bonds with the carboxylic acid. In addition, the anthranilic acid phenyl ring of **3** and Phe96 are engaged in an edge-to-face π-π binding interaction (not shown). Lastly, the distal 2-

trifluoromethyl substituted aromatic head group of **3** resides with the hydrophobic and vacuous β-ionone pocket and is positioned nearly orthogonal to the core piperidine ring. The image is of PDB ID ***3fmz*** was obtained from the RCSB Protein Data Bank (PDB) (www.rcsb.org). (B) Bioactive conformation and binding interactions of *N*-benzyl imidazole antagonist **6** with RBP4 as depicted within ***4psq***. The amide carbonyl of **6** engages in an H-bond interaction with Leu37 and the imidazole N2 nitrogen H-bonds with the ηNH_2 group of the Arg121 side chain. The distal 2-Cl substituted aromatic head group of **3** also resides with the hydrophobic β-ionone pocket in a nearly orthogonal position. The image is of PDB ID ***4psq*** was obtained from the RCSB Protein Data Bank (PDB) (www.rcsb.org).

As previously reported, ***3fmz*** data was employed to construct a computational docking model (version 5.8, Schrödinger, LLC.), which was used to triage novel analogue proposals prior to synthesis by identifying compounds that were predicted to have good docking orientations within the RBP4 binding cavity. The docking and analysis of novel analogues in our ***3fmz*** data model of RBP4 was performed as previously described.[26, 27]

Drawing from the *N*-benzyl imidazole motif of **6**, we hypothesized that analogues presenting carboxamides of fused [5,6]-bicyclic heteroaromatic systems could also serve to position key H-bond accepting groups within close proximity to Arg121 and Leu37. Furthermore, such motifs remove the rotatable bonds of the *N*-benzyl appendage of **6** but still project and aromatic ring toward the opening of the binding pocket, which may provide analogues with improved potency and physicochemical properties. Indeed, our initial ***3fmz*** docking experiment with 3-carboxamido-1*H*-indazole **11** predicted that the N2 nitrogen of the 1*H*-indazole ring H-bonds with Arg121 while the carboxamide carbonyl

oxygen would serve as an H-bond acceptor with Leu37 (Figure 5). Encouraged by the docking result for **11**, we synthesized a sample set of 1*H*-indazole- (**11**–**21**) and benzisoxazole- (**22** and **23**) containing analogues.

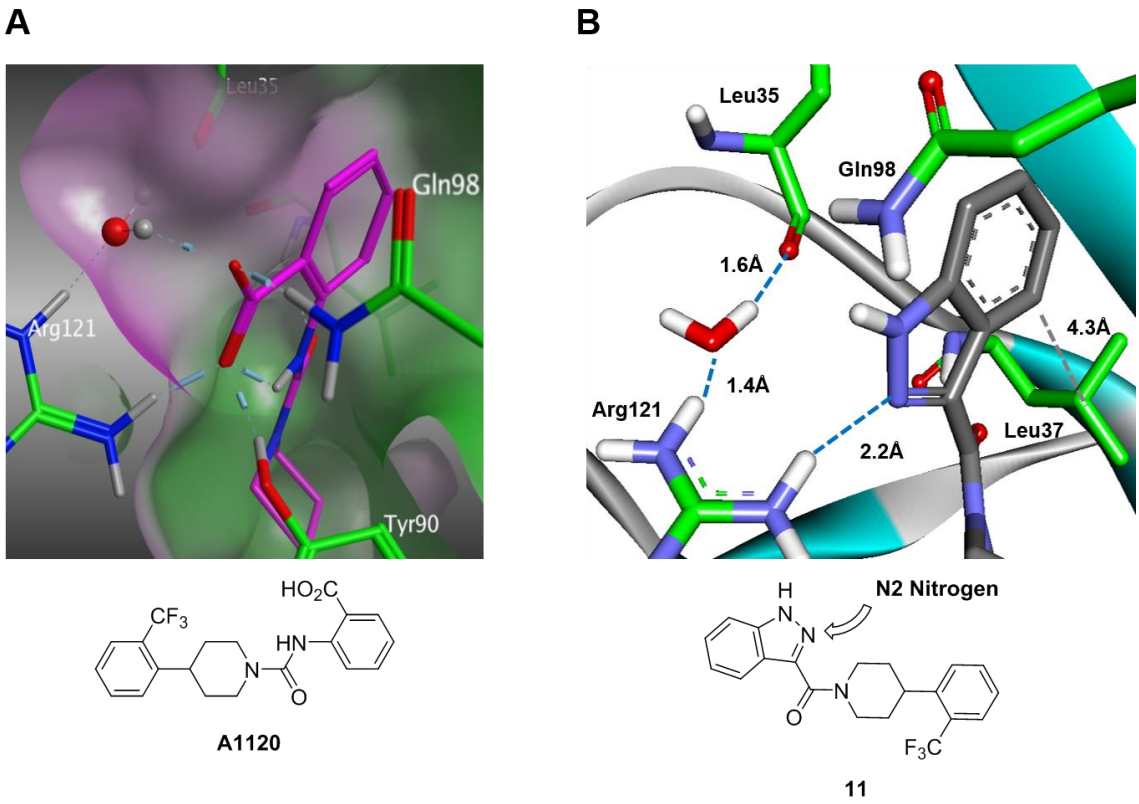

Figure 5. Comparison of the putative key binding interactions between anthranilic acid **3** and 3-carboxamido 1*H*-indazole **11** with RBP4. (A) Expanded view of the minimized bound conformation of **3**. H-bonds with Gln98 and Tyr90 and a salt bridge with Arg121 are shown (blue lines). An additional H-bond between the urea carbonyl oxygen of **11** with the backbone amide Leu37 is also present but out of view in this depiction. Hydrophobic molecular surfaces are shown as green and hydrophilic surfaces as purple. Contact preferences generated by MOE (Chemical Computing Group, Inc., Montreal, CA). (B) Expanded view of the 1*H*-indazole fragment of **11**. The 1*H*-indazole N2 nitrogen atom accepts an H-bond from Arg121. An additional H-bond between the amide

carbonyl oxygen of **11** with the backbone amide Leu37 is also present but out of view in this depiction. Furthermore, a potential van der Waals interaction may be occurring between the 1*H*-indazole ring and the isobutyl group of Leu37. The carbon atoms of **11** are grey and the carbon atoms of the resident RBP4 amino acid residues are green. Nitrogen atoms are shown as blue and oxygen atoms are shown as red. Grey lines indicate van der Waals contacts.

***In Vitro* Binding of Compounds to RBP4.** Binding affinities for RBP4 were measured using our scintillation proximity assay (SPA) as previously reported.[26-28, 34] Binding experiments were performed on white 96-well plates in a final assay volume of 100 µl/well. The reaction mixture contained 10 nM ^{3}H-Retinol (48.7Ci/mmol; PerkinElmer), 0.3 mg/well Streptavidin-PVT beads, 50 nM of RBP4 labeled with biotin. The SPA buffer contained 1X PBS, pH=7.4, 1 mM EDTA, 0.1% BSA, and 0.5% CHAPS. Nonspecific binding was measured in the presence of 20 µM of cold (unlabeled) retinol. Using these assay conditions, saturation binding of retinol to RBP4 afforded a K_d of 62.5 nM, which is in line with the previously reported 70–190 nM range of values. For compound characterization, competitive displacement of ^{3}H-retinol was measured. The concentration of ^{3}H-retinol was 10 nM, which corresponds to the generally recommended concentration of radioligand (1/10 of the K_d). The IC_{50} values were calculated from 8-point compound titrations using four-parameter nonlinear regression in GraphPad Prism (Version 8). Compounds with appreciable RBP4 binding potency (generally, with IC_{50} <150 nM) were further assessed for their ability to inhibit the retinol-dependent RBP4-TTR interaction using a homogenous time resolved fluorescence (HTRF) assay. [26-28, 34]

Antagonism of RBP4-TTR Interaction HTRF Assay. The ability of the compounds to disrupt the retinol-induced interaction of RBP4 with TTR was examined using our HTRF assay as described previously.[26-28, 34] Bacterially expressed Maltose Binding Protein (MBP)-tagged RBP4 and Eu^{3+}-cryptate-labeled commercially available human TTR were used along with a d2-conjugated anti-MBP monoclonal antibody. Retinol at 1 µM concentration stimulates the formation of the RBP4-TTR complex, which brings europium in close proximity to the d2 dye, resulting in the fluorescence energy transfer (FRET) to d2. The FRET emission signal (668 nm) was normalized using the europium emission (620 nm) to compensate for the pipetting and dispensing errors. Following a 12-point dose titration (30 µM–0.1 nM), the IC_{50} values were calculated using four-parameter nonlinear regression in GraphPad Prism (Version 8). To monitor the correlation between RBP4 binding affinity of the compounds and their potency as antagonists of the retinol-dependent RBP4-TTR interaction, the ratio of their IC_{50} values in the HTRF and SPA assays was tracked. For most compounds, a ratio in the 5–20 range was observed, despite the differences in their binding affinities.

Analogue SAR. 1*H*-indazole-3-carboxamide analogues containing substituents at the 5-, 6-, and 7-position of the 1*H*-indazole ring (**11**, **13–18**) and on the N1 nitrogen atom (**12**, **19–21**) were initially prepared from piperidine hydrochloride **10**. *In vitro* RBP4 potency, kinetic aqueous solubility, and liver microsomal metabolic stability for these compounds are shown in Table 1. The majority of these analogues exhibited excellent *in vitro* potency in the RBP4 SPA and HTRF assays. 1*H*-Indazole **11** presented an approximate 2-fold improvement in RBP4 SPA binding affinity relative to benchmark **3** and a nearly 3-

fold improvement in HTRF functional antagonist activity. Substitution with either F or Cl at the 5-, 6- or 7-position of the 1*H*-indazole ring (**13–16**, **18**) provided analogues of comparable potency to parent **11**. However, installation of an OCH_3 group at the 5-position (**17**) significantly diminished RBP4 SPA and HTRF potency. It is unclear whether the increased steric bulk, polarity, or the electron-donating capability of the OCH_3 group (or any combination thereof) contributed to the loss of potency observed for **17** relative to **13–16** and **18**.

The N1 1*H*-indazole nitrogen also provided a handle with which to install various groups that could further probe the RBP4 binding cavity. Methylation to give **12** neither improved nor diminished *in vitro* RBP4 potency relative to parent **11**, whereas increasing the bulk of the N1 substituent from methyl to ethyl (**19**) and isopropyl (**20**) significantly reduced potency. Interestingly, installation of the N1 oxetane appendage (**21**) restored potency comparable to **12**. Lastly, isosteric benzisoxazoles **22** and **23** were also found to be of comparable potency to **11**. The favorable *in vitro* RBP4 potencies observed for this initial sample set confirmed that fused [5,6]-bicyclic systems may be viable replacements for the carboxylic of **3** and **5** and the *N*-benzyl imidazole of **6**. However, enthusiasm for this series was tempered as the compounds generally exhibited very poor kinetic aqueous solubility or poor microsomal metabolic stability (or both), which was likely attributable in part to their relatively high lipophilicity and sub-optimal lipophilic ligand efficiency (LLE) (RBP4 SPA pIC_{50} - cLogP).[35]

Table 1. RBP4 Binding Affinity, Functional RBP4-TTR Antagonism, Kinetic Aqueous Solubility, and Liver Microsomal Metabolic Stability Data for 3-Carboxamido Indazole and Benzisoxazole RBP4 Antagonists.

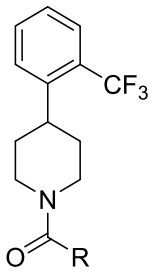

Compound Number	R	RBP4 SPA[a] IC_{50} (nM)	RBP4 HTRF[a] IC_{50} (nM)	Kinetic Solubility[b] (μM)	Microsomal Stability (% remaining)			cLogP	LLE
					HLM[c]	RLM[d]	MLM[e]		
3	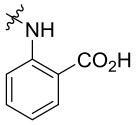	15.0 ± 0.005	122± 0.035	ND	3.0	85	ND	4.85	2.97
11	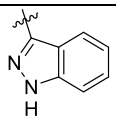	6.42	46	7.4	7.5	0.0	0.6	4.21	3.98
12	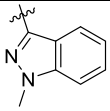	3.71	56.1	3.6	0.7	0.0	0.2	3.87	4.56
13	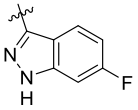	4.71	49.0	3	68	0.2	8.7	4.41	3.91
14	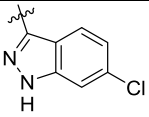	7.53	67.1	< 1.6	100	0.1	100	4.98	3.14
15	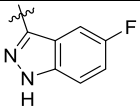	4.71	48.3	1.9	36	0.5	6.8	4.41	3.91

16	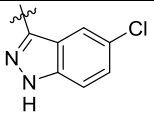	6.99	58.6	< 1.6	100	0.8	51	4.98	3.17
17	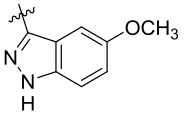	44.6	843	ND	ND	ND	ND	4.34	3.01
18	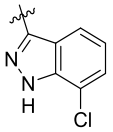	5.47	82.5	2.5	78	0.2	34	4.98	3.28
19	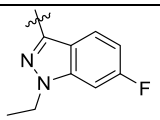	9.54	242	2.1	1.3	0.3	1.2	4.55	3.47
20	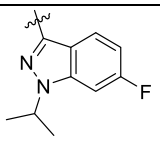	128	ND	ND	ND	ND	ND	4.86	2.03
21		4.12	35.6	4.7	0.1	10	4.3	3.57	4.81
22	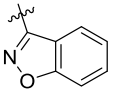	6.28	79.5	8.4	0.4	0.0	0.0	3.97	4.23
23	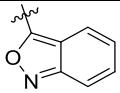	8.26	98.8	6.2	1.5	0.0	0.0	3.97	4.11

[a]For compounds tested more than twice, IC_{50} is represented as the mean ± standard deviation. Otherwise, IC_{50} is shown as the mean of two independent experiments. [b]Kinetic aqueous solubility measured in PBS, pH 7.4. Verapamil and tamoxifen were used as controls. [c]HLM = human liver microsomes. [d]RLM = rat liver microsomes. [e]MLM = mouse liver microsomes. Compound concentration was 10 μM and incubation time with either human, rat or mouse microsomes was

30 minutes. Testosterone was used as a positive control. cLogP derived from ChemDraw Professional (ChemOffice Professional, CambridgeSoft and Perkin Elmer). LLE = lipophilic ligand efficiency: RBP4 SPA pIC_{50} – cLogP. ND = not determined.

We next explored less lipophilic [1,2,4]triazolo[4,3-*a*]pyridine-3-carboxamides with the piperidine core of **10** (**34**–**38**, **48**, **49**) and the bicyclic core of **31** (**39**–**43**, **50**–**53**). Data for these compounds are highlighted in Table 2. We were encouraged to find that the [1,2,4]triazolo[4,3-*a*]pyridine motif afforded antagonists with excellent *in vitro* potency. Importantly, a direct comparison of the fluorinated 1*H*-indazole **15** with its less lipophilic congener **34** revealed that the latter exhibits comparable SPA potency, improved HTRF potency, and improved LLE (**15** LLE = 4.41; **34** LLE = 5.45). Indeed, the [1,2,4]triazolo[4,3-*a*]pyridine series as a whole demonstrated a general improvement in LLE trends relative to the previous 1*H*-indazole series, which also correlated with improved solubility and metabolic stability for compounds within this sample set, as exemplified by nitrile **48** (LLE = 6.08).

Table 2. RBP4 Binding Affinity, Functional RBP4-TTR Antagonism, Kinetic Aqueous Solubility, and Liver Microsomal Metabolic Stability Data For [1,2,4]Triazolo[4,3-*a*]pyridine RBP4 Antagonists.

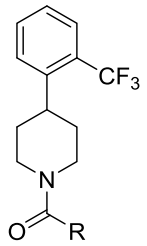

Scaffold Core A

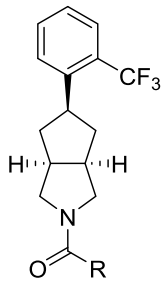

Scaffold Core B

Compound Number/ Scaffold Core	R	RBP4 SPA[a] IC_{50} (nM)	RBP4 HTRF[a] IC_{50} (nM)	Kinetic Solubility[b] (μM)	Microsomal Stability (% remaining)			cLogP	LLE
					HLM[c]	RLM[d]	MLM[e]		
34/A	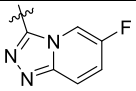	4.55	22.5	8	80	4.9	2.4	2.89	5.45
35/A	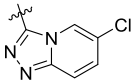	4.01	25.2	11	81	22	44	3.46	4.93
36/A	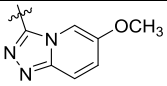	3.70	12.8	25	74	31	32	3.17	5.26
37/A	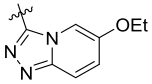	3.97	20.6	2.5	77	31	2.5	3.70	4.70
38/A	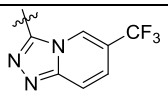	3.75	28.3	1.9	85	92	98	3.64	4.78

39/B	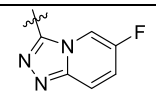	4.1	67.5	9.3	53	1.6	44	3.21	5.17
40/B	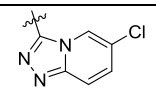	4.5	49.3	< 1.6	61	2.3	3	3.78	4.56
41/B	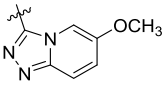	6.0	61.7	4.5	47	7.8	7.2	3.48	4.74
42/B	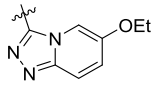	2.7	71.4	< 1.6	57	39	8.2	4.01	4.55
43/B	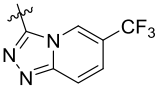	3.4	10.6	< 1.6	76	69	61	3.95	4.51
48/A	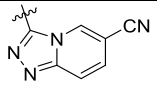	5.14	60.9	44	99	82	100	2.20	6.08
49/A	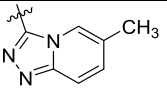	3.9	16.6	28.6	100	57	27	3.25	5.15
51/B	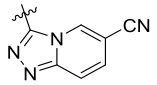	6.0	90.3	< 1.6	27	31	45	2.51	5.71
52/B	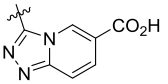	32.8	895	84	81	83	72	3.16	4.32
53/B	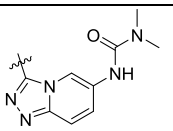	14.6	240.6	17	19	19	4.2	2.85	4.98
54/B	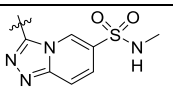	10.0	211.5	< 1.6	25	61	40	2.80	5.20

[a]For compounds tested more than twice, IC_{50} is represented as the mean ± standard deviation. Otherwise, IC_{50} is shown as the mean of two independent experiments. [b]Kinetic aqueous solubility

measured in PBS, pH 7.4. Verapamil and tamoxifen were used as controls. [c]HLM = human liver microsomes. [d]RLM = rat liver microsomes. [e]MLM = mouse liver microsomes. Compound concentration was 10 μM and incubation time with either human, rat or mouse microsomes was 30 minutes. Testosterone was used as a positive control. cLogP derived from ChemDraw Professional (ChemOffice Professional, CambridgeSoft and Perkin Elmer). LLE = lipophilic ligand efficiency: RBP4 SPA pIC_{50} – cLogP. ND = not determined.

Exploration of aryl head group SAR for standout analogue **48** was conducted with a focused set of fluorinated 2-trifluoromethyl phenyl bearing analogues (**59**, **61**, **62**, **64**) (Table 3). All of the compounds of this sample set presented *in vitro* RBP4 SPA potency comparable to des-fluoro parent **48**. However, with the exception of **64**, the fluorinated analogues exhibited an approximate 3-fold improvement in HTRF potency. Furthermore, fluorination *ortho* or *meta* to the 2-trifluoromethyl group did not diminish kinetic solubility relative to **48**, while *para* fluorination led to a precipitous drop in solubility. Lastly, unlike **61**, **62**, and **64**, analogue **59** maintained a favorable microsomal metabolic stability profile across multiple species and it quickly emerged as a lead.

Table 3. RBP4 Binding Affinity, Functional RBP4-TTR Antagonism, Kinetic Aqueous Solubility, and Liver Microsomal Stability Data for [1,2,4]Triazolo[4,3-*a*]pyridine RBP4 Antagonists with Fluorinated Aryl Head Groups.

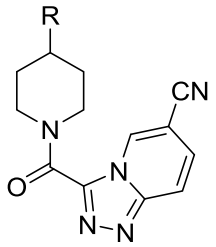

Compound Number	R	RBP4 SPA[a] IC_{50} (nM)	RBP4 HTRF[a] IC_{50} (nM)	Kinetic Solubility[b] (μM)	Microsomal Stability (% remaining)			cLogP	LLE
					HLM[c]	RLM[d]	MLM[e]		
59	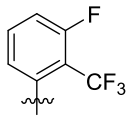	5.73	16.05	33	100	60	87	2.34	5.90
61	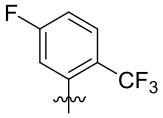	4.88	23.21	7.5	78	8.9	59	2.34	5.97
62	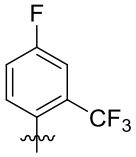	9.06	19.77	31	ND	ND	ND	2.34	5.70
64	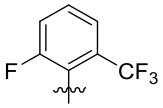	5.84	92.02	28	ND	ND	ND	2.34	5.89

[a]For compounds tested more than twice, IC_{50} is represented as the mean ± standard deviation. Otherwise, IC_{50} is shown as the mean of two independent experiments. [b]Kinetic aqueous solubility measured in PBS, pH 7.4. Verapamil and tamoxifen were used as controls. [c]HLM = human liver microsomes. [d]RLM = rat liver microsomes. [e]MLM = mouse liver microsomes. Compound concentration was 10 μM and incubation time with either human, rat or mouse microsomes was 30 minutes. Testosterone was used as a positive control. cLogP derived from ChemDraw Professional (ChemOffice Professional, CambridgeSoft and Perkin Elmer). ND = not determined.

Docking of **48** and **59** into our ***3fmz*** computational model showed both compounds extending their respective aryl head groups into the hydrophobic β-ionone cavity where they orient themselves into a nearly orthogonal position relative to their corresponding piperidine rings (Figure 6). The carboxamides for both compounds serve as H-bond acceptors for Leu37 and their respective [1,2,4]triazolo[4,3-*a*]pyridine N2 nitrogen atoms are engaged in H-bond interactions with Arg121. We postulate that the 3-fold improvement in RBP4 HTRF potency observed for fluorinated **59** relative to **48** may be due in part to additional van der Waals contacts within hydrophobic β-ionone cavity, which may serve to better secure the compound within the binding pocket and allow for more stabilized H-bond interactions with Leu37 and Arg121.

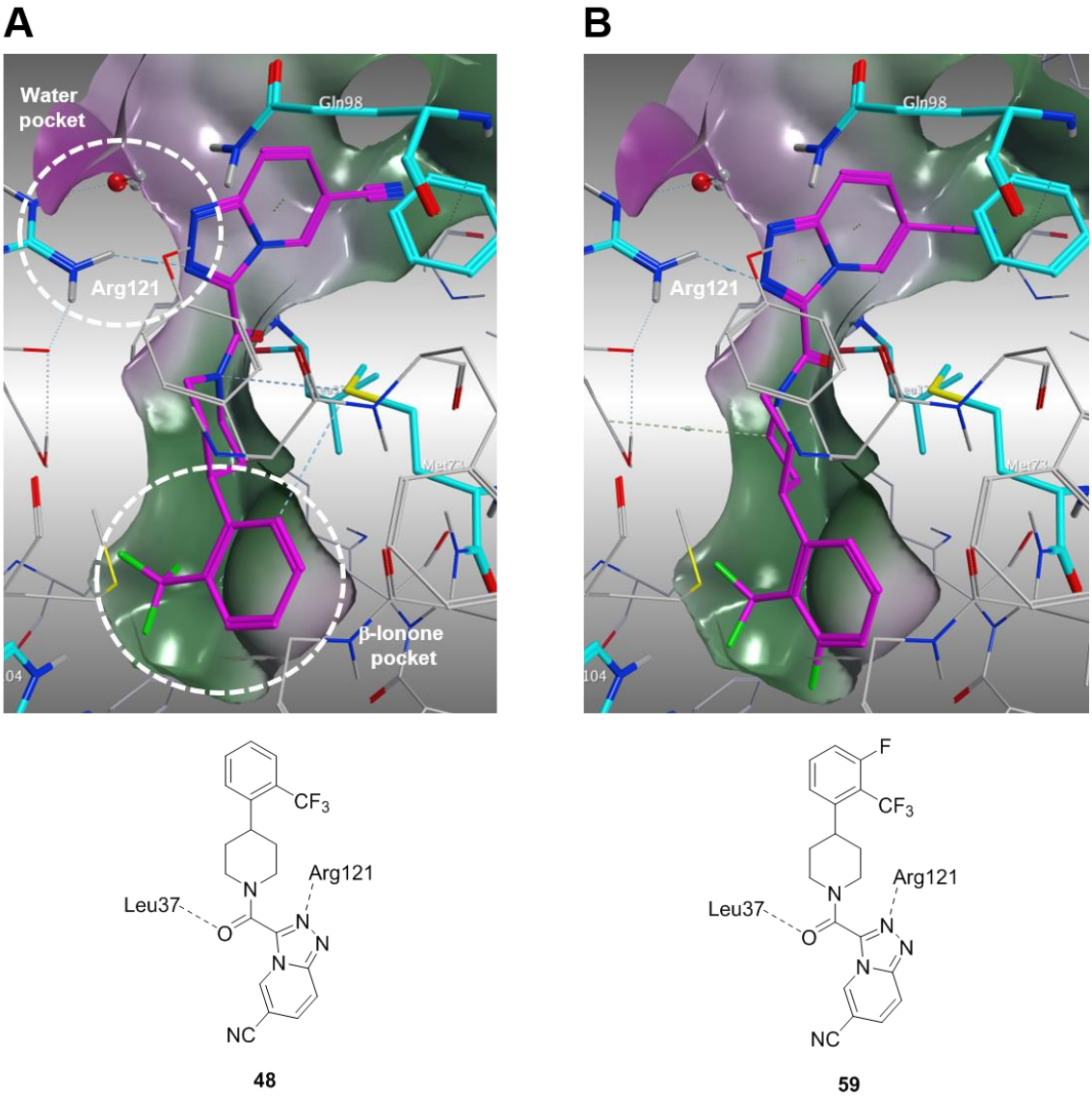

Figure 6. (A) Minimized bound conformation of RBP4 [1,2,4]triazolo[4,3-*a*]pyridine antagonist **48** within ***3fmz***. (B) Minimized bound conformation of RBP4 fluorinated antagonist **59** within ***3fmz***. H-bond interactions between the [1,2,4]triazolo[4,3-*a*]pyridine N2 nitrogen atom and Arg121 near the opening of the RBP4 binding cavity are highlighted. An H-bond between the carbonyl oxygen of **48** and **59** with the backbone amide Leu37 is also present but out of view in this depiction. The aryl head groups of both compounds are shown residing within the hydrophobic β-ionone pocket located deep within the RBP4 binding cavity.

We next explored the effects of repositioning heteroaryl amide connectivity by preparing compounds featuring a 2-carboxamido fused [5,6]-bicyclic heteroaromatic moiety (**65**–**72**) (Table 4). The RBP4 SPA potencies of benzimidazole **65**, benzoxazole **66,** and benzothiazole **67** were all within 2-fold of **48** and **59**; however, all three compounds exhibited significantly diminished potency in the HTRF assay. Benzoxazole **66** also exhibited low solubility and poor microsomal metabolic stability. Indole analogue **68** presented RBP4 binding affinity that was within 3-fold of **48** and **59**, but its HTRF potency was diminished by nearly two orders of magnitude. Interestingly, the specific placement of an additional nitrogen atom within the indole ring to give *aza*-indoles **69** and **70** had a dramatic effect on HTRF potency. Placement of a nitrogen atom at the 6-position of the indole ring to give aza-indole **69** resulted in a 5-fold loss in RBP4 binding affinity and a 2-fold loss in HTRF potency compared to parent indole **68**. However, placement of a nitrogen at the 4-position to give the aza-indole congener **70** restored binding affinity while significantly improving HTRF potency relative to **68**. Our docking model suggests that the position of the indole ring nitrogen of **70** brings it within closer proximity to Gln98 and a putative structural water in the binding site relative to the nitrogen of **69**, resulting in more stable H-bonds (Figure 7). However, despite the intriguing activity of **70**, the compound exhibited very poor kinetic solubility and metabolically stability. Lastly, we also explored analogues incorporating a 2-carboxamido imidazo[1,2-*a*]pyridine- (**71**) and imidazo[1,2-*b*]pyridazine (**72**) moiety. Both compounds exhibited comparable RBP4 SPA binding affinity, however **71** was 10-fold more potent than **72** in the HTRF assay. Despite

the poor metabolic stability observed for **72**, we were encouraged by its excellent RBP4 potency and proceeded to explore a small sample set of follow-up analogues.

Table 4. RBP4 Binding Affinity, Functional RBP4-TTR Antagonism, Kinetic Aqueous Solubility, and Liver Microsomal Stability Data for 2-Carboxamido RBP4 Antagonists of Diverse Fused [5,6]-Bicyclic Heteroaromatic Systems.

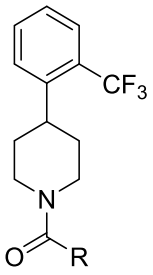

Compound Number	R	RBP4 SPA[a] IC_{50} (nM)	RBP4 HTRF[a] IC_{50} (nM)	Kinetic Solubility[b] (μM)	Microsomal Stability (% remaining)		
					HLM[c]	RLM[d]	MLM[e]
65	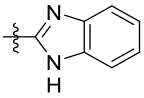	6.82	343	ND	ND	ND	ND
66	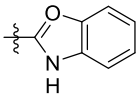	8.5	157	2.9	0.4	0.0	0.0
67	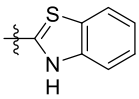	9.61	472	ND	ND	ND	ND
68	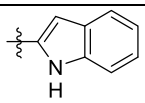	15.9	1780	ND	ND	ND	ND
69	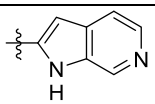	84.2	3720	ND	ND	ND	ND

70	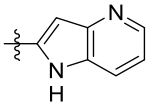	29.8	141	< 1.6	49	1.0	6.7
71	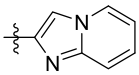	9.71	211	51	9.0	0.0	0.0
72	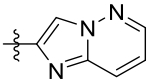	4.98	27.9	83	3.7	0.5	0.3

[a]For compounds tested more than twice, IC_{50} is represented as the mean ± standard deviation. Otherwise, IC_{50} is shown as the mean of two independent experiments. [b]Kinetic aqueous solubility measured in PBS, pH 7.4. Verapamil and tamoxifen were used as controls. [c]HLM = human liver microsomes. [d]RLM = rat liver microsomes. [e]MLM = mouse liver microsomes. Compound concentration was 10 μM and incubation time with either human, rat or mouse microsomes was 30 minutes. Testosterone was used as a positive control. ND = not determined.

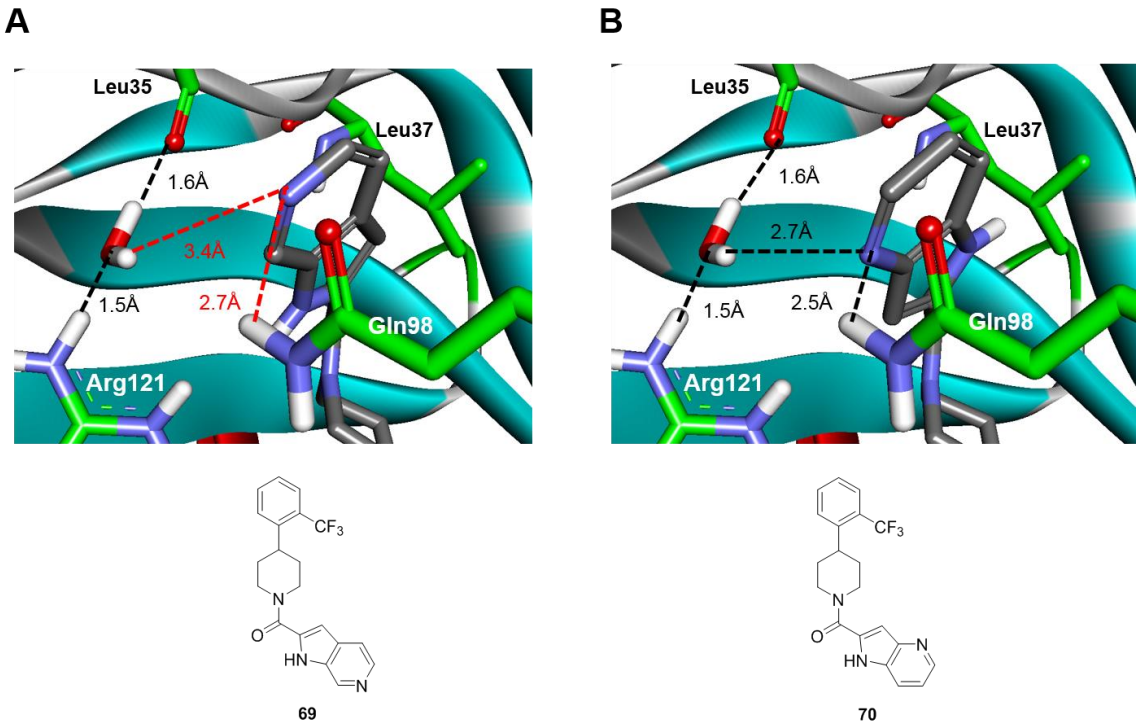

Figure 7. (A) Minimized bound conformation of RBP4 aza-indole antagonist **69** within ***3fmz***. (B) Minimized bound conformation of RBP4 aza-indole antagonist **70** within ***3fmz***. The 6-position of the indole ring of **69** resulted in a 5-fold loss in RBP4 binding affinity and a 2-fold loss in HTRF potency compared to parent indole **68**. However, positioning a nitrogen at the 4-position to give **70** restored binding affinity while significantly improving HTRF potency relative to **68**. Our docking model suggests that the position of the 1*H*-pyrrolo[3,2-*b*]pyridine nitrogen of **70** brings it within closer proximity to Gln98 and a putative structural water in the binding site relative to the indole ring nitrogen of **68**, resulting in more stable H-bonds. H-bond interactions are indicated with red and black lines.

Table 5 highlights additional imidazo[1,2-*b*]pyridazine-2-carboxamide analogues prepared (**74–78**). All five compounds presented robust RBP4 potency in the SPA binding assay and analogues **74** and **75** also displayed exceptional potency in the HTRF assay.

Within this series, morpholine **78** presented a favorable balance of RBP4 potency, solubility, and metabolic stability.

Table 5. RBP4 Binding Affinity, Functional RBP4-TTR Antagonism, Kinetic Aqueous Solubility, and Liver Microsomal Stability Data for Imidazo[1,2-*b*]pyridazine-2-carboxamide Analogues.

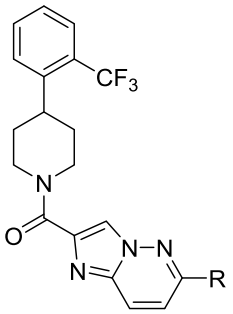

Compound Number	R	RBP4 SPA[a] IC_{50} (nM)	RBP4 HTRF[a] IC_{50} (nM)	Kinetic Solubility[b] (μM)	Microsomal Stability (% remaining)		
					HLM[c]	RLM[d]	MLM[e]
74		2.66	32.6	72	67	12	0.2
75		6.36	36.8	47	99	47	1.0
76		3.6	103	14	73	51	0.4
77		10.8	134	5.6	45	2.1	4.9
78	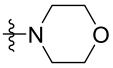	6.74	112	47	65	53	44

[a]For compounds tested more than twice, IC_{50} is represented as the mean ± standard deviation. Otherwise, IC_{50} is shown as the mean of two independent experiments. [b]Kinetic aqueous solubility measured in PBS, pH 7.4. Verapamil and tamoxifen were used as controls. [c]HLM = human liver microsomes. [d]RLM = rat liver microsomes. [e]MLM = mouse liver microsomes. Compound concentration was 10 μM and incubation time with either human, rat, or mouse microsomes was 30 minutes. Testosterone was used as a positive control. ND = not determined.

Encouraged by the excellent RBP4 potency, suitable kinetic solubility and good microsomal stability, previously described **48** and **59**were further studied in a battery of preclinical ADME studies. Their *in vitro* pharmacological profiles are shown in Table 6. Both **48** and **59** presented low microsomal CL_{int} for human, dog, and cynomolgus monkey liver microsomes with moderate CL_{int} for rat. Both compounds did not exhibit appreciable potency in a standard cytochrome P450 (CYP) inhibition panel (all CYP inhibition IC_{50} > 4.7 μM) and their corresponding percent plasma protein binding (%PPB) values are in an optimal range and indicate relatively low fraction unbound.

Table 6. *In Vitro* Metabolic Stability, CYP Inhibition, and %PPB Profiles for 48 and 59.

No.	Microsomal CL_{int} (μL/min/mg)[a]				CYP Inhibition (μM IC_{50})				%PPB[b]			tPSA[c,d]	cLogP[d]
	H	R	D	cyno	2C9	2C19	2D6	3A4	H	R	M		
48	5.9	31	4.9	9.4	4.7	30	>100	50	96.9	97.9	95.1	72.06	2.20
59	5.9	29	7.7	8.6	11	22	>100	74	97.0	98.7	98.5	72.06	2.34

[a]Intrinsic clearance (CL_{int}) in the presence of microsomes; H = human; R = rat; D = dog; cyno = cynomolgus monkey. [b]%PPB = percent plasma protein binding. H = human; R = rat; M = mouse. [c]tPSA = topological surface area. [d]tPSA and cLogP derived from ChemDraw Professional (ChemOffice Professional, CambridgeSoft and Perkin Elmer).

Compounds **48** and **59** were devoid of ancillary activity at the hERG channel or CYP-induction liabilities in the PXR activation assay (Table 7). Both compounds showed no signs of genotoxicity and mutagenicity in the Ames study. In a CEREP screening panel comprising fifty-five GPCRs, enzymes, ion channels, and transporters, **48** exhibited weak activity at the kappa opioid receptor (KOR) with an EC_{50} = 4 μM. Conversely, compound **59** did not display any off-target pharmacology at KOR or at any other target within the screening panel. Lastly, both compounds were highly permeable in the MDR1-MDCK assay.

Additional *in vitro* CYP experiments revealed that **48** and **59** demonstrate moderate time-dependent inhibition (TDI) at CYP2D6. IC_{50} determinations with or without a pre-

incubation step preceding the co-incubation of test compound, a CYP-selective substrate, and human liver microsomes (HLM) were conducted in parallel for each compound. Two pre-incubation arms of the assay were conducted; 1) one arm involves test compound incubated with HLM in the absence of NADPH ((-) NADPH), and 2) a second arm involves test compound incubated with HLM in the presence of NADPH ((+)NADPH) (Table 7). A 16- and 20-fold leftward shift was observed in the (+)NADPH IC_{50} curve relative to the (-)NADPH IC_{50} curve for compounds **48** and **59**, respectively. The inactivation parameters K_I, k_{inact}, and k_{inact}/K_I were next determined for both compounds in order to better characterize their inhibitory potential at CYP2D6.[36] The values of k_{inact} and K_I were determined by incubating different concentrations of the test compounds with human liver microsomes in the presence of NADPH over a specific time-course and these values are captured in Table 7. The k_{inact} values for both compounds were low and the K_I values were orders of magnitude higher than the respective RBP4 SPA and HTRF IC_{50} values for each compound. Taken collectively, the k_{inact}/K_I data suggest that both compounds are TDI-negative and do not pose a risk as a perpetrator of CYP2D6-mediated drug-drug interactions (DDI).

Table 7. *In Vitro* ADMET Profiles for 48 and 59 Continued.

No.	hERG[a] (IC_{50})	PXR Activation[b]	Selectivity Panel Screen[c] (10 μM)	Full Ames[d]	MDCK-MDR1 Permeability P_{app} (× 10^{-6} cm/s)			Time-Dependent CYP2D6 Inhibition IC_{50} Shift	CYP2D6 K_I/K_{inact}		
					A-B	B-A	ER		K_{inact} (1/min)	K_I (μM)	K_I/K_{inact} (mL/min/μmol)
48	>30 μM	No Induction	KOR, 79% Inhibition; EC_{50} = 4 μM	Negative	42.9	39.9	0.9	(-) NADPH; IC_{50} = 54 μM (+) NADPH; IC_{50} = 3.4 μM IC_{50} Shift = 16-fold	0.0597	3.13	19.4
59	>30 μM	No Induction	No Limiting Off-Target Pharmacology	Negative	53.4	40.5	0.8	(-) NADPH; IC_{50} = 61 μM (+) NADPH; IC_{50} = 2.9 μM IC_{50} Shift = 21-fold	0.0278	0.72	40.5

[a]hERG activity was assessed using a Patch-Xpress patch-clamp assay with HEK293 cells stably expressing the channel; compounds were tested in a five-point concentration-response to generate IC_{50} values (n = 3). [b]PXR = pregnane X receptor; the assay measures a dose-response increase of PXR activity in the presence of compound relative to DMSO controls in DPX2 cells. [c]Compounds **48** and **59** were independently screened at a 10 μM concentration against a standard Cerep selectivity panel of 50 diverse receptors, enzymes, ion channels, and transporters. [d]Strains of *salmonella typhimurium* tested in the full Ames studies: TA97, TA98, TA100, TA102, TA1535, TA1537 and TA1538.

***In Vivo* Activity: PK Characteristics of 48 and 59 in Rodents.** Both **48** and **59** possessed favorable PK profiles in naïve male CD-1 mice and adult Sprague-Dawley male rats (Table

8). The compounds exhibited moderate to low clearance and good half-lives ($t_{1/2}$) in both species. Adequate exposures (AUC_{last}) and good oral bioavailability (%F) were also achieved. The good oral bioavailability, moderate half-lives, and decent exposures achieved in mice coupled with favorable ADME profiles fully justified the use of **48** and **59** to establish PK/PD and ultimately proof-of-concept murine animal models.

Table 8. *In Vivo* PK Data for Analogues 48 and 59 Following IV and PO Administration in Rodents.

No.	Species	CL[a] (mL/h/kg)	C_{max}[b] (ng/mL)	T_{max}[c] (h)	$T_{1/2}$[d] (h)	V_{ss}[e] (mL/Kg)	AUC_{last}[f] (hr•ng/mL)	%F[g]
48	Mouse[h]	163.5	1590	2.00	4.7	1123	16402	53.7
	Rat[h]	755 ± 49	410 ± 165	1.00 ± 0.0	6.0 ± 0.5	2203 ± 479	2815 ± 908	42.6 ± 13.7
59	Mouse[h]	350	517	4	6.2	2954	8721	61.6
	Rat[h]	1134	175	1.5	10.53	4281	1771	42.0

Dosing groups consisted of three drug naïve male CD-1 mice or adult male Sprague-Dawley rats. Data represented as mean ± SD. [a]Total body clearance. [b]Maximum observed concentration of compound in plasma. [c]Time of maximum observed concentration of compound in plasma after oral administration. [d]Apparent half-life of the terminal phase of elimination of compound from plasma. [e]Volume of distribution at steady state. [f]Area under the plasma concentration versus time curve from 0 to the last time point compound was quantifiable in plasma. [g]Bioavailability; F = (AUC_{INFpo} × $Dose_{iv}$) ÷ AUC_{INFiv} × $Dose_{po}$). [h]IV formulation = 3% DMA/45% PEG300/12%

ethanol/40% sterile water; IV dosing volume = 2 mL/kg; PO formulation = 2% Tween 80 in 0.9% saline; PO dosing volume = 5 mL/kg. Dosing regimen for **48** in mouse and rat: 2.0 mg/kg i.v., 5 mg/kg p.o. Dosing regimen for **59** in mouse: 2.0 mg/kg i.v., 5 mg/kg p.o. Dosing regimen for **59** in rat: 1.0 mg/kg i.v., 2.0 mg/kg i.v., 5 mg/kg p.o.

***In Vivo* Activity: PK/PD Correlations of Compound 59 in Mouse.** Before testing **59** in the murine transgenic model of hepatic steatosis, we conducted acute dosing studies with **59** in mouse to measure the compound's effect on circulating plasma RBP4 levels and to establish PK/PD correlations (Figure 8). After a single oral dose of **59** (5 mg/kg), 85% maximal reduction in plasma RBP4 was observed (Figure 8, A), while plasma RBP4 was decreased by 81% following a 2 mg/kg intravenous dose (Figure 8, B). *In vivo* serum RBP4 lowering after both oral and intravenous dosing of **59** (Figure 8, A and B) showed a good correlation with the compound concentration in plasma (Figure 8, C and D). The long exposure and moderate to low clearance of **59** achieved after a single oral dose (Table 1) correlated well with the extent of the RBP4 reduction (85% reduction at the 12 h time point) and the duration of the RBP4 lowering effect (71% reduction at the 24 h time point). Furthermore, the magnitude of RBP4 lowering correlated very well with the projected free drug concentration of **59** in the plasma, which exceeded that required for disrupting the RBP4-TTR interaction measured in the *in vitro* HTRF assay. This data confirms in vivo target engagement for **59** and reveals an excellent PK/PD relationship between compound exposure and biological response in mice, additionally justifying characterization of **59** in the mouse transgenic model of hepatic steatosis.

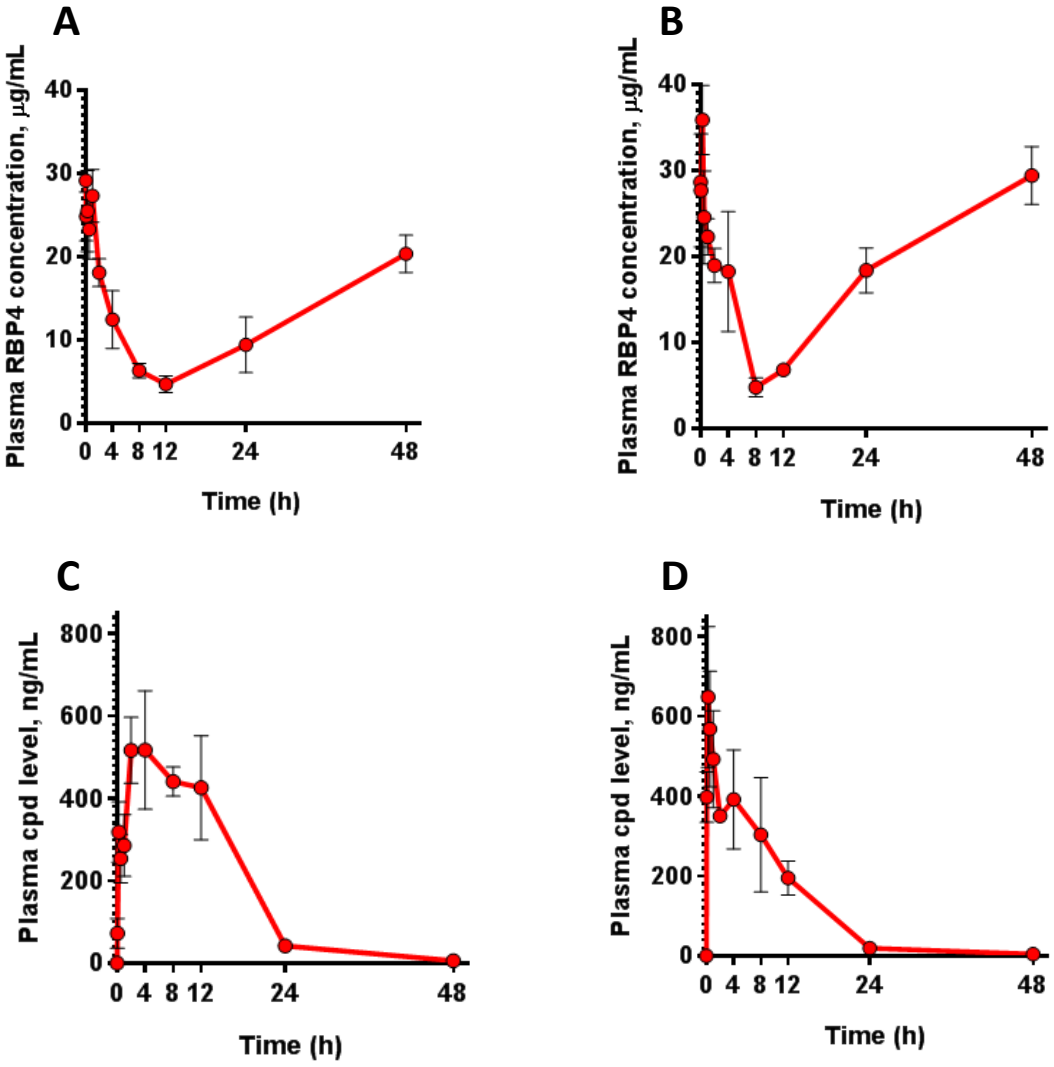

Figure 8. **PK/PD properties of 59 in mice**. (A, B) Plasma RBP4 levels in CD-1 mice following a single 5 mg/kg oral (A) and a single 2 mg/kg intravenous (B) administration of **59**. (C, D) Plasma compound levels following administration of a single oral 5 mg/kg dose (C) and a 2 mg/kg intravenous dose (D) of **59**. Data represented as the mean ± SD. For each time point of blood collection, three mice were used in the study.

Analogue 59 Reduces Circulating Levels of Adipose-Derived RBP4 in the Mouse Transgenic Model of Hepatic Steatosis. As was reported previously by Blaner and coworkers,[22] the mouse genetic model of hepatic steatosis was generated by targeting the human RBP4 (hRBP) cDNA construct with a *loxP-neo*^{r}-stop cassette to the mouse Rosa26 locus. To specifically express hRBP4 in mouse adipocytes, knock-in mice were bred with *adiponectin-Cre* mice.[22] Specific expression of human RBP4 in mouse adipocytes yielded no significant elevation in the circulating levels of RBP4 and no changes in retinoid levels in plasma, liver and adipose tissue while inducing obesity, impaired glucose tolerance, and pronounced increase in hepatic triglyceride levels.[22] To examine the effect of **59** on metabolic parameters in male adi-hRBP4 mice, we administered the compound as a formulated into the HFD chow at a dose of 20 mg/kg/day for 29 days. Compound administration started at 20 weeks of age when the animals were switched from a standard chow to a high-fat diet (60% of calories from fat). Chronic oral administration of **59** induced a 90% decrease in circulating levels of both mouse and human (adipose tissue-secreted) serum RBP4 (Figure 9). In un-treated adi-hRBP4 mice, circulating levels of adipose-derived human RBP4 (2-3 μg/ml) represented a small 3-5% fraction of mouse-specific serum RBP4 produced predominantly in the liver (Figure 9). Remarkably, this modest increase in circulating levels of RBP4 conferred by adipocyte secretion was sufficient to trigger the induction of the strong metabolic phenotype.

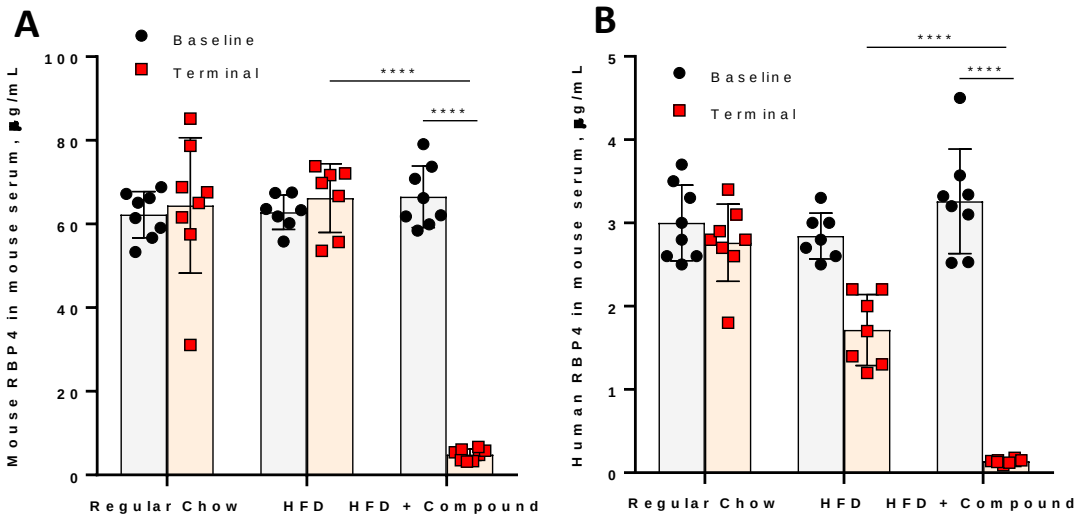

Figure 9. **Effect of oral administration of compound 59 on circulating levels of serum RBP4 in adi-hRBP4 mice.** Serum levels of mouse (A) and human (B) RBP4 were measured at baseline (black circles) and at the end of the 29-day compound treatment (red squares) with species-specific rodent or human ELISA tests as described in Supporting Information. Compared to baseline, statistically significant 90% reduction was seen for both human and mouse RBP4 at the study end in the **59**-treated mice (Two-way ANOVA with Holm-Sidak *post-hoc* test , ****P < 0.0001). A significant reduction in human and mouse RBP4 concentrations was detected in **59**-treated adi-hRBP4 mice in comparison to vehicle-treated knockout controls (Two-way ANOVA with Holm-Sidak *post-hoc* test, P < 0.0001). Error bars show SD; graph bars show mean. Each data point on the graph represents a serum RBP4 concentration from an individual animal. The number of male adi-hRBP4 mice per treatment group were 8 for normal chow, 7 for HFD and 8 for HFD with **59.**

Analogue 59 Reduces Body Weight Gain in Obese adi-hRBP4 mice. Over the 29-day study period, the adi-hRBP4 mice on high-fat diet gained significantly more weight than transgenic animals kept on a standard chow (Figure 10, A). A statistically significant

difference between the chow-fed and HFD adi-hRBP mice in percent weight gain was evident 5 days after initiation of the high-fat feeding (Figure 10, A). Body weight gain in HFD animals was significantly reduced by administration of analogue **59.** A statistically significant difference in body weight gains between **59**-treated and untreated HFD mice was evident after 19 days of high fat diet feeding (Figure 10, A). At the end of the 29-day treatment period, the mean body weight gain in the **59**-treated animals (2.2 ± 1.7 g) was 53% less than in the untreated animals on HFD (4.7 ± 1.6 g). Reduction in the body weight gain in **59**-treated adi-RBP4 mice was not associated with decreased food intake as **59** did not alter consumption of the HFD chow (Figure 10, B).

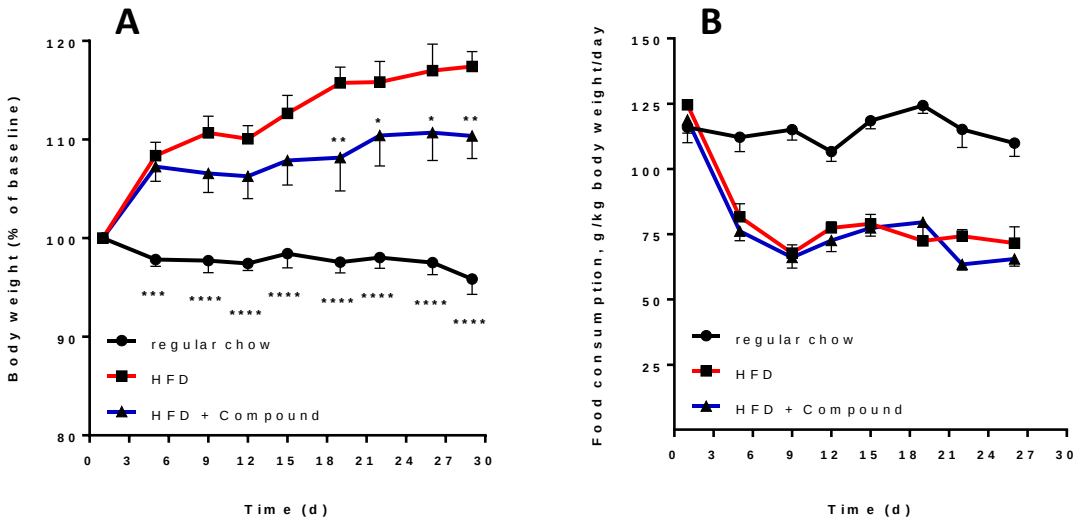

Figure 10. **Analogue 59 partially prevents high fat diet-induced obesity in adi-hRBP4 mice.** (A), Weight gains for male adi-hRBP4 mice fed with normal chow (n=8), HFD (n=7), and HFD with **58** (n=8). In comparison to the untreated HFD group, compound-treated HFD mice registered significantly decreased weight gain at four time points starting from Day 19 (Two-way RM ANOVA with Holm-Sidak *post-hoc* test, *$P < 0.05$; **$P < 0.01$). The body weight gain in chow-fed mice was

lower than in the HFD group at all time points studied (Two-way RM ANOVA with Holm-Sidak *post-hoc* test, ***$P < 0.001$; ****$P < 0.0001$). Values represent mean percent weight change from baseline. Error bars show SD. Body weights of individual animals from three treatment groups are shown in Supplementary Table S1. (B), Daily food consumption normalized to body weight in male adi-hRBP4 mice fed with normal chow, HFD, and HFD with **59**. No difference in food consumption between the untreated HFD group and compound-treated HFD mice was detected (Two-way RM ANOVA with Holm-Sidak *post-hoc* test). Values represent mean normalized daily chow consumption. Error bars show SD.

Reduction of Hepatic Lipid Levels by Analogue 59 in Obese adi-hRBP4 Mice. In accordance with the previous report,[22] hepatic free fatty acid (FFA) and triglyceride (TG) levels in adi-hRBP4 mice maintained on the high-fat diet were significantly higher than in transgenic animals kept on a standard chow (Figure 11; P<0.0001 for both FFA and TG). Administration of **59** lowered the FFA levels by 30% (Figure 11, A; P = 0.0107) and TG levels by 29% (Figure 11, B; P = 0.0104).

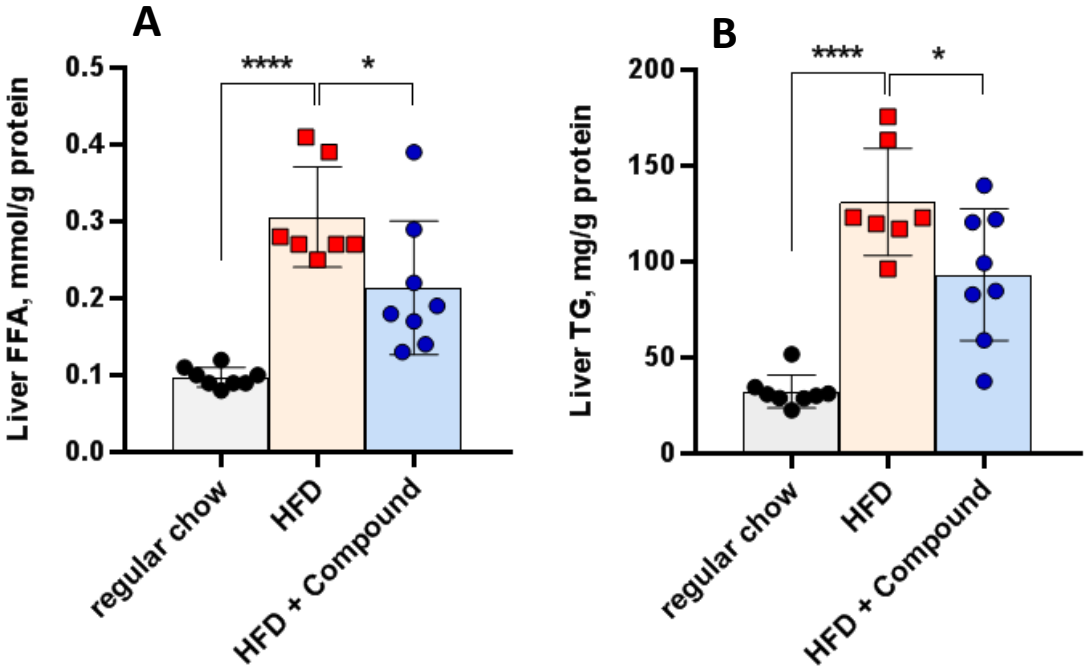

Figure 11. **Effect of analogue 59 orally administered at the 20 mg/kg dose on hepatic free fatty acid and triglyceride levels in obese adi-hRBP4 mice.** Liver levels of FFA (A) and TG (B) in male adi-hRBP4 mice fed with normal chow (n=8), HFD (n=7), and HFD with **59** (n=8). In comparison to the untreated HFD group, **59**-treated HFD mice have significantly decreased hepatic levels of FFA (P=0.0107, 1-way ANOVA with Holm-Sidak *post-hoc* test) and triglycerides (P=0.0104, one-way ANOVA with Holm-Sidak *post-hoc* test). Graph bars show mean; error bars show SD; *P < 0.05; ****P < 0.0001. Each data point on the graph represents a FFA or TG concentration from an individual animal.

Consistent with the dynamics of hepatic TG accumulation, histological examination of oil red O-stained frozen liver sections (Figure 12, A) and hepatic steatosis grading (Figure 12, B) confirmed significantly more steatosis in adi-hRBP4 mice maintained on HFD in comparison to the chow-fed transgenic mice, which showed no evidence of hepatic

steatosis. Significant improvement in hepatic steatosis was seen in the **59**-treated adi-hRBP4 obese mice, which exhibited fewer and smaller lipid droplets in comparison to the un-treated adi-hRBP4 mice maintained on HFD (Figure 12, A). Hepatic steatosis grading (Figure 12, B) revealed a significant 43% reduction in the degree of steatosis in **59**-treated HFD-fed adi-hRBP4 mice ($P<0.001$), which further confirmed the ability of **59** to alleviate hepatic steatosis in adi-hRBP4 mice.

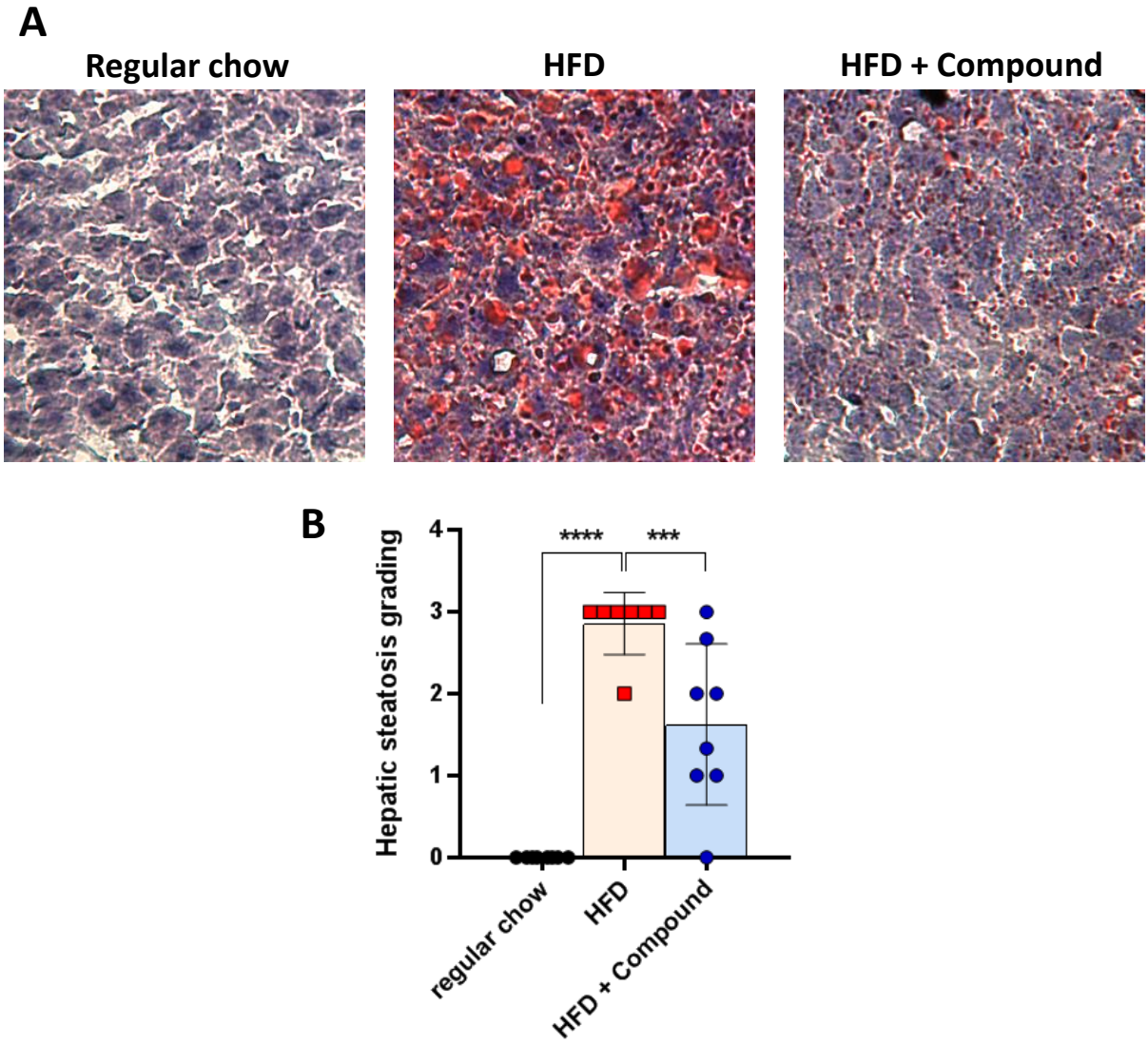

Figure 12. **Effect of analogue 59 on hepatic lipid disposition in adi-hRBP4 mice.** (A), Representative liver cryosections stained with oil red O illustrating fatty liver states in chow-fed, HFD, and **59**-treated HFD adi-hRBP4 mice. Compound was orally administered at the 20 mg/kg dose. (B), Histological scoring of oil red O-stained liver cryosections from chow-fed, HFD, and **59**-treated HFD adi-hRBP4 mice. Hepatic steatosis was graded as 0 (0% hepatocytes have macrovesicular steatosis), 1 (<33% hepatocytes have macrovesicular steatosis), 2 (33-66% hepatocytes have macrovesicular steatosis), and 3 (>66% hepatocytes have macrovesicular steatosis). Data was analyzed using one-way ANOVA with Holm-Sidak *post-hoc* test. Graph bars

show mean; error bars show SD; ***$P < 0.001$. Each data point on the graph represents a steatosis histology score from an individual animal. The number of male adi-hRBP4 mice per treatment group were 8 for normal chow, 7 for HFD and 8 for HFD with **59.**

Binding of Fatty Acid Ligands to RBP4. Blaner and coworkers reported that hepatic steatosis observed in the adi-hRBP4 mouse model results from the increased mobilization of fatty acids from adipose tissue which led to elevation in plasma levels of fatty acids and enhanced hepatic uptake of circulating free fatty acids.[22] It remains unclear how modestly increased expression of RBP4 in adipose tissue contributes to the development of hepatic steatosis. One can surmise that this ability of RBP4 may relate to binding and trafficking of endogenous non-retinoid ligands, which the nature of and abundance is unknown at this point. Consistent with the ability of RBP4 to interact with non-retinoid ligands, previous crystallographic studies of heterologously expressed RBP4 revealed fortuitous fatty acid ligands from the expression host (oleic acid and linoleic acid) bound within the ligand binding pocket of RBP4.[23, 24] Recent x-ray crystallographic and mass spectrometry findings reported by Monaco and coworkers confirmed that RBP4 is capable of binding fatty acids.[25] The capacity of retinol-binding proteins to bind hydrophobic non-retinoid ligands may be general as illustrated by recently described interactions of cellular retinol-binding protein 1 (CRBP1) with certain cannabinoids.[37] We tested the affinity of palmitic acid, oleic acid, linoleic acid, and docosahexaenoic acid for RBP4 using a SPA assay[34] that measures displacement of radioactive retinol from purified human RBP4 (Figure 13, A). These competition binding experiments confirmed the ability of the tested fatty acids to

function as weak RBP4 ligands. Our docking model is also consistent with the ability of RBP4 to bind fatty acid ligands. Figure 13, B presents overlays of **48** and the fatty acids palmitic acid, oleic acid, linoleic acid, and docosahexaenoic acid docked within our ***3fmz*** model and of **1** docked within our ***5nu7*** (holo-RBP4) model. The figure shows good overlay between **1** and **48** as both present similar geometric poses and project their polar fragments toward the opening of the binding cavity where they engage in H-bond interactions with Gln98 and Arg121, respectively. Similar to **1** and **48**, the fatty acids also extend their hydrophobic tails through the narrow β-barrel and into the β-ionone pocket and their polar carboxylic acids bind to residues residing closer to the opening of the binding cavity, namely Leu36 and Phe36.

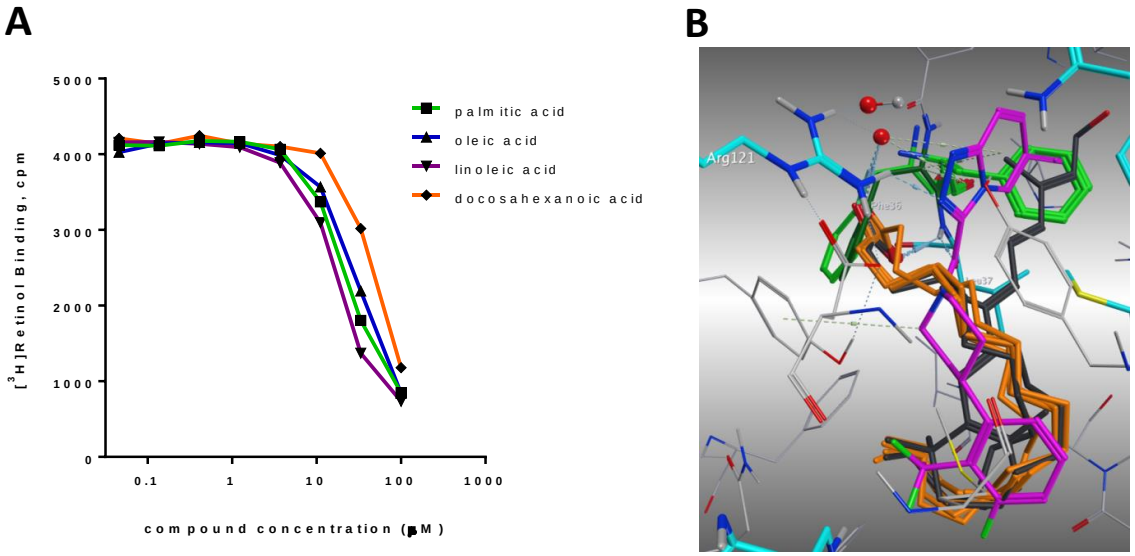

Figure 13. Binding of fatty acids to RBP4. (A), Isotherms of palmitic acid, oleic acid, linoleic acid, and docosahexaenoic acid binding to human RBP4. ^{3}H-retinol at 10 nM was used as a radioligand. (B), Overlays of minimized bound conformations of retinol (black, ***5nu7***), antagonist **48** (purple,

3fmz), and palmitic acid, oleic acid, linoleic acid, and docosahexaenoic acid (orange). Phe36 is as dark-green in the ***3fmz*** (within close proximity to the fatty acid carboxylic acid groups) and as light green in the ***5nu7*** model (within close proximity to the alcohol group of **1**). Contacting residues are labeled and illustrated in stick format (MOE, Chemical Computing Group, Inc., Montreal, CA).

▪ CONCLUSIONS

Epidemiologic evidence suggests that elevated circulating levels of RBP4 may have significant metabolic effects. Non-retinoid RBP4 antagonists represent an important pharmacological tool for assessing the role of RBP4 in pathogenesis of metabolic disorders such as NAFLD and NASH. We previously reported efforts to develop novel RBP4 antagonists using **3** and ***3fmz*** as springboards for our structure-based drug design strategies. Our investigations ultimately led us to discover the bicyclic antagonists **4** and **5**. However, in addition to exploring analogues with isosteric replacements for the piperidine core of **3**, we also sought to investigate novel appendages that did not bear a carboxylic acid group. Drawing from compound **6** and ***4spq***, we investigated various 2- and 3-carboxamido fused [5,6]-biaryl heteroaromatic systems that featured either a piperidine or bicyclic core to which the *ortho*-trifluoromethylphenyl head group of **3** was retained. Of these diverse sets of compounds, **48** was selected as the lead compound displaying unique *in vitro* RBP4 potency, good solubility, and robust *in vitro* microsomal stability. Focused SAR exploration of the aryl head group afforded analogue **59**, which displayed a similar profile to **48** but with improved HTRF potency. Analogues **48** and **59** were subjected to detailed *in vitro* and *in vivo* evaluation and displayed favorable ADME

profiles, no deleterious off-target binding *in vitro*, and excellent PK properties in rodents. Consistent with its good PK properties, **59** induced a robust 80-85% plasma RBP4 reduction after administration of a single oral or intravenous dose in mice (Figure 8). A general safety concerns for the class of RBP4 antagonists exemplified by analogue **59** is whether such a profound reduction in serum RBP4 may induce symptoms of systemic vitamin A deficiency. Based on the available evidence, pharmacological downregulation of serum RBP4 cannot be considered analogous to systemic deprivation of vitamin A. While RBP4-TTR complex is the major trafficking system for retinol delivery to vitamin A-dependent tissues, retinoid delivery to organs can occur via several complementary RBP4-independent pathways.[38-43] Following the absorption of **1** in the gut, dietary retinoids are incorporated into chylomicrons, which transport retinoids predominantly to the liver. However, extrahepatic vitamin A-dependent tissues are responsible for the uptake of about 25-33% of postprandial retinoid-laden chylomicrons.[38] Retinoic acid can also be delivered to the target organs in a complex with serum albumin.[39] In addition, biosynthesis of **1** from dietary β-carotene in RPE cells and other tissues has been reported.[39, 44] Patients with compound heterozygous missense mutations in RBP4 have plasma RBP4 levels below the limit of detection while showing no clinical symptoms of systemic vitamin A deficiency.[42] *Rbp4*$^{-/-}$ mice are phenotypically normal without systemic abnormalities[38, 40, 41] or histological signs of retinal degeneration .[45] At weaning, *Rbp4*$^{-/-}$ mice have reduced electroretinographic amplitudes, which completely normalize on standard chow that contains standard levels of **1**.[38, 40] Symptoms of vitamin A deficiency do not occur in TTR knock-out mice, despite low serum RBP4 levels and the absence of

the circulating retinol-RBP4-TTR complex.[46] We recently reported that administration of analogue **5** at doses inducing 90% serum RBP4 lowering in mice partially reduced the level of retinoids in the retina and significantly inhibited bisretinoid synthesis without negatively affecting the rate of the visual cycle or inhibiting retinal function as assessed by electroretinography.[47] In sum, pharmacological reduction of serum RBP4 by orally active RBP4 antagonists is unlikely to result in systemic vitamin A deficiency in patients who maintain a normal, vitamin A- and β-carotene-sufficient diet. While adverse effects related to induction of systemic vitamin A deficiency are unlikely, the long-term use of the first-generation RBP4 antagonist fenretinide in cancer patients was associated with transient and reversible ocular side effects, such as diminished dark adaptation, in a small subset of patients (yearly prevalence: 5.8-6.7%).[48] For analogue **59** and related compounds, the balance between clinical efficacy and the extent of potential ocular adverse effects remains to be determined in future clinical trials.

Advanced ADME characterization of analogue **59** led to further studies in the mouse transgenic model of hepatic steatosis, adi-hRBP4 mice, in which a very modest 3-5% increase in circulated levels of RBP4 conferred by adipocyte secretion of human RBP4 was sufficient to trigger the induction of a strong metabolic phenotype. Chronic oral administration of **59** at a dose of 20 mg/kg/day induced a 90% decrease in circulating levels of both mouse RBP4 (produced predominantly in the liver) as well as human (adipose tissue-secreted) serum RBP4. Analogue **59** reduced the body weight gain in obese HFD-fed adi-hRBP4 mice by 53% without decreasing food intake. Hepatic free fatty acid and triglyceride levels in adi-hRBP4 mice maintained on the high-fat diet were

significantly higher than in transgenic animals kept on a standard chow. Administration of **59** lowered the hepatic FFA levels by 30% and TG levels by 29% in HFD-fed adi-hRBP4 mice. In accordance with the dynamics of hepatic TG accumulation, histological examination of frozen liver sections and hepatic steatosis grading confirmed significantly more steatosis in adi-hRBP4 mice maintained on HFD. Significant improvement in hepatic steatosis was seen in the **59**-treated adi-hRBP4 obese mice, which exhibited fewer and smaller lipid droplets than untreated HFD-fed adi-hRBP4 mice. Steatosis grading revealed a significant 43% reduction in the degree of steatosis in **59**-treated HFD-fed adi-hRBP4 mice. Taken collectively, these data confirmed the ability of **59** to alleviate hepatic steatosis in adi-hRBP4 mice suggesting that RBP4 antagonist **59** may serve as a potential orally bioavailable pharmacotherapy for NASH. Consistent with the idea that adipose tissue-secreted RBP4 may potentially function as a transporter for endogenous hydrophobic ligands other than retinol, our competition binding experiments, supported by the docking model data, confirmed the ability of RBP4 to bind hydrophobic non-retinoid ligands, such as fatty acids. Synthetic RBP4 antagonists capable of suppressing hepatic lipid accumulation may be considered as a novel class of therapeutics for the treatment of NASH, particularly in patients with elevated circulating levels of RBP4.

EXPERIMENTAL SECTION

General Chemistry. The reactions presented were conducted under an inert atmosphere of N_2 gas unless noted otherwise. Reactions indicating room temperature (rt) were conducted at 25 °C. Reagents and solvents acquired from commercial vendors

were used as is. Rotary evaporations were conducted with Buchi rotary evaporators and Teflon-linked KNF vacuum pumps. AnalTech No. 02521 1" x 3" glass-backed silica gel plates with fluorescent indicator were used for routine thin layer chromatography TLC and visualization of the plates was accomplished either via short wave UV light (254 nm lamp), 10% phosphomolybdic acid in ethanol, or with iodine vapors. Analtech, 20 × 20 cm, 1000 micron preparative plates were used for compounds requiring preparative thin layer chromatography for purification. Teledyne Isco CombiFlash Companion Unit was used for flash column chromatography. Teledyne Isco RediSep Rf silica gel columns were used for the stationary phase. In cases when reverse phase chromatography was required, a RediSep Gold C18 reverse phase column was employed. Proton NMR spectra were obtained either on 300 MHz Bruker Nuclear Magnetic Resonance Spectrometer or 500 MHz Bruker Nuclear Magnetic Resonance Spectrometer and chemical shifts Bruker Nuclear Magnetic Resonance Spectrometer and chemical shifts (δ) are reported in parts per million (ppm) and coupling constant (*J*) values are given in Hz, with the following spectral pattern designations: s, singlet; d, doublet; t, triplet, q, quartet; dd, doublet of doublets; m, multiplet; br, broad. Tetramethylsilane was used as an internal reference. MEL-TEMP Electrothermal melting point apparatus was used to generate reported melting points, which are uncorrected. Mass spectroscopic analyses were performed using the following: 1) ESI ionization on a Varian ProStar LCMS with a 1200L quadrapole mass spectrometer; 2) ESI, APCI, or DUIS ionization on a Shimadzu LCMS-2020 single quadrapole mass spectrometer. High pressure liquid chromatography (HPLC) purity analysis was performed using a Varian Pro Star HPLC system with a binary solvent system

A and B using a gradient elusion [A, H_2O with either 0.05% or 0.1% trifluoroacetic acid (TFA); B, CH_3CN with either 0.05% or 0.1% TFA] and flow rate = 1 mL/min, with UV detection at either 223 or 254 nm. All final compounds tested for *in vitro* and *in vivo* biological testing were purified to ≥95% purity and these purity levels were measured by using the following HPLC methods:

A) Method A mobile phase: A = H_2O with 0.05% TFA and B = CH_3CN with 0.05% TFA; gradient: 0–90% B (0.0–20.0 min); UV detection was measured at at 254 nm; Method A column: 3.0 × 250 mm Phenomenex C18(2) reverse phase column

B) Method B mobile phase: A = H_2O with 0.05% TFA and B = CH_3CN with 0.05% TFA; gradient: 0–90% B (0.0–20.0 min); UV detection was measured at 230 nm; Method B column: 3.0 × 250 mm Phenomenex C18(2) reverse phase column

C) Method C mobile phase: A = H_2O with 0.05% TFA and B = CH_3CN with 0.05% TFA; gradient: 0–100% B (0.0–20.0 min); UV detection at 254 nm; Method C column: 4.6 × 250 mm SunFire C18 5 μm reverse phase column

(1H-Indazol-3-yl)(4-(2-(trifluoromethyl)phenyl)piperidin-1-yl)methanone (11). *Step A*. To a solution of 1-bromo-2-(trifluoromethyl)benzene (**7**, 35.0 g, 156 mmol) in THF (350 mL) cooled to -78 °C was slowly added a solution of *n*-BuLi (70.4 mL, 2.5 M in THF, 176 mmol) over a period of 15 min. The mixture stirred at -78 °C for 40 min, was allowed to warm to 0 °C and then cooled back down to -78 °C. To this was added a solution of 1-benzylpiperidin-4-one (22.1 g, 117 mmol) in THF (80 mL) over a period of 10 min. The

resulting mixture continued to stir at -78 °C for 2 h. The reaction was carefully quenched with aqueous, saturated aqueous NH_4Cl solution (500 mL) and the mixture was extracted with EtOAc (3 × 100 mL). The combined organic extracts were washed with H_2O, brine, dried over Na_2SO_4, filtered, and concentrated under reduced pressure. The resulting residue was chromatographed over silica gel (Isco CombiFlash Companion unit, 330 g RediSep column, 0–30% EtOAc in hexanes) to give 1-benzyl-4-(2-(trifluoromethyl)phenyl)piperidin-4-ol (**8**) as a light-yellow oil (29.2 g, 74%): ^{1}H NMR (500 MHz, $CDCl_3$) δ 7.78 (d, *J* = 1.6Hz, 1H), 7.59 (m, 1H), 7.47 (m, 1H), 7.36 (m, 5H), 7.31 (m, 2H), 3.58 (s, 2H), 2.80 (m, 2H), 2.55 (m, 2H), 2.27 (m, 2H), 1.88 (m, 2H); MS (ESI+) *m/z* 336 $[M + H]^+$.

Step B. A 0 °C cooled solution of 1-benzyl-4-(2-(trifluoromethyl)phenyl)piperidin-4-ol (**8**, 29.2 g, 87.1 mmol) in $SOCl_2$ (60 mL) stirred for 2 h and was then diluted with CH_2Cl_2 (250 mL). The mixture was carefully poured into a saturated aqueous $NaHCO_3$ solution (200 mL). The biphasic mixture was separated and the aqueous layer was further extracted with CH_2Cl_2 (2 × 200 mL). The combined organic layers were washed with brine, dried over Na_2SO_4, filtered and concentrated. The resulting residue was chromatographed over silica gel (Isco CombiFlash Companion unit, 330 g RediSep column, 0–30% EtOAc in hexanes) to give 1-benzyl-4-(2-(trifluoromethyl)phenyl)-1,2,3,6-tetrahydropyridine (**9**) as a light-yellow oil (13.5 g, 49%): ^{1}H NMR (500 MHz, $CDCl_3$) δ 7.63 (d, *J* = 1.6Hz, 1H), 7.48 (m, 1H), 7.39 (m, 5H), 7.28 (m, 2H), 5.56 (s, 1H), .68 (s, 2H), 3.14 (m, 2H), 2.70 (m, 2H), 2.39 (m, 2H); MS (ESI+) *m/z* 318 $[M + H]^+$.

Step C. A mixture of 1-benzyl-4-(2-(trifluoromethyl)phenyl)-1,2,3,6-tetrahydropyridine (**9**, 13.6 g, 42.5 mmol), 10% Pd/C (3.0 g), and HCO_2NH_4 (26.8 g, 425 mmol) in CH_3OH (800 mL) was heated at reflux for 2 h. The mixture cooled to rt and was filtered over Celite. The filtrate was concentrated and the resulting residue was chromatographed over silica gel (Isco CombiFlash Companion unit, 330 g RediSep column, 0–10% CH_3OH with 1% NH_4OH in CH_2Cl_2) to give 4-(2-(trifluoromethyl)phenyl)piperidine as a colorless oil (2.0 g, 21%): ^{1}H NMR (500 MHz, $CDCl_3$) δ 7.61 (d, *J* = 1.7Hz, 1H), 7.52 (m, 2H), 7.29 (m, 1H), 3.21 (m, 2H), 3.07 (m, 1H), 2.80 (m, 2H), 2.33 (bs, 1H), 1.77 (m, 4H); MS (ESI+) *m/z* 230 $[M + H]^+$. To a solution of 4-(2-(trifluoromethyl)phenyl)piperidine (5.6 g, 24.5 mmol) in CH_3CN (30 mL) was added a 4 M solution of HCl in 1,4-dioxane (6.1 mL, 24.5 mmol) at rt. The mixture stirred for 2 h and was then concentrated under reduced pressure to give 4-(2-(trifluoromethyl)phenyl)piperidine hydrochloride (**10**) as a white solid (6.4 g, >99%): MS (ESI+) *m/z* 230 $[M + H]^+$.

Step D. A mixture of 4-(2-(trifluoromethyl)phenyl)piperidine hydrochloride (**10**, 0.115 g, 0.436 mmol), 1H-indazole-3-carboxylic acid (0.070 g, 0.436 mmol), Et_3N (0.18 mL, 1.308 mmol), and HBTU (0.248 g, 0.651 mmol) in DMF (5 mL) was stirred at rt for 16 h. The mixture was diluted with H_2O (20 mL) and extracted with EtOAc (3 × 50 mL). The combined organic extracts were washed with H_2O (3 × 50 mL), brine, dried over Na_2SO_4, filtered and concentrated under reduced pressure. The resulting residue was purified by silica gel chromatography (10–50% EtOAc in hexanes) to afford (1H-indazol-3-yl)(4-(2-(trifluoromethyl)phenyl)piperidin-1-yl)methanone (**11**) as a white solid (0.114 g, 70%): mp = 175–177 ^{o}C; ^{1}H NMR (500 MHz, $CDCl_3$) δ 10.26 (bs, 1H), 8.16 (d, *J* = 7.8 Hz, 1H), 7.64 (m,

1H), 7.52 (m, 2H), 7.43 (m, 2H), 7.28 (m, 2H), 5.00 (m, 2H), 3.28 (m, 2H), 2.98 (m, 1H), 1.85 (m, 4H); MS (ESI+) *m/z* 374 $[M+H]^+$; HPLC 98.9% purity (AUC), t_R = 13.6 min (Method A).

(1-Methyl-1H-indazol-3-yl)(4-(2-(trifluoromethyl)phenyl)piperidin-1-yl)methanone (12). Compound **12** was prepared according to a similar procedure described for the synthesis of **11**. ^{1}H NMR (500 MHz, $CDCl_3$) δ 8.14 (d, *J* = 7.8 Hz, 1H), 7.64 (m, 1H), 7.51 (m, 1H), 7.43 (m, 3H), 7.28 (m, 2H), 5.02 (m, 2H), 4.11 (s, 3H), 3.27 (m, 2H), 2.92 (m, 1H), 1.85 (m, 4H); MS (ESI+) *m/z* 388 $[M+H]^+$; HPLC 98.4% purity (AUC), t_R = 14.8 min (Method A).

(6-Fluoro-1H-indazol-3-yl)(4-(2-(trifluoromethyl)phenyl)piperidin-1-yl)methanone (13). Compound **13** was prepared according to a similar procedure described for the synthesis of **11**. mp 210–212 °C; ^{1}H NMR (500 MHz, DMSO-d_6) δ 13.54 (s, 1H), 8.04–8.01 (m, 1H), 7.71–7.60 (m, 3H), 7.44–7.39 (m, 2H), 7.13–7.10 (m, 1H), 4.96–4.78 (m, 2H), 3.25–3.17 (m, 2H), 2.92–2.90 (m, 1H), 1.82–1.77 (m, 4H); ESI MS *m/z* 392 $[M + H]^+$; HPLC >99% purity (AUC), t_R = 10.5 min (Method A).

(6-Chloro-1H-indazol-3-yl)(4-(2-(trifluoromethyl)phenyl)piperidin-1-yl)methanone (14). Compound **14** was prepared according to a similar procedure described for the synthesis of **11**. mp = 221–223 °C; ^{1}H NMR (300 MHz, DMSO-d_6) δ 13.64 (s, 1H), 8.02 (d, *J* = 8.7 Hz, 1H), 7.72-7.60 (m, 4H), 7.42 (t, *J* = 7.4 Hz, 1H), 7.26 (dd, *J* = 1.7 Hz, *J* = 8.7 Hz, 1H), 4.94 (d, *J* = 13.5 Hz, 1H), 4.79 (d, *J* = 12.1 Hz, 1H), 3.32-3.11 (m, 2H), 2.91 (t, *J* = 9.6 Hz, 1H), 1.89-1.70 (m, 4H); MS (APCI+) *m/z* 408, 410 $[M+H]^+$; HPLC >99% purity (AUC), t_R = 15.4 min (Method A).

(5-Fluoro-1H-indazol-3-yl)(4-(2-(trifluoromethyl)phenyl)piperidin-1-yl)methanone (15). Compound **15** was prepared according to a similar procedure described for the

synthesis of **11**. mp 188–190 °C; ^{1}H NMR (500 MHz, DMSO-d_6) δ 13.64 (s, 1H), 7.73–7.59 (m, 5H), 7.45–7.39 (m, 1H), 7.36–7.29 (m, 1H), 5.08–4.99 (m, 1H), 4.83–4.74 (m, 1H), 3.29–3.13 (m, 2H), 2.95–2.85 (m, 1H), 1.86–1.71 (m, 4H); ESI MS *m/z* 392 [M + H]$^+$; HPLC >99% purity (AUC), t_R = 10.5 min (Method A).

(5-Chloro-1H-indazol-3-yl)(4-(2-(trifluoromethyl)phenyl)piperidin-1-yl)methanone (16). Compound **16** was prepared according to a similar procedure described for the synthesis of **11**. mp = 210–212 °C; ^{1}H NMR (300 MHz, DMSO-d_6) δ 13.73 (s, 1H), 8.05 (s, 1H), 7.75–7.62 (m, 4H), 7.48–7.39 (m, 2H), 5.03 (d, *J* = 12.8 Hz, 1H), 4.79 (d, *J* = 11.8 Hz, 1H), 3.29–3.17 (m, 2H), 2.99–2.87 (m, 1H), 1.81 (t, *J* = 6.9 Hz, 4H); MS (APCI+) *m/z* 408, 410 [M+H]$^+$; HPLC >99% purity (AUC), t_R = 15.6 min (Method A).

(5-Methoxy-1H-indazol-3-yl)(4-(2-(trifluoromethyl)phenyl)piperidin-1-yl)methanone (17). Compound **17** was prepared according to a similar procedure described for the synthesis of **11**. mp = 168–170 °C; ^{1}H NMR (500 MHz, DMSO-d_6) δ 8.75 (s, 1H), 7.69-7.62 (m, 3H), 7.42 (t, *J* = 6.3 Hz, 1H), 7.34 (d, *J* = 2.9 Hz, 1H), 7.28 (d, *J* = 8.9 Hz, 1H), 7.22 (dd, *J* = 2.9 Hz , *J* = 8.9 Hz, 1H), 4.24 (d, *J* = 13.5 Hz, 2H), 3.79 (s, 3H), 3.09 (t, *J* = 11.4 Hz, 1H), 2.94 (t, *J* = 11.8 Hz, 2H), 1.86-1.68 (m, 4H); MS (APCI+) *m/z* 404 [M+H]$^+$; HPLC >99% purity (AUC), t_R = 14.3 min (Method A).

(7-Chloro-1H-indazol-3-yl)(4-(2-(trifluoromethyl)phenyl)piperidin-1-yl)methanone (18). Compound **18** was prepared according to a similar procedure described for the synthesis of **11**. mp = 192–195 °C; ^{1}H NMR (500 MHz, DMSO-d_6) δ 14.03 (s, 1H), 7.98 (d, *J* = 8.2 Hz, 1H), 7.69 (d, *J* = 8.2 Hz, 2H), 7.64 (t, *J* = 7.4 Hz, 1H), 7.53 (d, *J* = 6.8 Hz, 1H), 7.42 (t, *J* = 7.8 Hz, 1H), 7.24 (t, *J* = 7.5 Hz, 1H), 4.87 (d, *J* = 13.0 Hz, 1H), 4.79 (d, *J* = 12.7 Hz, 1H),

3.29-3.16 (m, 2H), 3.03-2.83 (m, 1H), 1.89-1.70 (m, 4H); MS (APCI+) *m/z* 408, 410 $[M+H]^+$; HPLC 99.4% purity (AUC), t_R = 11.4 min (Method A).

(1-Ethyl-6-fluoro-1H-indazol-3-yl)(4-(2-(trifluoromethyl)phenyl)piperidin-1-yl)methanone (19). To a solution of (6-fluoro-1*H*-indazol-3-yl)(4-(2-(trifluoromethyl)phenyl)piperidin-1-yl)methanone (**13**, 0.05 g, 0.13 mmol) and iodoethane (0.015 mL, 0.19 mmol) in DMF (2 mL) was added K_2CO_3 (0.044 g, 0.32 mmol). The mixture stirred for 4 h at rt and was then diluted with H_2O (5 mL). The aqueous mixture was extracted with EtOAc (3 × 5 mL) and the combined organic extracts were dried over Na_2SO_4, filtered, and concentrated under reduced pressure. The resulting residue was chromatographed over silica gel (Parallex Flex unit, YMC-Pack ODS-A column, 5% to 95% CH_3CN in H_2O) to give (1-ethyl-6-fluoro-1*H*-indazol-3-yl)(4-(2-(trifluoromethyl)phenyl)piperidin-1-yl)methanone as a white solid (0.020 g, 37%): mp = 44–46 °C; ^{1}H NMR (500 MHz, $CDCl_3$) δ 7.83 (dd, *J* = 2.4 Hz , *J* = 8.9 Hz, 1H), 7.64 (d, *J* = 7.7 Hz, 1H), 7.52 (t, *J* = 7.7 Hz, 1H), 7.46 (d, *J* = 7.9 Hz, 1H), 7.37 (dd, *J* = 4.0 Hz , *J* = 9.1 Hz, 1H), 7.31 (t, *J* = 7.6 Hz, 1H), 7.20 (dt, *J* = 2.4 Hz, *J* = 8.9 Hz, 1H), 5.07 (d, *J* = 47.2 Hz, 2H), 4.44 (q, *J* = 7.3 Hz, 2H), 3.38–3.24 (m, 2H), 2.93 (br s, 1H), 1.99-1.81 (m, 4H), 1.54 (t, *J* = 7.3 Hz, 3H); MS (APCI+) *m/z* 420 $[M+H]^+$; HPLC 97.0% purity (AUC), t_R = 16.6 min (Method A).

(6-Fluoro-1-isopropyl-1H-indazol-3-yl)(4-(2-(trifluoromethyl)phenyl)piperidin-1-yl)methanone (20). Compound **20** was prepared according to a similar procedure described for the synthesis of **19**. mp = 50–53 °C; ^{1}H NMR (500 MHz, $CDCl_3$) δ 7.85 (dd, *J* = 2.4 Hz , *J* = 8.9 Hz, 1H), 7.64 (d, *J* = 7.8 Hz, 1H), 7.52 (t, *J* = 7.7 Hz, 1H), 7.46 (d, *J* = 7.8 Hz, 1H), 7.40 (dd, *J* = 4.0 Hz , *J* = 9.1 Hz, 1H), 7.31 (t, *J* = 7.6 Hz, 1H), 7.18 (dt, *J* = 2.5 Hz, *J* = 8.9

Hz, 1H), 5.09 (br s, 2H), 4.89-4.80 (m, 1H), 3.32-2.94 (m, 3H), 1.93–1.81 (m, 4H), 1.59 (d, *J* = 6.7 Hz, 6H); MS (APCI+) *m/z* 434 $[M+H]^+$; HPLC 95.7% purity (AUC), t_R = 17.4 min (Method A).

(6-Fluoro-1-(oxetan-3-yl)-1H-indazol-3-yl)(4-(2-(trifluoromethyl)phenyl)piperidin-1-yl)methanone (21). Compound **21** was prepared according to a similar procedure described for the synthesis of **19** using 3-iodooxetane and with heating at 60 °C for 24 h. mp = 70–73 °C; ^{1}H NMR (500 MHz, $CDCl_3$) δ 7.86 (dd, *J* = 2.2 Hz , *J* = 8.8 Hz, 1H), 7.65 (d, *J* = 7.8 Hz, 1H), 7.54-7.45 (m, 3H), 7.32 (t, *J* = 7.7 Hz, 1H), 7.23 (dd, *J* = 2.5 Hz, *J* = 8.9 Hz, 1H), 5.82–5.76 (m, 1H), 5.25 (t, *J* = 6.6 Hz, 2H), 5.16–5.11 (m, 3H), 5.02 (d, *J* = 12.1 Hz, 1H), 3.34–3.27 (m, 2H), 2.97–2.94 (m, 1H), 2.05-1.81 (m, 4H); MS (APCI+) *m/z* 448 $[M+H]^+$; HPLC >99% purity (AUC), t_R = 15.4 min (Method A).

Benzo[*d*]isoxazol-3-yl(4-(2-(trifluoromethyl)phenyl)piperidin-1-yl)methanone (22). Compound **22** was prepared according to a similar procedure described for the synthesis of **11**. ^{1}H NMR (500 MHz, $CDCl_3$) δ 7.94 (d, *J* = 7.8 Hz, 1H), 7.65 (m, 2H), 7.52 (m, 1H), 7.45 (m, 1H), 7.37 (m, 2H), 4.14 (m, 1H), 4.92 (m, 1H), 4.66 (m, 1H), 3.36 (m, 2H), 2.98 (m, 1H), 1.99 (m, 4H); MS (ESI+) *m/z* 375 $[M+H]^+$; HPLC 96.7% purity (AUC), t_R = 15.4 min (Method A).

Benzo[*c*]isoxazol-3-yl(4-(2-(trifluoromethyl)phenyl)piperidin-1-yl)methanone (23). Compound **23** was prepared according to a similar procedure described for the synthesis of **11**. mp = 106–108 °C; ^{1}H NMR (500 MHz, DMSO-d_6) δ 7.86 (d, *J* = 8.9 Hz, 1H), 7.45 (t, *J* = 9.1 Hz, 2H), 7.70–7.63 (m, 2H), 7.52–7.48 (m, 1H), 7.43 (t, *J* = 7.6 Hz, 1H), 7.28–7.24 (m, 1H), 4.74-4.65 (m, 1H), 4.27-4.18 (m, 1H), 3.50-3.38 (m, 1H), 3.24-3.17 (m, 1H), 3.09-3.00

(m, 1H), 1.98–1.75 (m, 4H); MS (APCI+) *m/z* 375 $[M+H]^+$; HPLC >99% purity (AUC), t_R = 12.1 min (Method A).

(3aR,5r,6aS)-5-(2-(Trifluoromethyl)phenyl)octahydrocyclopenta[*c*]pyrrole Hydrochloride (31). *Step A*. To a 0 °C cooled solution of $LiAlH_4$ in THF (1.0 M, 800 mL, 800 mmol) in THF (800 mL) was carefully added (3aR,7aS)-3a,4,7,7a-tetrahydro-1H-isoindole-1,3(2H)-dione (**24**, 53.7 g, 0.35 mol) portion-wise. An exotherm of ~5 °C occurred upon each addition of **24**. Upon complete addition, the mixture was allowed to warm to rt followed by heating at 70 °C for 16 h. The mixture was allowed to cool back to rt and then further cooled to 0 °C. The reaction was carefully quenched by slow addition of H_2O (30 mL), 15% aqueous NaOH solution (30 mL), followed by another bolus of H_2O (90 mL). The rate of quenching was done carefully so as to maintain an internal temperature below 25 °C. The mixture stirred for 1 h and was filtered through celite. The aqueous filtrate was extracted with Et_2O (2 × 100 mL) and the combined organic extracts were concentrated under reduced pressure. The resulting residue was purified using a Kugelrorh distillation apparatus to give (3aR,7aS)-2,3,3a,4,7,7a-hexahydro-1H-isoindole as a clear, colorless oil (19.45 g, 44%): ^{1}H NMR (500 MHz, $CDCl_3$) δ 5.29 (s, 2H), 3.88 (bs, 1H), 3.26 (m, 2H), 2.82 (m, 2H), 2.41-2.19 (m, 4H), 1.96 (m, 2H).

Step B. To a 0 °C cooled solution of (3aR,7aS)-2,3,3a,4,7,7a-hexahydro-1H-isoindole (11.5 g, 93.5 mmol) in CH_2Cl_2 (200 mL) was added Boc_2O (24.5 g, 112 mmol) and the mixture stirred at rt for 16 h. The mixture was washed with H_2O (100 mL), brine (100 mL), dried over Na_2SO_4, filtered, and concentrated under reduced pressure. The residue was purified by flash column chromatography (0% to 30% EtOAc in hexanes) to give (3a*R*,7a*S*)-

tert-butyl 3a,4,7,7a-tetrahydro-1H-isoindole-2(3H)-carboxylate (**25**) as a an oil (20.10 g, 49%): ^{1}H NMR (500 MHz, $CDCl_3$) δ 5.64 (s, 2H), 3.39 (m, 2H), 3.20 (m, 2H), 3.15 (m, 2H), 2.23-2.19 (m, 4H), 1.97 (m, 2H), 1.57 (s, 9H).

Step C. To a 0 °C cooled mixture of (3a*R*,7a*S*)-*tert*-butyl 3a,4,7,7a-tetrahydro-1H-isoindole-2(3H)-carboxylate (**25**, 66.78 g, 224 mmol) in CH_3CN (600 mL), CCl_4 (400 mL), and H_2O (800 mL) was added $NaIO_4$ (192.3 g, 899 mmol) followed by RuO_2•H_2O (1.19 g, 8.94 mmol). The mixture was stirred at rt for 24 h with mechanical stirring and then filtered through celite. The filter cake was washed with 10% CH_3OH in CH_2Cl_2 (200 mL) and the biphasic mother liquor was separated. The aqueous phase was further extracted with CH_2Cl_2 (3 × 150 mL) and the combined organic extracts were washed with H_2O (100 mL), brine (100 mL), dried over Na_2SO_4, filtered, and concentrated under reduced pressure. The residue was filtered through a plug of silica gel using a CH_3OH/CH_2Cl_2 eluent system (2%–10% CH_3OH in CH_2Cl_2). The filtrate was concentrated under reduced pressure to give 2,2'-((3*S*,4*R*)-1-(*tert*-butoxycarbonyl)pyrrolidine-3,4-diyl)diacetic acid (**26**) as a solid (46.75 g, 72%): ^{1}H NMR (500 MHz, DMSO-d_6) δ 12.2 (s, 2H), 3.38 (m, 2H), 3.02 (m, 2H), 2.49 (m, 2H), 2.32 (m, 2H), 2.29 (m, 2H), 1.42 (s, 9H).

Step D. To a suspension of 2,2'-((3*S*,4*R*)-1-(*tert*-butoxycarbonyl)pyrrolidine-3,4-diyl)diacetic acid (**26**, 6.97 g, 24.31 mmol) in Ac_2O (50 mL) was added NaOAc (1.99 g, 24.31 mmol) and the mixture was heated at 120 °C for 3 h. The mixture cooled to rt and filtered through celite. The filter cake was washed with Et_2O (5 × 50 mL) and the mother liquor was concentrated under reduced pressure. The resulting residue was purified by flash column chromatography (0%–30% EtOAc in hexanes) to give (3aR,6aS)-*tert*-butyl 5-

oxohexahydrocyclopenta[c]pyrrole-2(1H)-carboxylate (**27**) as a white foam (2.17 g, 40%): ^{1}H NMR (500 MHz, $CDCl_3$) δ 3.69 (m, 2H), 3.22 (m, 2H), 2.91 (m, 2H), 2.50 (m, 2H), 2.17 (m, 2H), 1.46 (s, 9H).

Step E. To a -78 °C cooled solution of (3aR,6aS)-*tert*-butyl 5-oxohexahydrocyclopenta[c]pyrrole-2(1H)-carboxylate (**27**, 22.35 g, 99.2 mmol) in THF (500 mL) was slowly added a solution of LiHMDS in THF (1.0 M, 129 mL). The mixture continued to stir at -78 °C for 30 min, then a solution of 1,1,1-trifluoro-*N*-phenyl-*N*-((trifluoromethyl)sulfonyl)methanesulfonamide (49.65 g, 139 mmol) in THF (150 mL) was slowly added. The mixture stirred for an additional 1 h at -78 °C and was then allowed to stir at rt for 2 h. The mixture was concentrated under reduced pressure and the residue was purified by flash column chromatography (0%–50% EtOAc in hexanes) to give (±)-(3aS,6aS)-*tert*-butyl 5-(((trifluoromethyl)sulfonyl)oxy)-3,3a,6,6a-tetrahydrocyclopenta[c]pyrrole-2(1H)-carboxylate ((±)-**28**) as a clear, viscous oil (1.56 g, quantitative): ^{1}H NMR (500 MHz, $CDCl_3$) δ 5.58 (s, 1H), 3.62 (m, 1H), 3.53 (m, 1H), 3.46 (m, 2H), 3.19 (m, 1H), 2.95 (m, 2H), 2.46 (m, 1H), 1.47 (s, 9H).

Step F. To an N_2 degassed mixture of (±)-(3aS,6aS)-*tert*-butyl 5-(((trifluoromethyl)sulfonyl)oxy)-3,3a,6,6a-tetrahydrocyclopenta[c]pyrrole-2(1H)-carboxylate ((±)-**28**, 14.79 g, 41.4 mmol), 2-trifluoromethylphenylboronic acid (19.70 g, 104 mmol), and a 2 M aqueous solution of Na_2CO_3 (250 mL) in DME (500 mL) was added $Pd(PPh_3)_4$ (4.80 g, 4.16 mmol). The mixture was heated at 80 °C for 6 h, then cooled to rt and diluted with H_2O (500 mL). The aqueous mixture was extracted with EtOAc (2 × 200 mL) and the combined organic extracts were washed with H_2O (200 mL), brine (200 mL),

dried over Na_2SO_4, filtered, and concentrated under reduced pressure. The residue was purified by flash column chromatography (0%–10% EtOAc in hexanes) to give (±)-(3aR,6aS)-*tert*-butyl 5-(2-(trifluoromethyl)phenyl)-3,3a,6,6a-tetrahydrocyclopenta[*c*]pyrrole-2(1H)-carboxylate ((±)-**29**) as a clear, viscous oil (13.70 g, 94%): ^{1}H NMR (500 MHz, $CDCl_3$) δ 7.65 (m, 1H), 7.47 (m, 2H), 7.25 (m, 1H), 5.58 (s, 1H), 3.85-3.42 (m, 4H), 3.23 (m, 1H), 2.98 (m, 2H), 2.49 (m, 1H), 1.47 (s, 9H).

Step G. A mixture of (±)-(3aR,6aS)-*tert*-butyl 5-(2-(trifluoromethyl)phenyl)-3,3a,6,6a-tetrahydrocyclopenta[*c*]pyrrole-2(1H)-carboxylate ((±)-**29**, 8.63 g, 24.41 mmol) and 10% Pd/C (1.57 g, wet, 10% w/w) in CH_3OH (50 mL) was subjected to an atmosphere of H_2 gas (40 psi) using a Parr Shaker apparatus at rt for 16 h. The mixture was filtered through celite and the filtrate was concentrated under reduced pressure. The resulting residue was purified by flash column chromatography (0%–30% EtOAc in hexanes) to give (3aR,5r,6aS)-*tert*-butyl 5-(2-(trifluoromethyl)phenyl)hexahydrocyclopenta[c]pyrrole-2(1H)-carboxylate (**30**) as a clear, viscous oil (0.910 g, 85%): ^{1}H NMR (500 MHz, $CDCl_3$) δ 7.69 (m, 1H), 7.51 (m, 2H), 7.25 (m, 1H), 3.49 (m, 5H), 2.75 (m, 2H), 2.92 (m, 2H), 1.52 (m, 2H), 1.48 (s, 9H).

Step H. To a 0 °C cooled solution of (3aR,5r,6aS)-*tert*-butyl 5-(2-(trifluoromethyl)phenyl)hexahydrocyclopenta[*c*]pyrrole-2(1H)-carboxylate (**30**, 7.94 g, 22.32 mmol) in CH_2Cl_2 (60 mL) was added a 2 M HCl solution in Et_2O (60 mL), and the mixture was allowed to stir at rt for 24 h. The mixture was diluted with Et_2O (200 mL) and the precipitated product was filtered to give (3a*R*,5*r*,6a*S*)-5-(2-(trifluoromethyl)phenyl)octahydrocyclopenta[c]pyrrole hydrochloride (**31**) as a white

solid (5.90 g, 91%): ^{1}H NMR (500 MHz, $CDCl_3$) δ 10.17 (bs, 1H), 8.06 (m, 1H), 7.59 (m, 1H), 7.53 (m, 1H), 7.27 (m, 1H), 3.42 (m, 2H), 3.38 (m, 3H), 3.01 (m, 2H), 2.36 (m, 2H), 1.96 (m, 2H); MS (ESI+) *m/z* 256 $[M + H]^+$.

6-Fluoro-[1,2,4]triazolo[4,3-*a*]pyridin-3-yl)(4-(2-(trifluoromethyl)phenyl)piperidin-1-yl)methanone (34). *Step A*. A solution of 5-fluoro-2-hydrazinylpyridine (0.460 g, 3.62 mmol) and ethyl 2-oxoacetate (50% in toluene, 0.739 g, 3.62 mmol) in CH_3OH (20 mL) was heated at 60 °C for 1 h. The mixture was then allowed to cooled to rt and concentrated under reduced pressure. The residue was dissolved in CH_2Cl_2 (20 mL) and $PhI(OAc)_2$ (1.28 g, 3.98 mmol) was added. The resulting mixture stirred for 1 h and was subsequently concentrated under reduced pressure. The residue was chromatographed over silica gel (0–80% EtOAc in hexanes) to give ethyl 6-fluoro-[1,2,4]triazolo[4,3-*a*]pyridine-3-carboxylate as an off- white solid (0.331 g, 43%): ^{1}H NMR (300 MHz, $CDCl_3$) δ 9.18 (m, 1H), 8.00–7.95 (m, 1H), 7.49–7.42 (m, 1H), 4.60 (q, *J* = 7.1 Hz, 2H), 1.52 (t, *J* = 7.1 Hz, 3H); MS (ESI+) *m/z* 210 $[M+H]^+$.

Step B. To a solution of ethyl 6-fluoro-[1,2,4]triazolo[4,3-*a*]pyridine-3-carboxylate (0.100 g, 0.478 mmol) in THF (5 mL) was added a solution of $LiOH•H_2O$ (0.040 g, 0.956 mmol) in H_2O (2 mL). The mixture stirred for 20 min and was then acidified to pH 6 with 2 N aqueous HCl followed by subsequent concentration under reduced pressure. The resulting residue (**33a**) was added to a mixture of 4-(2-(trifluoromethyl)phenyl)piperidine hydrochloride (**10**, 0.127 g, 0.478 mmol), HBTU (0.423 g, 0.956 mmol), *i*-Pr_2NEt (0.185 g, 1.43 mmol) in DMF (4 mL). The mixture stirred at rt for 16 h and was then poured into H_2O and extracted with EtOAc (3 × 30 mL). The combined organic extracts were washed

with brine (2 × 30 mL), dried over Na_2SO_4, filtered, and concentrated under reduced pressure. The resulting residue was chromatographed over silica gel (0–50% EtOAc in hexanes) and freeze dried to give (6-fluoro-[1,2,4]triazolo[4,3-*a*]pyridin-3-yl)(4-(2-(trifluoromethyl)phenyl)piperidin-1-yl)methanone (**34**) as a white solid (0.101 g, 53%): mp 168–170 °C; ^{1}H NMR (300 MHz, $CDCl_3$) δ 9.18 (s, 1H), 7.88 (m, 1H), 7.66 (d, *J* = 7.5 Hz, 1H), 7.55–7.30 (m, 4H), 5.76 (m, 1H), 4.99 (m, 1H), 3.40–3.30 (m, 2H), 2.98 (m, 1H), 2.03–1.76 (m, 4H); MS (ESI+) *m/z* 393 $[M+H]^+$; HPLC 97.8% purity (AUC), t_R = 19.3 min (Method B).

(6-Chloro-[1,2,4]triazolo[4,3-*a*]pyridin-3-yl)(4-(2-(trifluoromethyl)phenyl)piperidin-1-yl)methanone (35). Compound **35** was prepared according to a similar procedure described for the synthesis of **34**. mp 158–160 °C; ^{1}H NMR (300 MHz, $CDCl_3$) δ 9.27 (m, 1H), 7.84 (m, 1H), 7.66 (d, *J* = 7.8 Hz, 1H), 7.55–7.30 (m, 4H), 5.73–5.68 (m, 1H), 5.00–4.94 (m, 1H), 3.39–3.28 (m, 2H), 3.03–2.93 (m, 1H), 2.04–1.76 (m, 4H); MS (ESI+) *m/z* 408.9, 410.8, 412.0 $[M+H]^+$; HPLC 97.0% purity (AUC), t_R = 11.5 min (Method A).

(6-Methoxy-[1,2,4]triazolo[4,3-*a*]pyridin-3-yl)(4-(2 (trifluoromethyl)phenyl)piperidin-1-yl)methanone (36). Compound **36** was prepared according to a similar procedure described for the synthesis of **34**. mp 152–154 °C; ^{1}H NMR (300 MHz, $CDCl_3$) δ 8.70 (d, *J* = 1.8 Hz, 1H), 7.76 (dd, *J* = 9.9, 1.0 Hz, 1H), 7.65 (d, *J* = 7.8 Hz, 1H), 7.55–7.44 (m, 2H), 7.32 (t, *J* = 7.8 Hz, 1H), 7.22 (dd, J = 9.9, 2.4 Hz, 1H), 5.76 (m, 1H), 4.97 (m, 1H), 3.90 (s, 3H), 3.39–3.29 (m, 2H), 2.98 (m, 1H), 2.03–1.77 (m, 4H); MS (ESI+) *m/z* 405 $[M+H]^+$; HPLC 99.4% purity (AUC), t_R = 16.4 min (Method A).

(6-Ethoxy-[1,2,4]triazolo[4,3-*a*]pyridin-3-yl)(4-(2-(trifluoromethyl)phenyl)piperidin-1-yl)methanone (37). Compound **37** was prepared according to a similar procedure

described for the synthesis of **34**. mp 113–115 °C; ^{1}H NMR (300 MHz, $CDCl_3$) δ 8.68 (d, *J* = 1.8 Hz, 1H), 7.76 (m, 1H), 7.65 (d, *J* = 7.8 Hz, 1H), 7.54–7.44 (m, 2H), 7.34–7.19 (m, 2H), 5.78–5.73 (m, 1H), 4.96 (m, 1H), 4.12–4.04 (m, 2H), 3.37–2.29 (m, 2H), 3.01–2.92 (m, 1H), 2.03–1.76 (m, 4H), 1.48 (t, *J* = 7.2 Hz, 3H); MS (ESI+) *m/z* 419 $[M+H]^+$; HPLC >99% purity (AUC), t_R = 11.3 min (Method A).

(6-(Trifluoromethyl)-[1,2,4]triazolo[4,3-*a*]pyridin-3-yl)(4-(2 (trifluoromethyl)phenyl)piperidin-1-yl)methanone (38). Compound **38** was prepared according to a similar procedure described for the synthesis of **34**. mp 144–146 °C; ^{1}H NMR (300 MHz, $CDCl_3$) δ 9.60 (m, 1H), 8.00 (d, *J* = 9.6 Hz, 1H), 7.66 (d, *J* = 7.8 Hz, 1H), 7.59–7.43 (m, 3H), 7.33 (t, *J* = 7.5 Hz, 1H), 5.73–5.68 (m, 1H), 5.01–4.96 (m, 1H), 3.41–3.32 (m, 2H), 3.05–2.96 (m, 1H), 2.06–1.78 (m, 4H); MS (ESI+) *m/z* 443 $[M+H]^+$; HPLC 99.4% purity (AUC), t_R = 11.3 min (Method A).

(6-Fluoro-[1,2,4]triazolo[4,3-*a*]pyridin-3-yl)((3aR,5R,6aS)-5-(2 (trifluoromethyl)phenyl)hexahydrocyclopenta[*c*]pyrrol-2(1H)-yl)methanone (39). To a solution of ethyl 6-fluoro-[1,2,4]triazolo[4,3-*a*]pyridine-3-carboxylate (0.050 g, 0.239 mmol) in THF (4 mL) was added a solution of LiOH•H_2O (0.030 g, 0.717 mmol) in H_2O (3 mL). The mixture was stirred for 20 min, acidified with 2 N aqueous HCl to pH 6, and concentrated under reduced pressure. To a mixture of the resulting crude residue (**33a**) in DMF (4 mL) was added (3a*R*,5*R*,6a*S*)-5-(2-(trifluoromethyl)phenyl)octahydrocyclopenta[*c*]pyrrole hydrochloride (**31**, 0.070 g, 0.239 mmol), HBTU (0.211 g, 0.478 mmol), and *i*-Pr_2NEt (0.093 g, 0.717 mmol). The mixture stirred at rt for 16 h and then poured into H_2O (30 mL). The mixture was extracted with

EtOAc (3 × 30 mL) and the combined organic extracts were washed with brine (3 × 30 mL), dried over Na_2SO_4, filtered, and concentrated under reduced pressure. The resulting residue was chromatographed over silica gel (0%–50% EtOAc in hexanes) and freeze dried to give (6-fluoro-[1,2,4]triazolo[4,3-a]pyridin-3-yl)((3a*R*,5*R*,6a*S*)-5-(2-(trifluoromethyl)phenyl)hexahydrocyclopenta[*c*]pyrrol-2(1*H*)-yl)methanone (**39**) as a white solid (0.073 g, 73%): mp 139–141 °C; ^{1}H NMR (300 MHz, $CDCl_3$) δ 9.43 (m, 1H), 7.92–7.87 (m, 1H), 7.62 (d, *J* = 8.1 Hz, 1H), 7.54–7.47 (m, 2H), 7.43–7.36 (m, 1H), 7.28 (m, 1H), 4.53–4.41 (m, 2H), 4.00–3.85 (m, 2H), 3.63–3.53 (m, 2H), 2.47–2.36 (m, 2H), 1.73–1.60 (m, 2H); MS (ESI+) *m/z* 419 $[M+H]^+$; HPLC >99% purity (AUC), t_R = 18.0 min (Method A).

(6-Chloro-[1,2,4]triazolo[4,3-*a*]pyridin-3-yl)((3aR,5R,6aS)-5-(2-(trifluoromethyl)phenyl)hexahydrocyclopenta[*c*]pyrrol-2(1H)-yl)methanone (40). Compound **40** was prepared according to a similar procedure described for the synthesis of **39**. mp 147–150 °C; ^{1}H NMR (500 MHz, $CDCl_3$) δ 9.54 (m, 1H), 7.84 (m, 1H), 7.62 (d, *J* = 8.0 Hz, 1H), 7.53–7.48 (m, 2H), 7.41 (dd, *J* = 10.0, 2.0 Hz, 1H), 7.28 (t, *J* = 8.0 Hz, 1H), 4.50–4.41 (m, 2H), 3.99–3.86 (m, 2H), 3.63–3.55 (m, 1H), 3.04–2.87 (m, 2H), 2.44–2.37 (m, 2H), 1.70–1.62 (m, 2H); MS (ESI+) *m/z* 434.9, 436.4, 437.3 $[M+H]^+$; HPLC >99% purity (AUC), t_R = 12.1 min (Method A).

(6-Methoxy-[1,2,4]triazolo[4,3-*a*]pyridin-3-yl)((3aR,5R,6aS)-5-(2-(trifluoromethyl)phenyl)hexahydrocyclopenta[*c*]pyrrol-2(1H)-yl)methanone (41). Compound **41** was prepared according to a similar procedure described for the synthesis of **39**. mp 147–152 °C; ^{1}H NMR (300 MHz, $CDCl_3$) δ 9.00 (m, 1H), 7.78 (dd, *J* = 9.9, 0.6 Hz, 1H), 7.63–7.47 (m, 3H), 7.30–7.21 (3H), 4.54–4.42 (m, 2H), 4.00–3.85 (m, 5H), 3.66–3.53

(m, 1H), 3.04–2.87 (m, 2H), 2.46–2.36 (m, 2H), 1.74–1.61 (m, 2H); MS (ESI+) *m/z* 431 $[M+H]^+$; HPLC 99.8% purity (AUC), t_R = 14.5 min (Method A).

(6-Ethoxy-[1,2,4]triazolo[4,3-*a*]pyridin-3-yl)((3aR,5R,6aS)-5-(2-(trifluoromethyl)phenyl)hexahydrocyclopenta[*c*]pyrrol-2(1H)-yl)methanone (42). Compound **42** was prepared according to a similar procedure described for the synthesis of **39**. mp 110–112 °C; ^{1}H NMR (300 MHz, $CDCl_3$) δ 8.98 (d, *J* = 1.5 Hz, 1H), 7.77 (m, 1H), 7.61 (d, *J* = 7.8 Hz, 1H), 7.54–7.47 (m, 2H), 7.30–7.23 (m, 2H), 4.54–4.42 (m, 2H), 4.10 (q, *J* = 6.9 Hz, 2H), 3.99–3.84 (m, 2H), 3.65–3.52 (m, 1H), 3.06–2.84 (m, 2H), 2.46–2.35 (m, 2H), 1.74–1.60 (m, 2H), 1.48 (t, *J* = 6.9 Hz, 3H); MS (ESI+) *m/z* 445 $[M+H]^+$; HPLC >99% purity (AUC), t_R = 12.0 min (Method A).

(6-(Trifluoromethyl)-[1,2,4]triazolo[4,3-*a*]pyridin-3-yl)((3aR,5R,6aS)-5-(2-(trifluoromethyl)phenyl)hexahydrocyclopenta[*c*]pyrrol-2(1H)-yl)methanone (43). Compound **43** was prepared according to a similar procedure described for the synthesis of **39**. mp 154–156 °C; ^{1}H NMR (300 MHz, $CDCl_3$) δ 9.88 (m, 1H), 8.00 (d, *J* = 9.6 Hz, 1H), 7.63–7.49 (m, 4H), 7.27 (m, 1H), 4.53–4.41 (m, 2H), 4.02–3.86 (m, 2H), 3.65–3.50 (m, 1H), 3.06–2.89 (m, 2H), 2.48–2.36 (m, 2H), 1.72–1.61 (m, 2H); MS (ESI+) *m/z* 469 $[M+H]^+$; HPLC >99% purity (AUC), t_R = 12.6 min (Method A).

3-(4-(2-(Trifluoromethyl)phenyl)piperidine-1-carbonyl)-[1,2,4]triazolo[4,3-*a*]pyridine-6-carbonitrile (48). *Step A*. To a solution of ethyl 6-bromo-[1,2,4]triazolo[4,3-*a*]pyridine-3-carboxylate (0.365 g, 1.35 mmol) in THF (15 mL) was added a solution LiOH•H_2O (0.057 g, 1.35 mmol) in water (5 mL). The mixture stirred for 20 min, was acidified with aqueous 2 N HCl to pH 6, and concentrated under reduced pressure. To a

mixture of the resulting crude residue (**44**) in DMF (10 mL) was added 4-(2-(trifluoromethyl)phenyl)piperidine hydrochloride (**10**, 0.359 g, 1.35 mmol), HBTU (898 g, 2.03 mmol), and *i*-PrNEt (0.523 g, 4.05 mmol). The mixture stirred at rt for 16 h, was diluted with H_2O (50 mL), and extracted with EtOAc (3 × 50 mL). The combined organic extracts were washed with brine (3 × 60 mL), dried over Na_2SO_4, filtered, and concentrated under reduced pressure. The resulting residue was chromatographed over silica gel (0–60% EtOAc in hexanes) to give (6-bromo-[1,2,4]triazolo[4,3-*a*]pyridin-3-yl)(4-(2-(trifluoromethyl)phenyl)piperidin-1-yl)methanone (**45**) as a white solid (0.516 g, 84%): ^{1}H NMR (300 MHz, $CDCl_3$) δ 9.38 (m, 1H), 7.78 (dd, *J* = 9.6, 0.8 Hz, 1H), 7.66 (d, *J* = 7.8 Hz, 1H), 7.55–7.44 (m, 3H), 7.32 (t, *J* = 7.7 Hz, 1H), 5.72–5.67 (m, 1H), 5.00–4.94 (m, 1H), 3.39–3.30 (m, 2H), 3.03–2.93 (m, 1H), 2.01–1.81 (m, 4H); MS (ESI+) *m/z* 453 (M+H).

Step B. A mixture of **45** (0.080 g, 0.176 mmol), $ZnCN_2$ (0.041 g, 0.352 mmol), $Pd(PPh_3)_4$ (0.020 g, 0.0176 mmol), and DMF (1 mL) was heated under microwave irradiation at 130 °C for 30 min. After cooling to rt, the mixture was diluted with CH_2Cl_2 (30 mL), washed with brine (2 × 30 mL), dried over Na_2SO_4, filtered, and concentrated under reduced pressure. The resulting residue was chromatographed over silica gel (0–40% EtOAc in hexanes) to give 3-(4-(2-(trifluoromethyl)phenyl)piperidine-1-carbonyl)-[1,2,4]triazolo[4,3-*a*]pyridine-6-carbonitrile (**48**) as a white solid (0.063 g, 87%): ^{1}H NMR (300 MHz, $CDCl_3$) δ 9.72 (m, 1H), 7.97 (dd, *J* = 9.5, 1.0 Hz, 1H), 7.66 (d, *J* = 7.9 Hz, 1H), 7.55–7.42 (m, 3H), 7.33 (t, *J* = 7.6 Hz, 1H), 5.74–5.69 (m, 1H), 5.00–4.95 (m, 1H), 3.42–3.33 (m, 2H), 3.05–2.95 (m, 1H), 2.06–1.81 (m, 4H); MS (ESI+) *m/z* 400 $[M+H]^+$; HPLC >99% purity (AUC), t_R = 13.9 min (Method A).

(6-Methyl-[1,2,4]triazolo[4,3-*a*]pyridin-3-yl)(4-(2 (trifluoromethyl)phenyl)piperidin-1-yl)methanone (49). To a mixture of **45** (0.064 g, 0.141 mmol), $Fe(acac)_3$ (0.005 g, 0.0141 mmol), NMP (0.05 mmol), and THF (1 mL) was added CH_3MgBr (1.4 M solution in THF/toluene, 0.15 mL, 0.212 mmol) dropwise at 0 °C. The resulting mixture was allowed to warm to rt and stirred for 1 h. 2 N aqueous HCl (0.5 mL) was then added and the mixture was poured into saturated aqueous $NaHCO_3$ (10 mL). The aqueous mixture was extracted with EtOAc (3 × 10 mL) and the combined organic extracts were washed with brine, dried over Na_2SO_4, filtered, and concentrated under reduced pressure. The resulting residue was chromatographed over silica gel (0–70% EtOAc in hexanes) and freeze dried to give (6-methyl-[1,2,4]triazolo[4,3-*a*]pyridin-3-yl)(4-(2-(trifluoromethyl)phenyl)piperidin-1-yl)methanone (**49**) as a white solid (0.044 g, 80%): mp 145–147 °C; ^{1}H NMR (300 MHz, $CDCl_3$) δ 8.92 (m, 1H), 7.78 (m, 1H), 7.66 (d, J = 7.8 Hz, 1H), 7.55–7.44 (m, 2H), 7.34–7.26 (m, 2H), 5.70–5.65 (m, 1H), 4.98 (m, 1H), 3.38–3.28 (m, 2H), 3.02–2.92 (m, 1H), 2.39 (s, 3H), 2.07–1.67 (m, 4H); MS (ESI+) *m/z* 389 $[M+H]^+$; HPLC 98.6% purity (AUC), t_R = 14.1 min (Method A).

3-((3aR,5R,6aS)-5-(2-(Trifluoromethyl)phenyl)octahydrocyclopenta[*c*]pyrrole-2-carbonyl)-[1,2,4]triazolo[4,3-*a*]pyridine-6-carbonitrile (51). *Step A.* To a solution of ethyl 6-bromo-[1,2,4]triazolo[4,3-*a*]pyridine-3-carboxylate (0.485 g, 1.80 mmol) in THF (15 mL) was added a solution of $LiOH{\bullet}H_2O$ (0.076 g, 1.80 mmol) in H_2O (5 mL). The mixture was stirred for 20 min, acidified with 2 N HCl to pH 6 and concentrated under reduced pressure. To the residue were added **31** (0.525 g, 1.80 mmol), HBTU (1.20 g, 2.7 mmol), *i*-Pr_2NEt (0.698 g, 5.40 mmol), and DMF (15 mL). The

mixture was stirred at rt for 16 h and then poured into H_2O. The mixture was extracted with EtOAc (3 × 50 mL) and the combined organic extracts were washed with brine (2 × 150 mL), dried over Na_2SO_4, filtered, and concentrated under reduced pressure. The resulting residue was chromatographed over silica gel (0%–50% EtOAc in hexanes) to give (6-bromo-[1,2,4]triazolo[4,3-*a*]pyridin-3-yl)((3a*R*,5*R*,6a*S*)-5-(2-(trifluoromethyl)phenyl)hexahydrocyclopenta[*c*]pyrrol-2(1*H*)-yl)methanone (**50**) as a white solid (0.485 g, 56%): ^{1}H NMR (300 MHz, $CDCl_3$) δ 9.65 (m, 1H), 7.98 (dd, *J* = 9.6, 0.9 Hz, 1H), 7.62 (d, *J* = 7.9 Hz, 1H), 7.53–7.47 (m, 3H), 7.28 (m, 1H), 4.51–4.39 (m, 2H), 4.00–3.85 (m, 2H), 3.64–3.52 (m, 1H), 3.07–2.84 (m, 2H), 2.50–2.33 (m, 2H), 1.72–1.60 (m, 2H); MS (ESI+) *m/z* 479 $[M+H]^+$.

Step B. A mixture of **50** (0.080 g, 0.167 mmol), $ZnCN_2$ (0.039 g, 0.335 mmol), $Pd(PPh_3)_4$ (0.019 g, 0.0167 mmol), and DMF (2 mL) was heated at 130 °C under microwave irradiation for 30 min. After cooling to rt, the mixture was diluted with H_2O (50 mL) and extracted with EtOAc (3 × 50 mL). The combined organic extracts were washed with brine (2 × 50 mL), dried over Na_2SO_4, filtered, and concentrated under reduced pressure. The resulting residue was chromatographed over silica gel (0%–50% EtOAc in hexanes) to give 3-((3aR,5R,6aS)-5-(2-(trifluoromethyl)phenyl)octahydrocyclopenta[*c*]pyrrole-2-carbonyl)-[1,2,4]triazolo[4,3-*a*]pyridine-6-carbonitrile (**51**) as a white solid (0.073 g, 100%): mp 60–65 °C; ^{1}H NMR (300 MHz, $CDCl_3$) δ 9.98 (m, 1H), 7.99 (dd, *J* = 9.5, 0.9 Hz, 1H), 7.63 (d, *J* = 7.8 Hz, 1H), 7.53–7.47 (m, 3H), 7.28 (m, 1H), 4.51–4.40 (m, 2H), 4.02–3.86 (m, 2H), 3.66–3.54 (m, 1H), 3.09–2.86 (m, 2H), 2.49–2.37 (m, 2H), 1.71–1.60 (m, 2H); MS (ESI+) *m/z* 426 $[M+H]^+$; HPLC 99.5% purity (AUC), t_R = 14.1 min (Method A).

3-((3aR,5R,6aS)-5-(2-(trifluoromethyl)phenyl)octahydrocyclopenta[*c*]pyrrole-2-carbonyl)-[1,2,4]triazolo[4,3-*a*]pyridine-6-carboxylic Acid (52). *Step A*. A mixture of **50** (0.080 g, 0.167 mmol), $MO(CO)_6$ (0.066 g, 0.251 mmol), $Pd(OAc)_2$ (0.0037 g, 0.0167 mmol), xantphos (0.014 g, 0.0251 mmol), CH_3OH (0.054 g, 1.67 mmol), Cs_2CO_3(109 g, 0.334 mmol), and 1,4-dioxane (2 mL) was heated at 80 °C for 2 h in a sealed vessel. The mixture was allowed to cool to rt and then directly chromatographed over silica gel (0%–60% EtOAc in hexanes) to give methyl 3-((3a*R*,5*R*,6a*S*)-5-(2-(trifluoromethyl)phenyl)octahydrocyclopenta[*c*]pyrrole-2-carbonyl)-[1,2,4]triazolo[4,3-*a*]pyridine-6-carboxylate as a white solid (0.024 g, 31%): ^{1}H NMR (300 MHz, $CDCl_3$) δ 10.21 (s, 1H), 8.00–7.87 (m, 2H), 7.63–7.47 (m, 3H), 7.28 (m, 1H), 4.52–4.21 (m, 2H), 4.03–3.88 (m, 5H), 3.65–3.53 (m, 1H), 3.06–2.89 (m, 2H), 2.47–2.36 (m, 2H), 1.73–1.61 (m, 2H); MS (ESI+) *m/z* 459 $[M+H]^+$.

Step B. To a solution of 3-((3a*R*,5*R*,6a*S*)-5-(2-(trifluoromethyl)phenyl)octahydrocyclopenta[*c*]pyrrole-2-carbonyl)-[1,2,4]triazolo[4,3-*a*]pyridine-6-carboxylate (0.024 g, 0.0523 mmol) in THF (2 mL) was added a solution of $LiOH•H_2O$ (0.004 g, 0.105 mmol) in H_2O (1 mL). The mixture stirred for 30 min at rt, was acidified to pH 6 with 2 N aqueous HCl, and subsequently purified by C-18 reverse phase column chromatography (10%–60% CH_3CN in H_2O) to give 3-((3aR,5R,6aS)-5-(2-(trifluoromethyl)phenyl)octahydrocyclopenta[*c*]pyrrole-2-carbonyl)-[1,2,4]triazolo[4,3-*a*]pyridine-6-carboxylic acid (**52**) as a white solid (0.020 g, 86%): ^{1}H NMR (300 MHz, DMSO-d_6) δ 9.51 (s, 1H), 7.98 (d, *J* = 9.3 Hz, 1H), 7.80–7.74 (m, 2H), 7.66–7.61 (m, 2H), 7.38 (t, *J* = 7.5 Hz, 1H), 4.29–4.18 (m, 2H), 3.88–3.78 (m, 2H), 3.41 (m, 1H), 2.97–2.82 (m,

2H), 2.32–2.19 (m, 2H), 1.71–1.66 (m, 2H); MS (ESI+) *m/z* 445 $[M+H]^+$; HPLC 97.8% purity (AUC), t_R = 12.8 min (Method A).

1,1-Dimethyl-3-(3-((3aR,5R,6aS)-5-(2 (trifluoromethyl)phenyl)octahydrocyclopenta[*c*]pyrrole-2-carbonyl)-[1,2,4]triazolo[4,3-*a*]pyridin-6-yl)urea (53). A mixture of **50** (0.066 g, 0.138 mmol), $Pd(OAc)_2$ (0.003 g, 0.0138 mmol), xantphos (0.012 g, 0.0207 mmol), *N*,*N*-dimethylurea (0.018 g, 0.207 mmol), Cs_2CO_3 (0.067 g, 0.207 mmol), and 1,4-dioxane (2 mL) was heated at 100 °C for 6 h and cooled to rt. The mixture was chromatographed over silica gel (0%–10% CH_3OH in CH_2Cl_2) and further purified by C-18 reverse phase column chromatography (10%–60% CH_3CN in H_2O) to give 1,1-dimethyl-3-(3-((3aR,5R,6aS)-5-(2-(trifluoromethyl)phenyl)octahydrocyclopenta[*c*]pyrrole-2-carbonyl)-[1,2,4]triazolo[4,3-*a*]pyridin-6-yl)urea (**53**) as a white solid (0.023 g, 34%): mp 110–115 °C; ^1H NMR (300 MHz, $CDCl_3$) δ 9.43 (m, 1H), 7.79 (m, 1H), 7.69–7.47 (m, 4H), 7.30–7.25 (m, 1H), 4.48–4.37 (m, 2H), 3.97–3.83 (m, 2H), 3.63–3.51 (m, 1H), 3.06 (s, 6H), 3.02–2.83 (m, 2H), 2.45–2.34 (m, 2H), 1.72–1.59 (m, 2H); MS (ESI+) *m/z* 487 $[M+H]^+$; HPLC 99.7% purity (AUC), t_R = 12.2 min (Method A).

***N*-Methyl-3-((3aR,5R,6aS)-5-(2-(trifluoromethyl)phenyl)octahydrocyclopenta[*c*]pyrrole-2-carbonyl)-[1,2,4]triazolo[4,3-*a*]pyridine-6-sulfonamide (54)**. *Step A*. A mixture of **50** (0.090 g, 0.188 mmol), $Pd(OAc)_2$ (0.0042 g, 0.0188 mmol), xantphos (0.016 g, 0.0282 mmol), benzyl thiol (0.035 g, 0.282 mmol), *i*-Pr_2NEt (0.073 g, 0.564 mmol), and 1,4-dioxane (2 mL) was heated at 110 °C for 16 h. The mixture was allowed to cool to rt then directly chromatographed

over silica gel (0%–50% EtOAc in hexanes) to give (6-(benzylthio)-[1,2,4]triazolo[4,3-*a*]pyridin-3-yl)((3a*R*,5*R*,6a*S*)-5-(2-(trifluoromethyl)phenyl)hexahydrocyclopenta[*c*]pyrrol-2(1*H*)-yl)methanone as a mixture with unreacted benzyl mercaptan (0.090 g in a ratio of 1:1.4), a thick oil; MS (ESI+) *m/z* 523 $[M+H]^+$.

Step B. Crude (6-(benzylthio)-[1,2,4]triazolo[4,3-*a*]pyridin-3-yl)((3a*R*,5*R*,6a*S*)-5-(2-(trifluoromethyl)phenyl)hexahydrocyclopenta[*c*]pyrrol-2(1*H*)-yl)methanone was dissolved in HOAc (3 mL) and H_2O (1 mL). *N*-Chlorosuccinimide (NCS, 0.040 g, 0.296 mmol) was added and the mixture stirred for 3 h at rt, then concentrated under reduced pressure. The residue was partitioned between saturated aqueous Na_2CO_3 (50 mL) and CH_2Cl_2 (50 mL). The organic layer was separated and washed with brine (50 mL), dried over Na_2SO_4, filtered, and concentrated under reduced pressure. The resulting residue was chromatographed over silica gel (0%–50% EtOAc in hexanes) to give 3-((3a*R*,5*R*,6a*S*)-5-(2-(trifluoromethyl)phenyl)octahydrocyclopenta[*c*]pyrrole-2-carbonyl)-[1,2,4]triazolo[4,3-*a*]pyridine-6-sulfonyl chloride as a mixture with unreacted NCS (0.032 g), a thick oil; ^{1}H NMR (300 MHz, $CDCl_3$) δ 10.28 (m, 1H), 8.08 (dd, *J* = 9.7, 0.8 Hz, 1H), 7.89(dd, *J* = 9.7, 1.9 Hz, 1H), 7.62 (d, *J* = 7.8 Hz, 1H), 7.53–7.47 (m, 2H), 7.29 (m, 1H), 4.51–4.40 (m, 2H), 4.03–3.87 (m, 2H), 3.66–3.53 (m, 1H), 3.10–2.86 (m, 2H), 2.49–2.37 (m, 2H), 1.72–1.60 (m, 2H); MS (ESI+) *m/z* 499 $[M+H]^+$.

Step C. Crude 3-((3a*R*,5*R*,6a*S*)-5-(2-(trifluoromethyl)phenyl)octahydrocyclopenta[*c*]pyrrole-2-carbonyl)-[1,2,4]triazolo[4,3-*a*]pyridine-6-sulfonyl chloride was dissolved in CH_2Cl_2 (1 mL) and cooled to 0 °C. A mixture of *N*-methylamine (33% in EtOH, 0.018 g, 0.192 mmol) and *i*-Pr_2NEt (0.025 g, 0.192 mmol)

in CH_2Cl_2 (1 mL) was added. The mixture stirred at rt for 2 h and was then concentrated under reduced pressure. The residue was chromatographed by C-18 reverse phase column chromatography (10%–50% CH_3CN in H_2O) to give *N*-methyl-3-((3a*R*,5*R*,6a*S*)-5-(2-(trifluoromethyl)phenyl)octahydrocyclopenta[*c*]pyrrole-2-carbonyl)-[1,2,4]triazolo[4,3-*a*]pyridine-6-sulfonamide (**54**) as a white solid (6.0 mg, 6% over three steps): mp 148–152 °C; ^{1}H NMR (300 MHz, $CDCl_3$) δ 10.0 (m, 1H), 7.99 (dd, *J* = 9.6, 0.8 Hz, 1H), 7.73(dd, *J* = 9.6, 1.7 Hz, 1H), 7.62 (d, *J* = 7.2 Hz, 1H), 7.54–7.47 (m, 2H), 7.28 (m, 1H), 4.59 (q, *J* = 5.2 Hz, 1H), 4.50–4.39 (m, 2H), 4.01–3.86 (m, 2H), 3.65–3.53 (m, 1H), 3.08–2.86 (m, 2H), 2.81 (d, *J* = 5.3 Hz, 3H), 2.48–2.36 (m, 2H), 1.71–1.60 (m, 2H); MS (ESI+) *m/z* 494 $[M+H]^+$; HPLC 99.5% purity (AUC), t_R = 13.5 min (Method A).

3-(4-(3-Fluoro-2-(trifluoromethyl)phenyl)piperidine-1-carbonyl)-[1,2,4]triazolo[4,3-*a*]pyridine-6-carbonitrile (59). *Step A*. A solution of *tert*-butyl 4-oxopiperdine-1-carboxylte (**55**, 1.0 g, 5.02 mmol), in THF (30 mL) was cooled to -78 °C. LiHMDS (1.0 M solution in THF, 6.52 mL, 6.52 mmol) was added dropwise over 30 min. The mixture stirred at -78 °C for 1 h, then a solution of 1,1,1-trifluoro-*N*-phenyl-*N*-((trifluoromethyl)sulfonyl)methanesulfonamide (2.52 g, 7.05 mmol) in THF (5.0 mL) was added dropwise over 30 min. The mixture stirred at 0 °C for 3 h and was then concentrated under redued pressure. The residue was chromatographed over silical gel (0%–100% EtOAc in hexanes) to provide *tert*-butyl 4-(((trifluoromethyl)sulfonyl)oxy)-3,6-dihydropyridine-1(2H)-carboxylate (**56**) as a light-yellow viscous oil (1.50 g, 90%): ^{1}H NMR (300 MHz, $CDCl_3$) δ 5.75 (br s, 1H), 4.05–4.02 (m, 2H), 3.64–3.60 (m, 2H), 2.44–2.42 (m, 2H), 1.46 (s, 9H).

Step B. A mixture of *tert*-butyl 4-(((trifluoromethyl)sulfonyl)oxy)-3,6-dihydropyridine-1(2H)-carboxylate (**56**, 3.50 g, 10.6 mmol), 3-fluoro-(2-trifluoromethyl)phenylboronic acid (2.19 g, 10.6 mmol), $Pd(PPh_3)_4$ (1.22 g, 1.06 mmol), and 2.0 M aqueous Na_2CO_3 solution (65 mL) in DME (120 mL) was heated at 80 °C for 6 h. The mixture was allowed to cool to rt and was diluted with 5% aqueous LiCl solution (100 mL). The aqueous mixture was extracted with EtOAc (3 × 50 mL) and the combined organic extracts were washed with brine (2 × 50 mL) and concentrated under reduced pressure. The residue was diluted with CH_2Cl_2 (100 mL) and filtered through a 300 mL silica gel plug, eluting with 10% EtOAc in hexanes (800 mL). The resulting filtrate was concentrated under reduced pressure and chromatographed over silica gel (0%–50% EtOAc in hexanes) to provide *tert*-butyl 4-(3-fluoro-2-(trifluoromethyl)phenyl)-3,6-dihydropyridine-1(2H)-carboxylate (**57**) as a light-yellow oil (2.39 g, 69%): ^{1}H NMR (300 MHz, DMSO-d_6) δ 7.75–7.61 (m, 1H), 7.49–7.36 (m, 1H), 7.17 (d, *J* = 7.8 Hz, 1H), 5.63–5.54 (m, 1H), 3.97–3.86 (m, 2H), 3.57–3.45 (m, 2H), 2.31–2.18 (m, 2H), 1.42 (s, 9H).

Step C. A mixture of *tert*-butyl 4-(3-fluoro-2-(trifluoromethyl)phenyl)-3,6-dihydropyridine-1(2H)-carboxylate (**57**, 4.7 g, 13.6 mmol), and 10% Pd/C (1.0 g) in EtOH (100 mL) was placed under an atmosphere of H_2 (30 psi) at rt for 18 h. The mixture was filtered through celite and the filtrate was concentrated under reduced pressure to give *tert*-butyl 4-(3-fluoro-2-(trifluoromethyl)phenyl)piperidine-1-carboxylate as a clear oil (4.80 g, quantitative): ^{1}H NMR (300 MHz, DMSO-d_6) δ 7.72–7.60 (m, 1H), 7.46 (d, *J* = 8.1 Hz, 1H), 7.30 (dd, *J* = 12.3, 8.1 Hz, 1H), 4.18–4.00 (m, 2H), 3.11–2.95 (m, 1H), 2.92–2.64 (m, 2H), 1.76–1.51 (m, 4H), 1.42 (s, 9H).

Step D. To a solution of *tert*-butyl 4-(3-fluoro-2-(trifluoromethyl)phenyl)piperidine-1-carboxylate (4.70 g, 13.6 mmol) in CH_2Cl_2 (40 mL) was added 2.0 M HCl in Et_2O (40 mL). The mixture stirred at rt for 18 h and was diluted with Et_2O (100 mL). A precipitate formed, which was collected by filtration to give 4-(3-fluoro-2-(trifluoromethyl)phenyl)piperidine hydrochloride (**58**) as a white powder (3.69 g, 96%): ^{1}H NMR (300 MHz, DMSO-d_6) δ 9.09–8.80 (m, 2H), 7.83–7.70 (m, 1H), 7.44–7.29 (m, 2H), 3.42–3.31 (m, 2H), 3.29–3.15 (m, 1H), 3.14–2.95 (m, 2H), 2.11–1.91 (m, 2H), 1.89–1.76 (m, 2H); ESI MS *m/z* = 248 $[M+H]^+$.

Step E. To a solution of ethyl 6-bromo-[1,2,4]triazolo[4,3-*a*]pyridine-3-carboxylate (0.075 g, 0.28 mmol) in THF (2.5 mL) was added a solution of LiOH•H_2O (0.023 g, 0.56 mmol) in H_2O (1.5 mL). The mixture was stirred for 20 min and was subsequently neutralized with 2 N aqueous HCl. The mixture was concentrated under reduced pressure and the resulting residue was diluted in DMF (3.0 mL). To this mixture was added 4-(3-fluoro-2-(trifluoromethyl)phenyl)piperidine hydrochloride (**58**, 0.078 g, 0.28 mmol), HBTU (0.245 g, 0.55 mmol) and *i*-Pr_2NEt (0.11 mL, 0.83 mmol). The resulting mixture stirred at rt for 16 h. The mixture was subsequently diluted with H_2O (20 mL) and extracted with EtOAc (4 × 30 mL). The combined organic extracts were washed with bine, dried over Na_2SO_4, filtered, and concentrated under reduced pressure. The resulting residue was chromatographed over silica gel (0%–50% EtOAc in hexanes) to provide (6-bromo-[1,2,4]triazolo[4,3-a]pyridin-3-yl)(4-(3-fluoro-2-(trifluoromethyl)phenyl)piperidin-1-yl)methanone as an orange oil (0.087 g, 66%): ^{1}H NMR (300 MHz, DMSO-d_6) δ 9.13–9.10 (m, 1H), 7.75–7.62 (m 2H), 7.52–7.46 (m, 1H), 7.38–7.25 (m, 1H), 5.30–5.17 (m, 1H), 4.78–

4.64 (m, 1H), 3.42–3.28 (m, 3H), 3.11–2.92 (m, 1H), 1.98–1.70 (m, 4H); ESI MS *m/z* = 471 $[M+H]^+$.

Step F. A solution of (6-bromo-[1,2,4]triazolo[4,3-a]pyridin-3-yl)(4-(3-fluoro-2-(trifluoromethyl)phenyl)piperidin-1-yl)methanone (0.087 g, 0.19 mmol) and $ZnCN_2$ (0.043 g, 0.37 mmol) in DMF (2.0 mL), was sparged with Ar for 10 min. To this solution was then added $Pd(PPh_3)_4$ (0.021 g, 0.019 mmol) and the vessel was sealed and the mixture was heated to 130 °C via microwave irradiation for 30 min. The mixture was allowed to cool to rt and then diluted with saturated aqueous $NaHCO_3$ solution (30 mL). The aqueous mixture was extracted with EtOAc (3 × 30 mL) and the combined organic extracts were concentrated under reduced pressure. The resulting residue was chromatographed over silica gel (0%–70% EtOAc in hexanes) to provide 3-(4-(3-fluoro-2-(trifluoromethyl)phenyl)piperidine-1-carbonyl)-[1,2,4]triazolo[4,3-a]pyridine-6-carbonitrile (**59**) was a white solid (0.052 g, 67%): ^{1}H NMR (500 MHz, DMSO-d_6) δ 9.54–9.51 (m, 1H), 8.13 (dd, *J* = 9.5, 1.0 Hz, 1H), 7.81 (dd, *J* = 9.5, 1.5 Hz, 1H), 7.71–7.65 (m, 1H), 7.48 (d, *J* = 8.0 Hz, 1H), 7.32 (dd, *J* = 12.5, 8.5 Hz, 1H), 5.17–5.09 (m, 1H), 4.78–4.70 (m, 1H), 3.44–3.28 (m, 2H), 3.09–3.00 (m, 1H), 1.97–1.75 (m, 4H); ESI MS *m/z* = 418 $[M+H]^+$; HPLC >99% purity (AUC), t_R = 16.7 min (Method A).

3-(4-(5-Fluoro-2-(trifluoromethyl)phenyl)piperidine-1-carbonyl)-[1,2,4]triazolo[4,3-*a*]pyridine-6-carbonitrile (61). *Step A*. A mixture of *tert*-butyl 4-(((trifluoromethyl)sulfonyl)oxy)-3,6-dihydropyridine-1(2H)-carboxylate (**56**, 1.10 g, 3.32 mmol), 5-fluoro-(2-trifluoromethyl)phenylboronic acid (0.690 g, 3.32 mmol), $Pd(PPh_3)_4$ (0.384 g, 0.332 mmol), and 2.0 M aqueous Na_2CO_3 solution (20 mL) in DME (50 mL) was

heated at 80 °C for 6 h. The mixture was allowed to cool to rt, diluted with EtOAc (50 mL), and filtered through celite to remove solids. The filtrate was washed with brine (4 × 50 mL) and concentrated under reduced pressure. The resulting residue was chromatographed over silica gel (0%–80% EtOAc in hexanes) to provide *tert*-butyl 4-(5-fluoro-2-(trifluoromethyl)phenyl)-3,6-dihydropyridine-1(2H)-carboxylate as a clear oil (0.542 g, 48%): ^{1}H NMR (300 MHz, DMSO-d_6) δ 7.80 (dd, *J* = 8.4, 6.0 Hz, 1H), 7.42–7.27 (m, 2H), 5.62 (br s, 1H), 3.97–3.87 (m, 2H), 3.51 (t, *J* = 5.7 Hz, 2H), 2.34–2.23 (m, 2H), 1.42 (s, 9H).

Step B. To a solution of *tert*-butyl 4-(5-fluoro-2-(trifluoromethyl)phenyl)-3,6-dihydropyridine-1(2H)-carboxylate (0.542 g, 1.58 mmol) in CH_2Cl_2 (20 mL) was added 2.0 M HCl in Et_2O (10 mL). The mixture stirred at rt for 18 h and was diluted with Et_2O (30 mL). A precipitate formed, which was collected by filtration to give 4-(5-fluoro-2-(trifluoromethyl)phenyl)-1,2,3,6-tetrahydropyridine hydrochloride (**60a**) as a white solid (0.393 g, 88%): ^{1}H NMR (300 MHz, DMSO-d_6) δ 9.26–9.00 (m, 2H), 7.84 (dd, *J* = 8.7, 5.4 Hz, 1H), 7.46–7.36 (m, 1H), 7.24 (dd, *J* = 9.3, 2.4 Hz, 1H), 5.67 (br s, 1H), 3.76–3.64 (m, 2H), 3.27 (t, *J* = 5.7 Hz), 2.70–2.40 (m, 2H).

Step C. A mixture of 4-(5-fluoro-2-(trifluoromethyl)phenyl)-1,2,3,6-tetrahydropyridine hydrochloride (**60a**, 0.393 g, 1.41 mmol) and Pt_2O (0.095 g, 0.42 mmol) in EtOAc (14 mL) was stirred under a balloon of H_2 (1 atm) at rt for 72 h. The mixture was then filtered through celite and the filtrate was concentrated under reduced pressure. The resulting residue was dissolved in CH_2Cl_2 (4 mL) and 2.0 M HCl in Et_2O (4 mL) was then added. The mixture stirred at rt for 18 h and the resulting solids were collected via filtration to provide

4-(5-fluoro-2-(trifluoromethyl)phenyl)piperidine hydrochloride as a white solid (0.309 g, 78%): ^{1}H NMR (300 MHz, DMSO-d_6) δ 8.81 (br s, 2H), 7.80 (dd, *J* = 9.3, 6.0 Hz, 1H), 7.39–7.26 (m, 2H), 3.43–3.30 (m, 1H), 3.24–2.97 (m, 3H), 2.11–1.90 (m, 2H), 1.88–1.75 (m, 2H); ESI MS *m/z* = 248 $[M+H]^+$.

Step D. To a solution of ethyl 6-bromo-[1,2,4]triazolo[4,3-*a*]pyridine-3-carboxylate (0.075 g, 0.28 mmol) in THF (2.5 mL) was added a solution of LiOH•H_2O (0.015 g, 0.35 mmol) in H_2O (1.5 mL). The mixture was stirred for 20 min and was subsequently neutralized with 2 N aqueous HCl. The mixture was concentrated under reduced pressure and the resulting residue was diluted in DMF (3.0 mL). To this mixture was added 4-(5-fluoro-2-(trifluoromethyl)phenyl)piperidine hydrochloride (0.089 g, 0.32 mmol), HBTU (0.280 g, 0.63 mmol) and *i*-Pr_2NEt (0.17 mL, 0.95 mmol). The resulting mixture stirred at rt for 16 h. The mixture was subsequently diluted with H_2O (20 mL) and extracted with EtOAc (3 × 20 mL). The combined organic extracts were washed with bine, dried over Na_2SO_4, filtered, and concentrated under reduced pressure. The resulting residue was chromatographed over silica gel (0%–50% EtOAc in hexanes) to provide (6-bromo-[1,2,4]triazolo[4,3-a]pyridin-3-yl)(4-(5-fluoro-2-(trifluoromethyl)phenyl)piperidin-1-yl)methanone as a white solid (0.097 g, 65%): ^{1}H NMR (500 MHz, DMSO-d_6) δ 9.16–9.14 (m, 1H), 7.98 (dd, *J* = 10.0, 1.0 Hz, 1H), 7.77 (dd, *J* = 8.5, 5.5 Hz, 1H), 7.72 (dd, *J* = 9.5, 1.5 Hz, 1H), 7.52 (dd, *J* = 11.0, 3.5 Hz, 1H), 7.29–7.23 (m, 1H), 5.31–5.24 (m, 1H), 4.76–4.70 (m, 1H), 3.42–3.32 (m, 1H), 3.27-3.19 (m, 1H), 3.06–2.96 (m, 1H), 1.98–1.75 (m, 4H).

Step E. A solution of (6-bromo-[1,2,4]triazolo[4,3-a]pyridin-3-yl)(4-(5-fluoro-2-(trifluoromethyl)phenyl)piperidin-1-yl)methanone (0.097 g, 0.21 mmol) and $ZnCN_2$ (0.048

g, 0.41 mmol) in DMF (2.5 mL), was purged with Ar for 10 min. To this solution was then added $Pd(PPh_3)_4$ (0.024 g, 0.021 mmol) and the vessel was sealed and the mixture was heated to 130 °C via microwave irradiation for 30 min. The mixture was allowed to cool to rt and then diluted with saturated aqueous $NaHCO_3$ solution (10 mL). The aqueous mixture was extracted with EtOAc (4 × 30 mL) and the combined organic extracts were concentrated under reduced pressure. The resulting residue was chromatographed over silica gel (0%–50% EtOAc in hexanes) to provide 3-(4-(5-fluoro-2-(trifluoromethyl)phenyl)piperidine-1-carbonyl)-[1,2,4]triazolo[4,3-a]pyridine-6-carbonitrile (**61**) was a white solid (0.035 g, 41%): ^{1}H NMR (500 MHz, DMSO-d_6) δ 9.54–9.53 (m, 1H), 8.14 (dd, *J* = 9.5, 6.0 Hz, 1H), 7.56 (dd, *J* = 10.5, 2.5 Hz, 1H), 7.78 (dd, *J* = 9.0, 6.0 Hz, 1H), 7.56 (dd, *J* = 10.5, 2.5 Hz, 1H), 7.30–7.24 (m, 1H), 5.20–5.10 (m, 1H), 4.73–4.71 (m, 1H), 3.43–3.34 (m, 1H), 3.29–3.20 (m, 1H), 3.08–3.00 (m, 1H), 1.99–1.77 (m, 4H); ESI MS *m/z* = 418 $[M+H]^+$; HPLC >99% purity (AUC), t_R = 16.8 min (Method A).

3-(4-(4-Fluoro-2-(trifluoromethyl)phenyl)piperidine-1-carbonyl)-[1,2,4]triazolo[4,3-*a*]pyridine-6-carbonitrile (62). Compound **62** was prepared according to a similar procedure described for the synthesis of **61**: mp 158–162 °C; ^{1}H NMR (300 MHz, DMSO-d_6) δ 9.53 (s, 1H), 8.14 (dd, *J* = 9.0, 0.9 Hz, 1H), 7.82 (dd, *J* = 9.6, 1.5 Hz, 1H), 7.77–7.67 (m, 1H), 7.61–7.67 (m, 2H), 5.19–5.04 (m, 1H), 4.80–4.67 (m, 1H), 3.46–3.14 (m, 2H), 3.12–2.94 (m, 1H), 2.02–1.70 (m, 4H); ESI MS *m/z* = 418 $[M+H]^+$; HPLC 98.5% purity (AUC), t_R = 10.6 min (Method A).

3-(4-(2-Fluoro-6-(trifluoromethyl)phenyl)piperidine-1-carbonyl)-[1,2,4]triazolo[4,3-*a*]pyridine-6-carbonitrile (64). *Step A*. A mixture of *tert*-butyl 4-

(((trifluoromethyl)sulfonyl)oxy)-3,6-dihydropyridine-1(2H)-carboxylate (**56**, 1.20 g, 3.62 mmol), (2-fluoro-6-(trifluoromethyl)phenyl)boronic acid (0.528 g, 2.53 mmol), $Pd(PPh_3)_4$ (0.292 g, 0.253 mmol), and 2.0 M aqueous Na_2CO_3 solution (20 mL) in DME (30 mL) was heated at 80 °C for 6 h. The mixture was allowed to cool to rt, diluted wth EtOAc (50 mL), and filtered through celite to remove solids. The filtrate was washed with brine (4 × 50 mL) and concentrated under reduced pressure. The resulting residue was chromatographed over silica gel (0%–10% EtOAc in hexanes) to provide *tert*-butyl 4-(2-fluoro-6-(trifluoromethyl)phenyl)-3,6-dihydropyridine-1(2H)-carboxylate as a clear oil (0.479 g, 39%): ^{1}H NMR (300 MHz, DMSO-d_6) δ 7.66–7.51 (m, 3H), 5.68 (s, 1H), 4.04–3.82 (m, 2H), 3.67–3.39 (m, 2H), 2.39–2.02 (m, 2H), 1.43 (s, 9H).

Step B. A mixture of *tert*-butyl 4-(2-fluoro-6-(trifluoromethyl)phenyl)-3,6-dihydropyridine-1(2H)-carboxylate (0.479 g, 1.41 mmol) and Pt_2O (0.095, 0.42 mmol) in EtOAc (15 mL) and HOAc (82 μL, 1.4 mmol) stirred at rt under a balloon of H_2 (1 atm) for 72 h. The mixture was diluted with EtOAc (50 mL) and filtered over celite. The filtrate was concentrated under reduced pressure and the resulting residue was chromatogrhed over silica gel (0%–10% EtOAc in hexanes) to afford *tert*-butyl 4-(2-fluoro-6-(trifluoromethyl)phenyl)piperidine-1-carboxylate (**63**) as a white solid: ^{1}H NMR (300 MHz, DMSO-d_6) δ 7.62–7.48 (m, 3H), 4.15–3.94 (m, 1H), 3.10–2.94 (m, 2H), 2.93–2.67 (m, 2H), 2.00–1.79 (m, 2H), 1.67–1.55 (m, 2H), 1.42 (s, 9H).

Step C. To a solution of *tert*-butyl 4-(2-fluoro-6-(trifluoromethyl)phenyl)piperidine-1-carboxylate (**63**, 0.219 g, 0.63 mmol) in CH_2Cl_2 (5 mL) was added 2.0 M HCl in Et_2O (4 mL). The mixture stirred at rt for 18 h and was diluted with Et_2O (50 mL). A precipitate formed,

which was collected by filtration to give 4-(2-fluoro-6-(trifluoromethyl)phenyl)piperidine hydrochloride as a white solid (0.158 g, 88%): ^{1}H NMR (300 MHz, DMSO-d_6) δ 8.82 (br s, 1H), 8.50 (br s, 1H), 7.66–7.48 (m, 3H), 3.24–2.95 (m, 3H), 2.35–2.15 (m, 2H), 1.87–1.74 (m, 2H); ESI MS *m/z* = 248 $[M+H]^+$.

Step D. To a solution of ethyl 6-bromo-[1,2,4]triazolo[4,3-*a*]pyridine-3-carboxylate (0.072 g, 0.27 mmol) in THF (2.5 mL) was added a solution of LiOH•H_2O (0.012 g, 0.29 mmol) in H_2O (1.5 mL). The mixture was stirred for 20 min and was subsequently neutralized with 2 N aqueous HCl. The mixture was concentrated under reduced pressure and the resulting residue was diluted in DMF (3.0 mL). To this mixture was added 4-(2-fluoro-6-(trifluoromethyl)phenyl)piperidine hydrochloride (0.075 g, 0.27 mmol), HBTU (0.236 g, 0.53 mmol) and *i*-Pr_2NEt (0.14 mL, 0.80 mmol). The resulting mixture stirred at rt for 16 h. The mixture was subsequently diluted with H_2O (20 mL) and extracted with EtOAc (3 × 20 mL). The combined organic extracts were washed with bine, dried over Na_2SO_4, filtered, and concentrated under reduced pressure. The resulting residue was chromatographed over silica gel (0%–50% EtOAc in hexanes) to provide (6-bromo-[1,2,4]triazolo[4,3-a]pyridin-3-yl)(4-(2-fluoro-6-(trifluoromethyl)phenyl)piperidin-1-yl)methanone as a white solid (0.080 g, 64%): ^{1}H NMR (300 MHz, DMSO-d_6) δ 9.12–9.10 (m, 1H), 8.00–7.95 (m, 1H), 7.74–7.68 (m, 1H), 7.65–7.50 (m, 3H), 5.29–5.15 (m, 1H), 4.82–4.68 (m, 1H), 3.41–3.19 (m, 2H), 3.07-2.97 (m, 1H), 2.34–2.19 (m, 1H), 2.15–2.02 (m, 1H), 1.93–1.75 (m, 2H); ESI MS *m/z* = 472 $[M+H]^+$.

Step E. A solution of (6-bromo-[1,2,4]triazolo[4,3-a]pyridin-3-yl)(4-(2-fluoro-6-(trifluoromethyl)phenyl)piperidin-1-yl)methanone (0.080 g, 0.17 mmol) and $ZnCN_2$ (0.040

g, 0.34 mmol) in DMF (2.5 mL), was sparged with Ar for 10 min. To this solution was then added $Pd(PPh_3)_4$ (0.019 g, 0.017 mmol) and the vessel was sealed and the mixture was heated to 130 °C via microwave irradiation for 30 min. The mixture was allowed to cool to rt and then diluted with saturated aqueous $NaHCO_3$ solution (10 mL). The aqueous mixture was extracted with EtOAc (4 × 30 mL) and the combined organic extracts were concentrated under reduced pressure. The resulting residue was chromatographed over silica gel (0%–50% EtOAc in hexanes) to provide 3-(4-(2-fluoro-6-(trifluoromethyl)phenyl)piperidine-1-carbonyl)-[1,2,4]triazolo[4,3-*a*]pyridine-6-carbonitrile (**64**) was a white solid (0.023 g, 33%): ^{1}H NMR (500 MHz, DMSO-d_6) δ 9.54–9.52 (m, 1H), 8.14–8.11 (m, 1H), 7.82–7.78 (m, 1H), 7.64–7.59 (m, 1H), 7.57–7.50 (m, 2H), 5.17–5.10 (m, 1H), 4.79–4.72 (m, 1H), 3.40–3.24 (m, 2H), 3.07–2.98 (m, 1H), 2.30–2.19 (m, 1H), 2.14–2.03 (m, 1H), 1.91–1.79 (m, 2H); ESI MS *m/z* = 418 $[M+H]^+$; HPLC >99% purity (AUC), t_R = 9.9 min (Method A).

(1H-Benzo[*d*]imidazol-2-yl)(4-(2-(trifluoromethyl)phenyl)piperidin-1-yl)methanone (65). A mixture of 4-(2-(trifluoromethyl)phenyl)piperidine hydrochloride (**10**, 0.128 g, 0.483 mmol), 1H-benzo[*d*]imidazole-2-carboxylic acid (0.070 g, 0.436 mmol), *i*-Pr_2NEt (0.25 mL, 1.49 mmol), and HBTU (0.274 g, 0.724 mmol) in DMF (5 mL) was stirred at rt for 16 h. The mixture was diluted with H_2O (20 mL) and extracted with EtOAc (3 × 50 mL). The combined organic extracts were washed with H_2O (3 × 50 mL), brine, dried over Na_2SO_4, filtered and concentrated under reduced pressure. The resulting residue was purified by silica gel chromatography (10–50% EtOAc in hexanes) to afford (1H-Benzo[d]imidazol-2-yl)(4-(2-(trifluoromethyl)phenyl)piperidin-1-yl)methanone (**65**) as a

white solid (0.121 g, 67%): mp 178–185 °C; ^{1}H NMR (500 MHz, DMSO-d_6) δ 13.11 (s, 1H), 7.74 (d, *J* = 8.0 Hz, 1H), 7.71–7.60 (m, 3H), 7.55 (d, *J* = 8.5 Hz, 1H), 7.45–7.38 (m, 1H), 7.35–7.29 (m, 1H), 7.28–7.22 (m, 1H), 5.83–5.77 (m, 1H), 4.79–4.73 (m, 1H), 3.35–3.27 (m, 1H), 3.25–3.16 (m, 1H), 3.00–2.90 (m, 1H), 1.95–1.71 (m, 4H); ESI MS *m/z* 374 [M + H]$^+$; HPLC 98.8% purity (AUC), t_R = 13.4 min (Method A).

Benzo[*d*]oxazol-2-yl(4-(2-(trifluoromethyl)phenyl)piperidin-1-yl)methanone (66). Compound **66** was prepared according to a similar procedure described for the synthesis of **65**. ^{1}H NMR (500 MHz, DMSO-d_6) δ 7.92–7.86 (m, 2H), 7.71–7.41 (m, 6H), 4.70–4.67 (m, 2H), 3.80–3.35 (m, 1H), 3.23–3.18 (m, 1H), 3.05–2.99 (m, 1H), 1.92–1.77 (m, 4H); ESI MS *m/z* 375 [M + H]$^+$; HPLC 99.4% purity (AUC), t_R = 15.1 min (Method A).

Benzo[*d*]thiazol-2-yl-(4-(2-(trifluoromethyl)phenyl)piperidin-1-yl)methanone (67). Compound **67** was prepared according to a similar procedure described for the synthesis of **65**. mp 151–153 °C; ^{1}H NMR (500 MHz, DMSO-d_6) δ 8.22–8.13 (m, 2H), 7.71–7.57 (m, 5H), 7.44–7.41 (m, 1H), 5.40–5.37 (m, 1H), 4.71–4.68 (m, 1H), 3.99–3.21 (m, 2H), 3.01–3.03 (m, 1H), 1.92–1.83 (m, 4H); ESI MS *m/z* 391 [M + H]$^+$; HPLC 98.4% purity (AUC), t_R = 16.6 min (Method A).

(1H-Indol-2-yl)(4-(2-(trifluoromethyl)phenyl)piperidin-1-yl)methanone (68). Compound **68** was prepared according to a similar procedure described for the synthesis of **65**. mp 189–192 °C; ^{1}H NMR (500 MHz, DMSO-d_6) δ 11.56 (s, 1H), 7.71–7.68 (m, 2H), 7.67–7.63 (m, 1H), 7.60 (d, *J* = 8.0 Hz, 1H), 7.45–7.40 (m, 2H), 7.20–7.16 (m, 1H), 7.06–7.02 (m, 1H), 6.82 (dd, *J* = 2.5, 1.0 Hz, 1H), 4.63 (d, *J* = 12.5 Hz, 2H), 3.23–2.94 (m, 3H),

1.88–1.75 (m, 4H); ESI MS *m/z* 373 [M + H]$^+$; HPLC 99.9% purity (AUC), t_R = 19.8 min (Method C).

(1H-Pyrrolo[2,3-*c*]pyridin-2-yl)(4-(2-(trifluoromethyl)phenyl)piperidin-1-yl)methanone (69). Compound **69** was prepared according to a similar procedure described for the synthesis of **65**. mp 214–218 °C; ^{1}H NMR (500 MHz, DMSO-d_6) δ 11.99 (s, 1H), 8.90 (s, 1H), 8.22 (d, *J* = 5.5 Hz, 1H), 7.72–7.68 (m, 2H), 7.67–7.63 (m, 1H), 7.46–7.40 (m, 1H), 7.38 (d, *J* = 6.0 Hz, 1H), 6.98 (d, *J* = 1.0 Hz, 1H), 4.73–4.44 (m, 2H), 3.08–2.77 (m, 3H), 1.93–1.74 (m, 4H); ESI MS *m/z* 374 [M + H]$^+$; HPLC 99.8% purity (AUC), t_R = 11.5 min (Method A).

(1H-Pyrrolo[3,2-*b*]pyridin-2-yl)(4-(2-(trifluoromethyl)phenyl)piperidin-1-yl)methanone (70). Compound **70** was prepared according to a similar procedure described for the synthesis of **65**. mp 275–278 °C decomp.; ^{1}H NMR (500 MHz, DMSO-d_6) δ 11.81 (s, 1H), 8.39 (dd, *J* = 6.0, 1.5 Hz, 1H), 7.79 (d, *J* = 8.5 Hz, 1H), 7.73–7.63 (m, 3H), 7.46–7.41 (m, 1H), 7.19 (dd, *J* = 8.5, 4.5 Hz, 1H), 6.93 (d, *J* = 1.5 Hz, 1H), 4.73–4.42 (m, 2H), 3.28–2.81 (m, 3H), 1.92–1.76 (m, 4H); ESI MS *m/z* 374 [M + H]$^+$; HPLC 99.5% purity (AUC), t_R = 13.0 min (Method A).

Imidazo[1,2-*a*]pyridin-2-yl(4-(2-(trifluoromethyl)phenyl)piperidin-1-yl)methanone (71). Compound **71** was prepared according to a similar procedure described for the synthesis of **65**. mp 130–133 °C; ^{1}H NMR (500 MHz, $CDCl_3$) δ 8.16 (d, *J* = 7.8 Hz, 1H), 8.09 (s, 1H), 7.62 (m, 2H), 7.53 (m, 2H), 7.48 (m, 1H), 7.30 (m, 1H), 6.82 (m, 1H), 5.42 (m, 1H), 4.91 (m, 1H), 3.26 (m, 2H), 2.98 (m, 1H), 1.83 (m, 4H); MS (ESI+) *m/z* 374 [M+H]$^+$; HPLC 97.6% purity (AUC), t_R = 9.9 min (Method A).

Imidazo[1,2-*b*]pyridazin-2-yl(4-(2-(trifluoromethyl)phenyl)piperidin-1-yl)methanone (72). Compound **72** was prepared according to a similar procedure described for the synthesis of **65**. mp 133–135 °C; ^{1}H NMR (500 MHz, DMSO-d_6) δ 8.61–8.58 (m, 2H), 8.21–8.18 (m, 1H), 7.70–7.60 (m, 3H), 7.44–7.39 (m, 1H), 7.33–7.29 (m, 1H), 5.15–5.06 (m, 1H), 4.77–4.67 (m, 1H), 3.28–3.12 (m, 2H), 2.93–2.81 (m, 1H), 1.90–1.67 (m, 4H); ESI MS *m/z* 375 $[M + H]^+$; HPLC 99.6 % purity (AUC), t_R = 9.5 min (Method A).

(6-Methylimidazo[1,2-*b*]pyridazin-2-yl)(4-(2-(trifluoromethyl)phenyl)piperidin-1-yl)methanone (74). *Step A*. A mixture of 4-(2-(trifluoromethyl)phenyl)piperidine hydrochloride (**10**, 0.996 g, 3.76 mmol), 6-chloroimidazo[1,2-*b*]pyridazine-2-carboxylic acid (0.743 g, 3.76 mmol), *i*-Pr_2NEt (1.96 mL, 11.28 mmol), and HBTU (2.13 g, 5.64 mmol) in DMF (80 mL) was stirred at rt for 16 h. The mixture was diluted with H_2O (150 mL) and extracted with EtOAc (3 × 150 mL). The combined organic extracts were washed with H_2O (3 × 100 mL), brine, dried over Na_2SO_4, filtered and concentrated under reduced pressure. The resulting residue was purified by silica gel chromatography (10–50% EtOAc in hexanes) to afford (6-chloroimidazo[1,2-*b*]pyridazin-2-yl)(4-(2-(trifluoromethyl)phenyl)piperidin-1-yl)methanone (**73**) as an off- white solid (1.35 g, 87%): ^{1}H NMR (300 MHz, $CDCl_3$) δ 8.40 (s, 1H), 7.91 (m, 1H), 7.65 (d, *J* = 8.0 Hz, 1H), 7.52–7.43 (m, 2H), 7.31 (t, *J* = 6.6 Hz, 1H), 7.13 (d, *J* = 9.5 Hz, 1H), 5.30–5.23 (m, 1H), 4.96–4.91 (m, 1H), 3.30–3.24 (m, 2H), 2.90 (m, 1H), 1.96–1.83 (m, 4H); MS (ESI+) *m/z* 409 $[M+H]^+$.

Step B. A mixture of (6-chloroimidazo[1,2-*b*]pyridazin-2-yl)(4-(2-(trifluoromethyl)phenyl)piperidin-1-yl)methanone (**73**, 0.030 g, 0.0734 mmol), trimethyl boroxine (0.014 g, 0.110 mmol), DPPF (0.006 g, 0.00734 mmol), K_2CO_3 (0.020 g, 0.147

mmol), 1,4-dioxane (2 mL) and H_2O (0.3 mL) was heated in sealed tube under an atmosphere of N_2 at 110 °C for 5 h. The mixture was allowed to cool to rt, diluted with EtOAc, and solids were filtered. The filtrate was concentrated under reduced pressure and the residue was chromatographed over silica gel (0-3% CH_3OH in CH_2Cl_2) to give (6-methylimidazo[1,2-*b*]pyridazin-2-yl)(4-(2-(trifluoromethyl)phenyl)piperidin-1-yl)methanone (**74**) as an off-white solid (0.015 g, 52%): mp 144–147 °C; ^{1}H NMR (300 MHz, $CDCl_3$) δ 8.35 (s, 1H), 7.82 (d, *J* = 9.4 Hz, 1H), 7.64 (d, *J* = 7.8 Hz, 1H), 7.53–7.44 (m, 2H), 7.30 (m, 1H), 6.96 (d, *J* = 9.4 Hz, 1H), 5.30 (m, 1H), 4.94 (m, 1H), 3.26 (m, 2H), 2.93 (m, 1H), 2.59 (s, 3H), 1.89–1.77 (m, 4H); MS (ESI+) *m/z* 489 $[M+H]^+$; HPLC 95.9% purity (AUC), t_R = 13.3 min (Method A).

(6-Methoxyimidazo[1,2-*b*]pyridazin-2-yl)(4-(2-(trifluoromethyl)phenyl)piperidin-1-yl)methanone (75). To a solution of **73** (0.060 g, 0.147 mmol) in CH_3OH (6 mL) was added a solution of $NaOCH_3$ in CH_3OH (0.5 M, 2.94 mL, 1.47 mmol). The mixture was heated 70 °C for 1 h, allowed to cool to rt and concentrated under reduced pressure. The residue was dissolved in CH_2Cl_2 and the solution was washed with saturated $NaHCO_3$, dried over Na_2SO_4, filtered, and concentrated under reduced pressure. The resulting residue was chromatographed over silica gel (0–70% EtOAc in hexanes) and lyophilized from CH_3CN and H_2O to give (6-methoxyimidazo[1,2-*b*]pyridazin-2-yl)(4-(2-(trifluoromethyl)phenyl)piperidin-1-yl)methanone (**75**) as a white solid (0.015 g, 25%): mp 120–123 °C; ^{1}H NMR (300 MHz, $CDCl_3$) δ 8.24 (s, 1H), 7.76 (d, *J* = 9.6 Hz, 1H), 7.64 (d, *J* = 8.1 Hz, 1H), 7.49 (m, 2H), 7.30 (m, 1H), 6.74 (d, *J* = 9.6 Hz, 1H), 5.38 (m, 1H), 4.93 (m, 1H),

4.00 (s, 3H), 3.25 (m, 2H), 2.88 (m, 1H), 1.89–1.77 (m, 4H); MS (ESI+) *m/z* 405 $[M+H]^+$; HPLC 96.6% purity (AUC), t_R = 13.9 min (Method A).

(6-Cyclopropylimidazo[1,2-*b*]pyridazin-2-yl)(4-(2 (trifluoromethyl)phenyl)piperidin-1-yl)methanone (76). A mixture of **73** (0.050 g, 0.122 mmol), potassium cyclopropyltrifluoroborate (0.026 g, 0.183 mmol), $Pd(OAc)_2$ (0.002 g, 0.0061 mmol), di-(1-admantyl)-*n*-butylphosphine (0.004 g, 0.0122 mmol), and Cs_2CO_3 (0.119 g, 0.366 mmol) in toluene (2 mL) and H_2O (0.2 mL) was heated at 100 °C for 3 h. The mixture was concentrated under reduced pressure and the resulting residue was chromatographed over silica gel (0–60% EtOAc in hexanes) to give (6-cyclopropylimidazo[1,2-*b*]pyridazin-2-yl)(4-(2-(trifluoromethyl)phenyl)piperidin-1-yl)methanone (**76**) as a white solid (0.035 g, 69%): ^{1}H NMR (300 MHz, $CDCl_3$) δ 8.30 (s, 1H), 7.78 (m, 1H), 7.63 (d, *J* = 7.8 Hz, 1H), 7.54–7.44 (m, 2H), 7.30 (t, *J* = 7.8 Hz, 1H), 6.88 (d, *J* = 9.6 Hz, 1H), 5.30 (m, 1H), 4.94 (m, 1H), 3.27 (m, 2H), 2.89 (m, 1H), 2.12–1.81 (m, 5H), 1.14–1.08 (m, 4H); MS (ESI+) *m/z* 415 $[M+H]^+$; HPLC 98.2% purity (AUC), t_R = 13.7 min (Method A).

(6-(Pyrrolidin-1-yl)imidazo[1,2-*b*]pyridazin-2-yl)(4-(2-(trifluoromethyl)phenyl)piperidin-1-yl)methanone (77). A mixture of **73** (0.030 g, 0.0734 mmol) and pyrrolidine (1.5 mL) was heated at 100 °C for 3 h. The mixture cooled to rt and was concentrated under reduced pressure. The residue was chromatographed over silica gel (0–70% EtOAc in hexanes) to give (6-(pyrrolidin-1-yl)imidazo[1,2-*b*]pyridazin-2-yl)(4-(2-(trifluoromethyl)phenyl)piperidin-1-yl)methanone (**77**) as an off-white solid (0.046 g, 85%): mp 170–171 °C; ^{1}H NMR (300 MHz, $CDCl_3$) δ 8.15 (s, 1H), 7.63 (d, *J* = 9.3 Hz, 1H), 7.53–7.44 (m, 2H), 7.30 (t, *J* = 7.8 Hz, 1H), 6.66 (d, *J* = 9.9 Hz, 1H), 5.42 (m, 1H), 4.93 (m,

1H), 3.50 (m, 4H), 3.24 (m, 2H), 2.87 (m, 1H), 2.07–1.80 (m, 8H); MS (ESI+) *m/z* 444 $[M+H]^+$; HPLC 99.2 % purity (AUC), t_R = 12.0 min (Method A).

(6-Morpholinoimidazo[1,2-*b*]pyridazin-2-yl)(4-(2-(trifluoromethyl)phenyl)piperidin-1-yl)methanone (78). A mixture of **73** (0.030 g, 0.0734 mmol) and morpholine (1.5 mL) was heated at 120 °C for 2 h. The mixture was allowed to cool to rt and was concentrated under reduced pressure. The resulting residue was dissolved in CH_2Cl_2 and the solution was washed with aqueous saturated $NaHCO_3$ solution, dried over Na_2SO_4, filtered, and concentrated under reduced pressure. The resulting residue was chromatographed over silica gel (0–100% EtOAc in hexanes) to give (6-morpholinoimidazo[1,2-*b*]pyridazin-2-yl)(4-(2-(trifluoromethyl)phenyl)piperidin-1-yl)methanone (**78**) as a white solid (0.015 g, 44%): mp 203–205 °C; ^{1}H NMR (300 MHz, $CDCl_3$) δ 8.17 (s, 1H), 7.71 (d, *J* = 10.0 Hz, 1H), 7.63 (d, *J* = 7.7 Hz, 1H), 7.53–7.43 (m, 2H), 7.30 (m, 1H), 6.96 (d, *J* = 10.0 Hz, 1H), 5.38 (m, 1H), 4.93 (m, 1H), 3.85 (m, 4H), 3.50 (m, 4H), 3.24 (m, 2H), 2.88 (m, 1H), 1.88–1.76 (m, 4H); MS (ESI+) *m/z* 460 $[M+H]^+$; HPLC 98.0 % purity (AUC), t_R = 12.1 min (Method A).

▪ ASSOCIATED CONTENT

ⓢSupporting Information

The Supporting Information is available free of charge on the ACS publications website at http://pubs.acs.org.

RBP4 *in vitro* assay protocols, mouse PK study protocols, rat PK study protocol, serum RBP4 collection and measurements, protocols for the adipocyte-specific

hRBP4 transgenic mouse experiments, general chemistry information, ^{1}H NMR, MS, and HPLC data for compounds **48** and **59** (PDF).

Docking was performed only with PDB entry ***3fmz*** (RBP4 co-crystallized with **3**) (PDB). Authors will release the atomic coordinates and experimental data upon article publication.

Molecular formula strings for biologically tested compounds (CSV).

▪ AUTHOR INFORMATION

Corresponding Authors

*Christopher L. Cioffi: phone, 518-694-7224; e-mail: christopher.cioffi@acphs.edu.

ORCID ID

0000-0003-0642-7905

* Konstantin Petrukhin: phone, 212-305-9040; e-mail: kep4@cumc.columbia.edu.

Notes

The authors declare the following competing financial interest(s): C.L.C., E.E.F., M.P.C., L.Z., P.C., G.J., and K.P. are inventors on the patent applications for compounds disclosed in this paper that are assigned to The Trustees of Columbia University in the City of New York.

▪ ACKNOWLEDGEMENTS

This study was supported by NIH Grants U01 NS074476 and R21 EY027027 to K.P. and R01 DK068437 and R01 DK101251 to W.S.B., as well as by unrestricted funds from

Research to Prevent Blindness (New York, NY) to the Department of Ophthalmology, Columbia University. This project has also been funded in whole or in part with Federal funds from the National Institute of Neurological Disorders and Stroke, the National Eye Institute, the NIH Blueprint Neurotherapeutics Network, Blueprint for Neuroscience Research Program, National Institutes of Health, Department of Health and Human Services, under Contract No. HHSN271201100013C.

▪ ABBREVIATIONS

Abca4, ATP-binding cassette, sub-family A (ABC1), member 4; NASH, non-alcoholic steatohepatitis; NAFLD, non-alcoholic fatty liver disease; AMD, age-related macular degeneration; RBP4, retinol-binding protein 4; TTR, transthyretin; CRBP1, cellular retinol-binding protein-1; Ar, argon; rt, room temperature; SPA, scintillation proximity assay; HTRF, homogenous time resolved fluorescence assay; HFD, high fat diet; HLM, human liver microsomes; RLM, rat liver microsomes; *n*-BuLi, *n*-butyl lithium; THF, tetrahydrofuran; DMF; *N*,*N*-dimethylformamide; DME, dimethoxyethane; Et_2O, diethyl ether; EtOAc, ethyl acetate; CH_3OH, methyl alcohol; EtOH, ethyl alcohol; Boc_2O, di-*tert*-butyl di-carbonate; HFD, high-fat diet; TFA, trifluoroacetic acid; $Pd(OAc)_2$, palladium (II) acetate; $Pd_2(dba)_3$, tris(dibenzylideneacetone)dipalladium(0); BINAP, 2,2′-bis(diphenylphosphino)-1,1′-binaphthalene; XantPhos, 4,5-bis(diphenylphosphino)-9,9-dimethylxanthene; JohnPhos, (2-biphenyl)di-*tert*-butylphosphine; Ac_2O, acetic anhydride; NaOAc, sodium acetate; LiHMDS, lithium bis(trimethylsilyl)amide; *i*-Pr_2NEt, *N*,*N*-diisopropylethylamine; Et_3N, triethylamine; $LiOH{\bullet}H_2O$, lithium hydroxide

monohydrate; NaOH, sodium hydroxide; $SOCl_2$, thionyl chloride; $Pd(PPh_3)_4$, tetrakis(triphenylphosphine)palladium(0); $PhN(SO_2CF_3)_2$, 1,1,1-trifluoro-*N*-phenyl-*N*-((trifluoromethyl)sulfonyl)methanesulfonamide; $LiAlH_4$, lithium aluminum hydride; Gly, glycine; Tyr, tyrosine; Arg, arginine; Gln, glutamine; Leu, leucine; Phe, phenylalanine; CYP, cytochrome P450; CYP2C9, cytochrome P450 2C9; CYP2C19, cytochrome P450 2C19; CYP2D6, cytochrome P450 2D6; CYP3A4, cytochrome P450 3A4; GPCR, G-protein coupled receptor; hERG, human ether-à-go-go-related gene; PK, pharmacokinetics; PD, pharmacodynamics; IV; intravenous; PO, oral; QD, once daily; Cl; clearance; Vss, volume of distribution at steady state; AUC, area under the curve; %F, % oral bioavailability; SAR, structure-activity relationship; SPR, structure-property relationship; ADME, Absorption, Distribution, Metabolism, Elimination; PPB, plasma protein binding; THF, tetrahydrofuran; DME, dimethoxyethane; CH_2Cl_2, dichloromethane; CH_3CN, acetonitrile; aq, aqueous

▪ REFERENCES

1. Schlehuber, S.; Skerra, A. Lipocalins in drug discovery: from natural ligand-binding proteins to "anticalins". *Drug Discovery Today* **2005**, *10*, 23-33.
2. Yang, Q.; Graham, T. E.; Mody, N.; Preitner, F.; Peroni, O. D.; Zabolotny, J. M.; Kotani, K.; Quadro, L.; Kahn, B. B. Serum retinol binding protein 4 contributes to insulin resistance in obesity and type 2 diabetes. *Nature* **2005**, *436*, 356-362.

3. Bobbert, T.; Raila, J.; Schwarz, F.; Mai, K.; Henze, A.; Pfeiffer, A. F. H.; Schweigert, F. J.; Spranger, J. Relation between retinol, retinol-binding protein 4, transthyretin and carotid intima media thickness. *Atherosclerosis* **2010**, *213*, 549-551.
4. Kawaguchi, R.; Zhong, M.; Kassai, M.; Ter-Stepanian, M.; Sun, H. Vitamin A transport mechanism of the multitransmembrane cell-surface receptor STRA6. *Membranes* **2015**, *5*, 425-453.
5. Alapatt, P.; Guo, F. J.; Komanetsky, S. M.; Wang, S. P.; Cai, J. J.; Sargsyan, A.; Diaz, E. R.; Bacon, B. T.; Aryal, P.; Graham, T. E. Liver retinol transporter and receptor for serum retinol-binding protein (RBP4). *J. Biol. Chem.* **2013**, *288*, 1250-1265.
6. Tsutsumi, C.; Okuno, M.; Tannous, L.; Piantedosi, R.; Allan, M.; Goodman, D. S.; Blaner, W. S. Retinoids and retinoid-binding protein expression in rat adipocytes. *J. Biol. Chem.* **1992**, *267*, 1805-1810.
7. Kotnik, P.; Fischer-Posovszky, P.; Wabitsch, M. RBP4: a controversial adipokine. *Eur. J. Endocrinol.* **2011**, *165*, 703-711.
8. Graham, T. E.; Yang, Q.; Bluher, M.; Hammarstedt, A.; Ciaraldi, T. P.; Henry, R. R.; Wason, C. J.; Oberbach, A.; Jansson, P. A.; Smith, U.; Kahn, B. B. Retinol-binding protein 4 and insulin resistance in lean, obese, and diabetic subjects. *N. Engl. J. Med.* **2006**, *354*, 2552-2563.
9. Aeberli, I.; Biebinger, R.; Lehmann, R.; L'Allemand, D.; Spinas, G. A.; Zimmermann, M. B. Serum retinol-binding protein 4 concentration and its ratio to serum retinol are associated with obesity and metabolic syndrome components in children. *J. Clin. Endocrinol. Metab.* **2007**, *92*, 4359-4365.

10. Kowalska, I.; Straczkowski, M.; Adamska, A.; Nikolajuk, A.; Karczewska-Kupczewska, M.; Otziomek, E.; Gorska, M. Serum retinol binding protein 4 is related to insulin resistance and nonoxidative glucose metabolism in lean and obese women with normal glucose tolerance. *J. Clin. Endocrinol. Metab.* **2008**, *93*, 2786-2789.

11. Ingelsson, E.; Sundstrom, J.; Melhus, H.; Michaelsson, K.; Berne, C.; Vasan, R. S.; Riserus, U.; Blomhoff, R.; Lind, L.; Arnlov, J. Circulating retinol-binding protein 4, cardiovascular risk factors and prevalent cardiovascular disease in elderly. *Atherosclerosis* **2009**, *206*, 239-244.

12. Qi, Q.; Yu, Z.; Ye, X.; Zhao, F.; Huang, P.; Hu, F. B.; Franco, O. H.; Wang, J.; Li, H.; Liu, Y.; Lin, X. Elevated retinol-binding protein 4 levels are associated with metabolic syndrome in Chinese people. *J. Clin. Endocrinol. Metab.* **2007**, *92*, 4827-4834.

13. Norseen, J.; Hosooka, T.; Hammarstedt, A.; Yore, M. M.; Kant, S.; Aryal, P.; Kiernan, U. A.; Phillips, D. A.; Maruyama, H.; Kraus, B. J.; Usheva, A.; Davis, R. J.; Smith, U.; Kahn, B. B. Retinol-binding protein 4 inhibits insulin signaling in adipocytes by inducing proinflammatory cytokines in macrophages through a c-Jun N-terminal kinase- and toll-like receptor 4-dependent and retinol-independent mechanism. *Mol. Cell. Biol.* **2012**, *32*, 2010-2019.

14. Moraes-Vieira, P. M.; Yore, M. M.; Dwyer, P. M.; Syed, I.; Aryal, P.; Kahn, B. B. RBP4 activates antigen-presenting cells, leading to adipose tissue inflammation and systemic insulin resistance. *Cell Metab.* **2014**, *19*, 512-526.

15. Farjo, K. M.; Farjo, R. A.; Halsey, S.; Moiseyev, G.; Ma, J. X., Retinol-binding protein 4 induces inflammation in human endothelial cells by an NADPH oxidase- and nuclear

factor kappa B-dependent and retinol-independent mechanism. *Mol. Cell. Biol.* **2012**, *32*, 5103-5115.

16. Berry, D. C.; Jacobs, H.; Marwarha, G.; Gely-Pernot, A.; O'Byrne, S. M.; DeSantis, D.; Klopfenstein, M.; Feret, B.; Dennefeld, C.; Blaner, W. S.; Croniger, C. M.; Mark, M.; Noy, N.; Ghyselinck, N. B. The STRA6 receptor is essential for retinol-binding protein-induced insulin resistance but not for maintaining vitamin A homeostasis in tissues other than the eye. *J. of Biol. Chem.* **2013**, *288*, 24528-24539.
17. Berry, D. C.; O'Byrne, S. M.; Vreeland, A. C.; Blaner, W. S.; Noy, N. Cross talk between signaling and vitamin A transport by the retinol-binding protein receptor STRA6. *Mol. Cell. Biol.* **2012**, *32*, 3164-3175.
18. Quadro, L.; Blaner, W. S.; Hamberger, L.; Van Gelder, R. N.; Vogel, S.; Piantedosi, R.; Gouras, P.; Colantuoni, V.; Gottesman, M. E. Muscle expression of human retinol-binding protein (RBP). Suppression of the visual defect of RBP knockout mice. *J. Biol. Chem.* **2002**, *277*, 30191-30197.
19. Motani, A.; Wang, Z.; Conn, M.; Siegler, K.; Zhang, Y.; Liu, Q.; Johnstone, S.; Xu, H.; Thibault, S.; Wang, Y.; Fan, P.; Connors, R.; Le, H.; Xu, G.; Walker, N.; Shan, B.; Coward, P. Identification and characterization of a non-retinoid ligand for retinol-binding protein 4 which lowers serum retinol-binding protein 4 levels in vivo. *J. Biol. Chem.* **2009**, *284*, 7673-7680.
20. Du, M.; Otalora, L.; Martin, A. A.; Moiseyev, G.; Vanlandingham, P.; Wang, Q. L.; Farjo, R.; Yeganeh, A.; Quiambao, A.; Farjo, K. M. Transgenic mice overexpressing serum

retinol-binding protein develop progressive retinal degeneration through a retinoid-independent mechanism. *Mol. Cell. Biol.* **2015**, *35*, 2771-2789.

21. Fedders, R.; Muenzner, M.; Weber, P.; Sommerfeld, M.; Knauer, M.; Kedziora, S.; Kast, N.; Heidenreich, S.; Raila, J.; Weger, S.; Henze, A.; Schupp, M. Liver-secreted RBP4 does not impair glucose homeostasis in mice. *J. Biol. Chem.* **2018**, *293*, 15269-15276.
22. Lee, S. A.; Yuen, J. J.; Jiang, H.; Kahn, B. B.; Blaner, W. S., Adipocyte-specific overexpression of retinol-binding protein 4 causes hepatic steatosis in mice. *Hepatology* **2016**, *64*, 1534-1546.
23. Huang, H.-J., Nanao, M., Stout, T., Rosen, J. PDB ID: 2WR6 Structure of the Complex of RBP4 with Linoleic Acid. 2009. Protein Data Bank.
24. Nanao, M., Mercer, D., Nguyen, L., Buckley, D., Stout, T.J. PDB ID: 2WQ9 Crystal Structure of RBP4 Bound to Oleic Acid. 2009. Protein Data Bank.
25. Perduca, M.; Nicolis, S.; Mannucci, B.; Galliano, M.; Monaco, H. L. Human plasma retinol-binding protein (RBP4) is also a fatty acid-binding protein. *Biochim. Biophys. Acta, Mol. Cell Biol. Lipids* **2018**, *1863*, 458-466.
26. Cioffi, C. L.; Dobri, N.; Freeman, E. E.; Conlon, M. P.; Chen, P.; Stafford, D. G.; Schwarz, D. M. C.; Golden, K. C.; Zhu, L.; Kitchen, D. B.; Barnes, K. D.; Racz, B.; Qin, Q.; Michelotti, E.; Cywin, C. L.; Martin, W. H.; Pearson, P. G.; Johnson, G.; Petrukhin, K. Design, synthesis, and evaluation of nonretinoid retinol binding protein 4 antagonists for the potential treatment of atrophic age-related macular degeneration and Stargardt disease. *J. Med. Chem.* **2014**, *57*, 7731-7757.

27. Cioffi, C. L.; Racz, B.; Freeman, E. E.; Conlon, M. P.; Chen, P.; Stafford, D. G.; Schwarz, D. M.; Zhu, L.; Kitchen, D. B.; Barnes, K. D.; Dobri, N.; Michelotti, E.; Cywin, C. L.; Martin, W. H.; Pearson, P. G.; Johnson, G.; Petrukhin, K. Bicyclic [3.3.0]-octahydrocyclopenta[c]pyrrolo antagonists of retinol binding protein 4: potential treatment of atrophic age-related macular degeneration and Stargardt disease. *J. Med. Chem.* **2015**, *58*, 5863-5888.

28. Racz, B.; Varadi, A.; Kong, J.; Allikmets, R.; Pearson, P. G.; Johnson, G.; Cioffi, C. L.; Petrukhin, K. A non-retinoid antagonist of retinol-binding protein 4 rescues phenotype in a model of Stargardt disease without inhibiting the visual cycle. *J. Biol. Chem.* **2018**, *293*, 11574-11588.

29. Lassila, T.; Hokkanen, J.; Aatsinki, S. M.; Mattila, S.; Turpeinen, M.; Tolonen, A. Toxicity of carboxylic acid-containing drugs: the role of acyl migration and coa conjugation investigated. *Chem. Res. Toxicol.* **2015**, *28*, 2292-2303.

30. Wang, Y.; Connors, R.; Fan, P.; Wang, X.; Wang, Z.; Liu, J.; Kayser, F.; Medina, J. C.; Johnstone, S.; Xu, H.; Thibault, S.; Walker, N.; Conn, M.; Zhang, Y.; Liu, Q.; Grillo, M. P.; Motani, A.; Coward, P.; Wang, Z. Structure-assisted discovery of the first non-retinoid ligands for retinol-binding protein 4. *Bioorg. Med. Chem. Lett.* **2014**, *24*, 2885-2891.

31. Swanson, D. M.; Dubin, A. E.; Shah, C.; Nasser, N.; Chang, L.; Dax, S. L.; Jetter, M.; Breitenbucher, J. G.; Liu, C.; Mazur, C.; Lord, B.; Gonzales, L.; Hoey, K.; Rizzolio, M.; Bogenstaetter, M.; Codd, E. E.; Lee, D. H.; Zhang, S. P.; Chaplan, S. R.; Carruthers, N. I., Identification and biological evaluation of 4-(3-trifluoromethylpyridin-2-yl)piperazine-

1-carboxylic acid (5-trifluoromethylpyridin-2-yl)amide, a high affinity TRPV1 (VR1) vanilloid receptor antagonist. *J. Med. Chem.* **2005**, *48*, 1857-1872.

32. (a) Dart, M. J.; Searle, X. B.; Tietje, K. R.; Toupence, R. B., Azabicyclic Compounds are Central Nervous System Active Agents. PCT Int. Appl. WO2004016604 A2. Google Patents: 2004; (b) Lauffer, D.; Li, P.; Waal, N.; Mcginty, K.; Tang, Q.; Ronkin, S.; Farmer, L.; Shannon, D.; Jacobs, D., C-Met Protein Kinase Inhibitors. PCT Int. Appl. WO2009045992 A2. Google Patents: 2009; (c) Guillemont, J. E. G.; Lançois, D. F. A.; Motte, M. M. S.; Koul, A.; Balemans, W. M. A.; Arnoult, E. P. A., Antibacterial Cyclopenta[c]pyrrole Substituted 3,4-Dihydro-1h-[1,8]naphthyridinones. PCT Int. Appl. WO2013021054 A1. Google Patents: 2013.
33. Motani, A.; Wang, Z.; Conn, M.; Siegler, K.; Zhang, Y.; Liu, Q.; Johnstone, S.; Xu, H.; Thibault, S.; Wang, Y.; Fan, P.; Connors, R.; Le, H.; Xu, G.; Walker, N.; Shan, B.; Coward, P. Identification and characterization of a non-retinoid ligand for retinol-binding protein 4 which lowers serum retinol-binding protein 4 levels in vivo. *J. Biol. Chem.* **2009**, *284*, 7673-7680.
34. Dobri, N.; Qin Q.; Kong, J.; Yamamoto, K.; Liu, Z.; Moiseyev, G.; Ma, J. X.; Allikmets, R.; Sparrow, J. R.; Petrukhin, K. A1120, a non-retinoid RBP4 antagonist, inhibits formation of cytotoxic bisretinoids in the animal model of enhanced retinal lipofuscinogenesis. *Invest. Ophthalmol. Vis. Sci.* **2013**, *54*, 85-95.
35. Johnson, T. W.; Gallego, R. A.; Edwards, M. P. Lipophilic efficiency as an important metric in drug design. *J. Med. Chem.* **2018**, *15*, 6401-6420.

36. Zimmerlin, A.; Trunzer, M.; Faller, B. CYP3A time-dependent inhibition risk assessment validated with 400 reference drugs. *Drug Metab. Dispos.* **2011**, *39,* 1039-1046.

37. Silvaroli, J. A.; Widjaja-Adhi, M. A. K.; Trischman, T.; Chelstowska, S.; Horwitz, S.; Banerjee, S.; Kiser, P. D.; Blaner, W. S.; Golczak, M. Abnormal cannabidiol modulates vitamin A metabolism by acting as a competitive inhibitor of CRBP1. *ACS Chem. Biol.* **2019**, doi: 10.1021/acschembio.8b01070 [Epub ahead of print].

38. Vogel, S.; Piantedosi, R.; O'Byrne, S. M.; Kako, Y.; Quadro, L.; Gottesman, M. E.; Goldberg, I. J.; Blaner, W. S. Retinol-binding protein-deficient mice: biochemical basis for impaired vision. *Biochemistry* **2000**, *41*, 15360-15368.

39. Biesalski, H. K.; Chichili, G. R.; Frank, J.; von Lintig, J.; Nohr, D. Conversion of beta-carotene to retinal pigment. *Vitam. Horm.* **2007**, *75*, 117-130.

40. Quadro, L.; Blaner, W. S.; Salchow, D. J.; Vogel, S.; Piantedosi, R.; Gouras, P.; Freeman, S.; Cosma, M. P.; Colantuoni, V.; Gottesman, M. E. Impaired retinal function and vitamin A availability in mice lacking retinol-binding protein. *EMBO J.* **1999**, *18*, 4633-4644.

41. Quadro, L.; Hamberger, L.; Colantuoni, V.; Gottesman, M. E.; Blaner, W. S. Understanding the physiological role of retinol-binding protein in vitamin A metabolism using transgenic and knockout mouse models. *Mol. Aspects Med.* **2003**, *24*, 421-430.

42. Wolf, G. A case of human vitamin A deficiency caused by an inherited defect in retinol-binding protein without clinical symptoms except night blindness. *Nutr. Rev.* **1999**, *57*, 258-260.

43. Seeliger, M. W.; Biesalski, H. K.; Wissinger, B.; Gollnick, H.; Gielen, S.; Frank, J.; Beck, S.; Zrenner, E. Phenotype in retinol deficiency due to a hereditary defect in retinol binding protein synthesis. *Invest. Ophthalmol. Visual Sci.* **1999**, *40*, 3-11.

44. Chichili, G. R.; Nohr, D.; Schaffer, M.; von Lintig, J.; Biesalski, H. K. beta-Carotene conversion into vitamin A in human retinal pigment epithelial cells. *Invest. Ophthalmol. Visual Sci.* **2005**, *46*, 3562-3569.

45. Thompson, C. L.; Blaner, W. S.; Van Gelder, R. N.; Lai, K.; Quadro, L.; Colantuoni, V.; Gottesman, M. E.; Sancar, A. Preservation of light signaling to the suprachiasmatic nucleus in vitamin A-deficient mice. *Proc. Natl. Acad. Sci. U. S. A.* **2001**, *98*, 11708-11713.

46. Wolf, G. Retinol transport and metabolism in transthyretin-"knockout" mice. *Nutr. Rev.* **1995**, *53*, 98-99.

47. Racz, B.; Varadi, A.; Kong, J.; Allikmets, R.; Pearson, P. G.; Johnson, G.; Cioffi, C. L.; Petrukhin, K. A non-retinoid antagonist of retinol-binding protein 4 rescues phenotype in a model of Stargardt disease without inhibiting the visual cycle. *J. Biol. Chem.* **2018** *293*, 11574-11588.

48. Camerini, T.; Mariani, L.; De Palo, G.; Marubini, E.; Di Mauro, M. G.; Decensi, A.; Costa, A.; Veronesi, U. Safety of the synthetic retinoid fenretinide: long-term results from a controlled clinical trial for the prevention of contralateral breast cancer. *J. Clin. Oncol.* **2001**, *19*, 1664-1670.

Table of Content Graphic